2019

Design, Synthesis and Biological Screening of Novel Cucs-inspired Estrone Analogs towards Treatment of Pancreatic Adenocarcinoma

Khaled Alseud
South Dakota State University

DESIGN, SYNTHESIS AND BIOLOGICAL SCREENING OF NOVEL CUCS-INSPIRED ESTRONE ANALOGS TOWARDS TREATMENT OF PANCREATIC ADENOCARCINOMA

BY

KHALED MOHAMMED ALSEUD

A dissertation submitted in partial fulfillment of the requirements for the

Doctor of Philosophy

Major in Chemistry

South Dakota State University

2019

DESIGN, SYNTHESIS AND BIOLOGICAL SCREENING OF NOVEL CUCS-INSPIRED ESTRONE ANALOGS TOWARDS TREATMENT OF PANCREATIC ADENOCARCINOMA

KHALED MOHAMMED ALSEUD

This thesis is approved as a credible and independent investigation by a candidate for Doctor of Philosophy in Chemistry degree and is acceptable for meeting the Dissertation requirements for this degree. Acceptance of this does not imply that the conclusions reached by the candidate are necessarily the conclusions of the major department.

Fathi T. Halaweish, Ph.D.
Thesis Advisor Date

Douglas Raynie, Ph.D.
Head, Department of Chemistry and Biochemistry Date

Dean, Graduate School Date

ACKNOWLEDGEMENTS

All the thanks to ALLAH who gave me the strength, guide me to the right path and help me to accomplish my dream.

Second, this dissertation is dedicated to my family, who has always stand for me and supported me.

My Parents

I could never have accomplished my dream without your prayers, supports and continuous encouragement. Thank you for everything and for your love.

My Advisor

To the scholar who taught me how to balance between my research and social life and succeed in both, Dr. Fathi Halaweish, who always supports and guides me. Thank you so much for having me in your lab.

My Family

To the women whom I love, respect and believe in, thank you so much for everything that you have done to me. My wife Fatimah Aalsaadah thank you so much for your support and prayers. To my two kids Mazen and Ahmed, thanks for being patient and showing your support for me.

My Friends

To the people who are always with me and make me laugh at the sad time, support me at the hard time. Thank you so much for the nice moments that we spent together in the lab.

CONTENTS

ABBREVIATIONS

ADME	Absorption, Distribution, Metabolism and Excretion
EGFR	Epidermal Growth Factors Receptor
ERK	Extracellular Signal-Related Kinase
PDAC	Pancreatic ductal adenocarcinoma
MAPK	Mitogen Activated Protein Kinase
MDR	Multidrug Resistance
MEK	MAPK/ERK kinase
MRP	Multidrug resistance protein
MTT	3-(4, 5-dimethylthiazol-2-yl)-2, 5-diphenyltetrazolium bromide
NMR	Nuclear Magnetic resonance
SAR	Structure Activity Relationship
STAT3	Signal Transducer and Activator of Transcription 3
JAK	Janus Kinase I
GLUT1	Glucose transporter I

LIST OF FIGURES

.

LIST OF TABLES

ABSTRACT

DESIGN, SYNTHESIS AND BIOLOGICAL SCREENING OF NOVEL CUCS-INSPIRED ESTRONE ANALOGS TOWARDS TREATMENT OF PANCREATIC ADENOCARCINOMA

KHALED MOHAMMED ALSEUD

2019

Pancreatic cancer is currently the fourth most deadly type of cancer globally. It is expected to become the second by 2030, due to its poor prognosis and its resistance to the current standard treatment, Gemcitabine. Moreover, the survival rate after treatment is low compared to other cancer types, which suggests an urgent need for new potent and safe treatment agents. Recently, the triterpenoid, cucurbitacin, has shown promising antiproliferative activity against human pancreatic cancer cells in a dose- and time-dependent manner, and decreased pancreatic tumor size in combination with gemcitabine in vivo. However, the use of cucurbitacin in clinical studies has been hindered by its low yield from natural sources and challenging total chemical synthesis. In order to overcome this obstacle, we have developed molecular-modeling based strategy that resulted in the installation of cucurbitacin pharmacophores onto an estrone scaffold to generate novel hybrid analogs that showed a promising antiproliferative activity. In-*silico* drug design results showed that modification of these compounds at C_{11} possessing high binding affinity towards more than one of pancreatic molecular targets such as EGFR, and Erk, kinase domains. Based on that total of 25 novel analogs have been synthesized by adopting multiple step organic synthesis. The ant proliferation activities of the novel analogs were biologically investigated against PANC-I, AsPC-I, and BXPC-3 pancreatic cell lines in 2D

and 3D models using MTT and CellTiter assays, respectively. Five analogs showed potent IC_{50} values compared to gemcitabine and cucurbitacin B, and were further studied for cell cycle inhibition, EGFR signaling and caspase 3/7 activity in 2D models. Additional studies showed these analogs arrested the cell cycle in the G1 phase, inhibited activation of EGFR and the downstream MAP kinase Erk. The present study shows, for the first time, that C_{11} modified cucurbitacin-estrone hybrid analogs possess more antiproliferative activities than the standard chemotherapy regimen against pancreatic cancer cell lines and provide potential drug candidates for preclinical application.

Chapter One

General Introduction

1.1. Drug Discovery and Development

Drug discovery research has contributed to the progress of medicine more than the research in other medical fields.[1] The drug discovery process is very complicated and requires a development period of 10-15 years and a cost estimated to be more than $1-3 billion dollars.[2] Moreover, 95% of these drug candidates fail to receive approval from NIH during the early or late stages of drug discovery or during the clinical phases.[3] The drug discovery process starts with the identification of a medical problem that needs to be treated, followed by identification of the molecular targets used to treat that disease and the screening of many compounds in vitro against these targets. Thousands of compounds are produced during this screening stage. Following this stage, the drug candidates undergo a preclinical studies where they are tested in vivo. Many disciplines contribute to this long process where the pharmacological activity and toxicity profile of these drugs are tested, mostly in mice. This stage will determine if the drug will be moved to clinical trials after approval from the FDA; at that point, it will obtain an investigational new drug (IND) license that allows researchers to start the clinical trial process. In the clinical trial stage, the pharmacological and toxicity effects are studied in healthy human subjects, as well as in human subjects who are affected by the targeted disease. This stage is divided into four phases.[4]

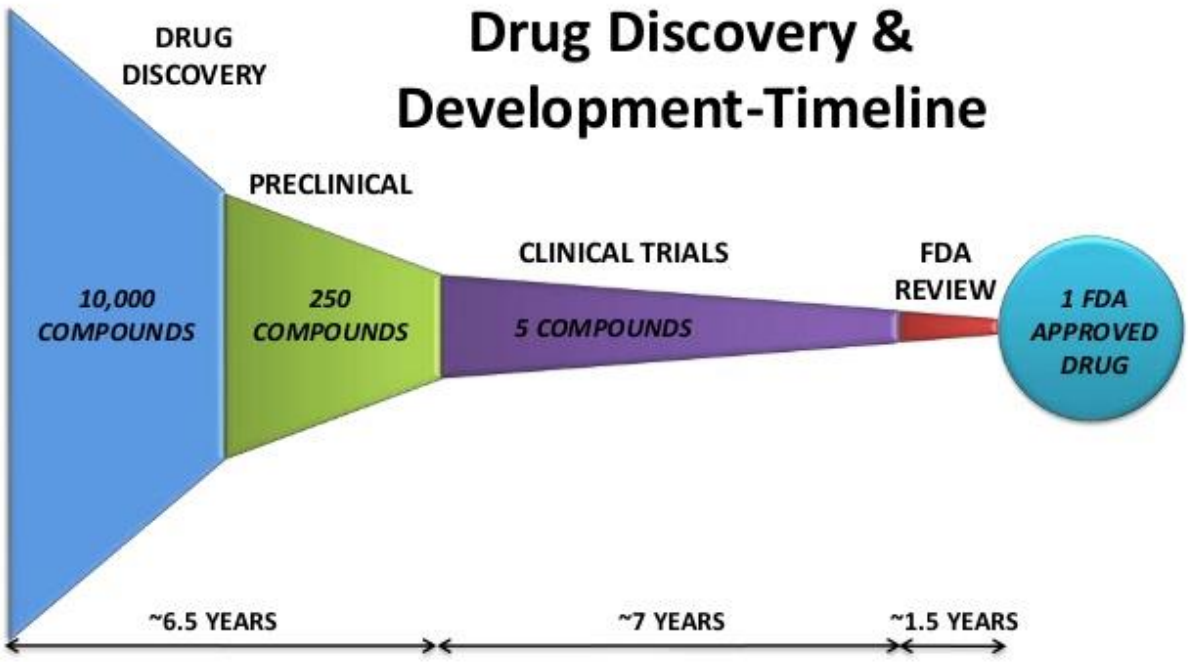

Figure 1.1. Timeline for the general stages of drug discovery and development.[5]

By benefiting from the failed drugs, medicinal chemists develop drug design concepts through which they can identify the functional groups that increase the binding to the targets compared to existing groups and groups that are known to be toxic, such as nitro groups. Also, an understanding of molecular targets facilitates the drug discovery process, especially since the advancements in bioinformatics. Through bioinformatics and genetic sequences, the researcher is able to identify the genetic mutations in biological molecules in different cancer types before they are overexpressed in vitro, and use them as targets for screening small molecules.[5] Through NMR spectroscopy, x-ray crystallography, and computational *in-silico* design programs, a better understanding of ligand-target interactions is gained and the first stage of the drug discovery process has been effectively minimized.[6]

One of the strategies used in the drug discovery process is *in-silico* drug design, where a library of small molecules is screened against a three-dimensional structure of a

macromolecule. In this strategy, small molecules are fitted into the space that is docked by the original ligand that crystalized with that macromolecule.[7] The first step in molecular docking includes the generation of a large library of small molecules and all possible conformers of these ligands by rotating the angles between their atoms. Then, the most stable conformer is chosen by using one of the force fields, such as UFF, GAFF or MMFF94.[8] After the preparation of the virtual library, docking programs with different parameters rank the binding of the molecules.[9] Docking programs such as FRED, Surflex and DOCK will run the exhaustive docking process that is used to rank the ligands based on different functions, such as shapeguass, PLP, chemgauss3, chemscore, and screenscore. These functions rank the ligands based on the molecular interactions between the ligand and the macromolecule. For example, all of these mentioned forces consider the fitting of the molecule in the pocket and the hydrogen bonding between the ligand and the target (with the exception of the chemguass function). Some interactions are unique to a specific function, such as desolvation which is used by chemguass3 but not the others. These scoring functions also vary in terms of their speed, exhaustive docking and optimization. After running the docking experiments, these compounds will be ranked according to a calculated consensus score that depends on the functions used in the docking. The lowest consensus score will be the ligand that best binds to the target. The promising candidates will be obtained either by purchasing, if they are commercially available, or by synthesizing them chemically.

After synthesizing the candidate compounds and testing their biological activity in vitro, another important step is necessary to gain information that might not be predicted by molecular modeling. Information such as the transport of the drug to the cell or the export

of the drug by a certain resistance mechanism requires that other kinds of optimization are performed to overcome the obstacles found in the biological evaluations of these candidates. These optimizations have different aspects, including changing the polarity of some functional group or completely changing the pharmacophores.

Many aspects of optimization have been carefully studied, leading to the development of drug discovery rules. For example, the Lipinski rule of five suggests that a compound should not exceed 5 hydrogen bond donors and 10 hydrogen bond acceptors, and its molecular weight should be less than 500 Daltons with a partition coefficient in terms of log *P* less than 5.[10] These rules are focused on the chemical and physical properties of the compound which affect its binding to the target and its bioavailability. Although these rules are not essential in determining if a drug will be a good candidate, it is important to take them into consideration and use them as an initial guide in designing drugs, thus keeping synthesized compounds within the mentioned ranges.

Another aspect of drug optimization uses a bioisosterism concept where a chemical group can be substituted with a different group having similar chemical properties to obtain better pharmacological activity or less toxic effects. Bioisosterism is based on the biological activity derived from a biological evaluation of previously known lead compounds and their derivatives.[11] Sometimes, bioisosterism is applied not only to change the biological activity of compounds, but to change their physical properties to improve their bioavailability, thus maintaining or improving the potency of the drug.

1.2. Natural products as an inspired source for drug discovery

Statistical studies regarding approved drugs indicate that natural products play an important role in drug discovery. Natural products contain unique pharmacophores, as noted through their complex stereochemistry. An example of a natural product-inspired drug is temsirolimus, which is an mTOR inhibitor with anticancer activity against renal cell carcinoma. It was developed from the natural product rapamycin.[12]

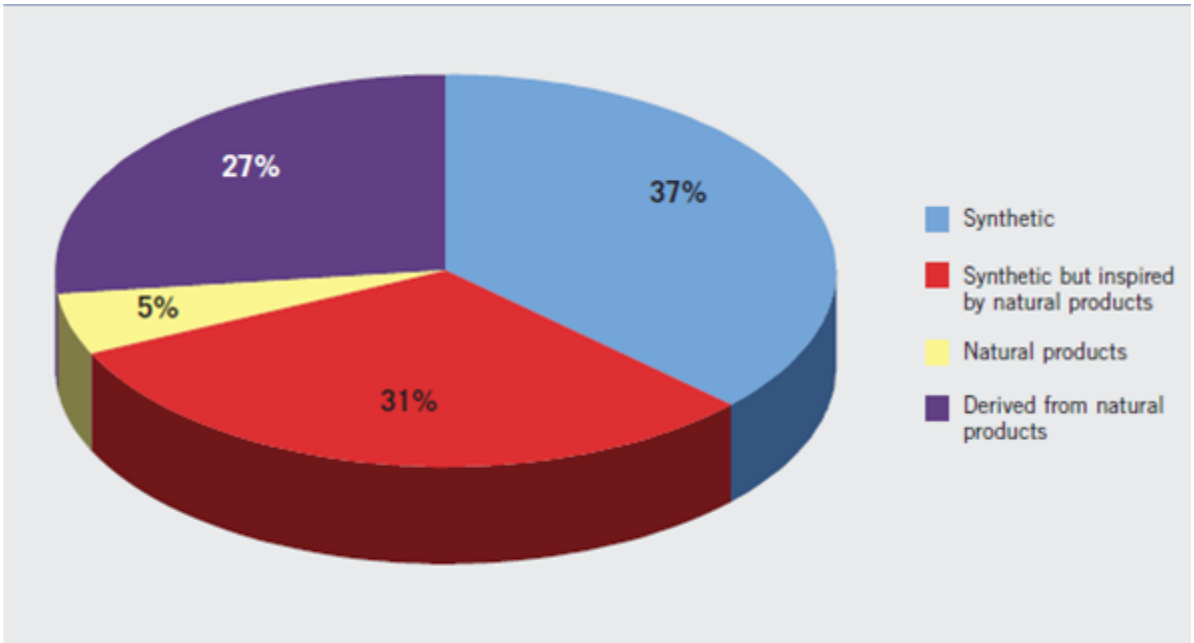

Figure 1.2. a diagram for the sources of the approved from the period of 1981-2011 shows that almost two thirds are derived from natural products.[13]

1.3. Cucurbitacins as Potential Natural Compounds Targeting Different Molecular Targets

Cucurbitacins are four-ring tetraterpenoid compounds that exist in very small amounts in Cucurbitaceae plants, such as Cayaponia tayuya, and Citrillus colocynthis.[14] This group of compounds, which consists of 18 types, was traditionally used as an anti-inflammatory and

anticancer agent are example of natural products that has been used for different pharmacological uses till today.[15]

1.3.1. Chemistry of Cucurbitacins

Cucurbitacins are tetracyclic triterpenes are characterized by high number of oxygen atoms and similar to steroids in structure (Figure 1.3). One of the common features of cucurbitacins and steroids, such as cholesterol and estrone, is the presence of the four ring system.[16] However, some differences and additional functional groups are found in cucurbitacin (cuc) that result in its unique pharmacological activities compared to steroids, such as the gem-dimethyl group at ring A, C_4, the methyl that exists between rings B and C, and C_9. In some cuc types, such as cuc A, C_{11} is hydroxylated, which is thought to be responsible for the selectivity of cuc A as it loses its anti-STAT3 inhibition activity.[17] Another feature of cucurbitacins is the presence of α-β-unsaturated ketone in the side chain, which is one of the major pharmacophores responsible for the antiproliferative activity of cucurbitacins. Upon comparing nine commonly found cucs compounds, common functional groups can be used to distinguish cuc family of compounds from the other four-membered ring steroidal compounds. These characteristics include the double bond between C_5 and C_6 and ring B, α-hydroxyl group at ring D, C_{16}, the hydroxyl group at C_2, and the ketone at C_3 of ring A. In all cucs compounds, except for cucs C and F, the ketone group is reduced to hydroxyl groups, while C_2 of cuc C is attached to hydrogen instead.

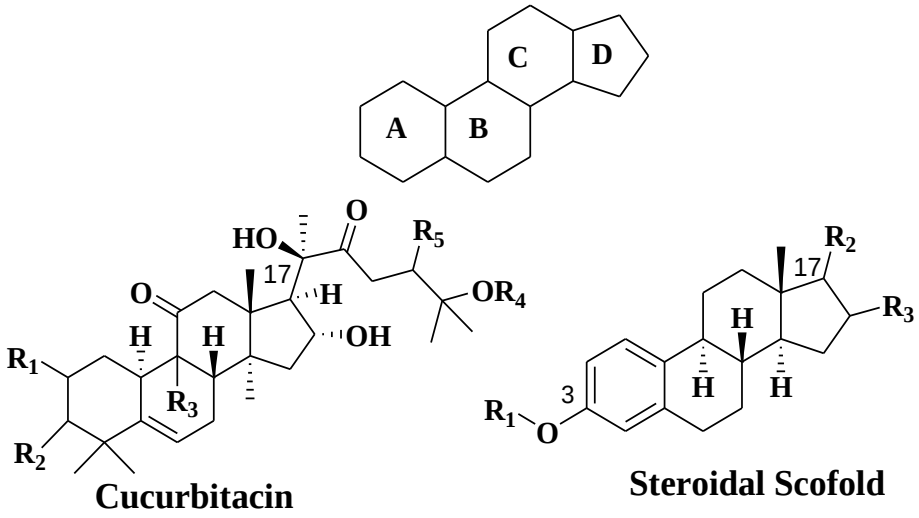

Figure 1.3. General structures of cucurbitacin and steroid.

The α-β-unsaturated ketone side chain of cucurbitacins either contains the tertiary hydroxylated group, as in cucs D and F-J, or are acetylated, as in the rest of cucs. Experimental data confirms the presence of acetyl-transferase enzyme as expressed in the gene biosynthetic cluster of these cucs types.[18]

1.3.2. Pharmacological Activities of Cucurbitacins

The unique oxygenated and unsaturated four rings of cucurbitacins, which differentiate them from the other steroidal scaffolds, give them unique biological and pharmacological activities.[19] Cucs were traditionally known for their anti-inflammatory activity, but recently, they became efficient antiproliferative agents for the treatment of different cancer types, such as lung, breast, colon, and pancreatic cancers.[17] Moreover, cucs have been reported to have antiviral activity**,** which opened another avenue of investigation for pharmacological uses for cucurbitacins.[20]

Cucurbitacins have been traditionally used as an anti-inflammatory agent by applying it topically. In this type of application, it has been proved to inhibit cyclooxygenase 2 (COX-2). Cyclooxygenase enzymes are involved in the biosynthesis of prostaglandins and thromboxane, so their inhibition relieves the symptoms of inflammation and pain.[21] Comparing cucs with the non-steroidal anti-inflammatory (NSAIDs) COX inhibitors, Recio *et al.* indicated that the COX-2 inhibitory rate of cucs is lower than NSAIDs. On the other hand, cucs are more selective COX-2 inhibitors. Other reports demonstrated that the saturation of carbons 23, 24 of cucs increased the inhibitory COX-2 activity.[22]

Cuc B has demonstrated comparable antiviral activity to acyclovir when it was examined against the enveloped-DNA virus Herpesviridae, with IC_{50} values of 0.94 and 1.74 μM, respectively.[23] The anti-HSV-1 activity of cucs against enveloped-DNA viruses, which are responsible for many antiviral infections, indicate other potential antiviral activities for these compounds. Moreover, cuc B showed a mono- and synergistic effect with tetracycline and oxacillin against *Staphylococcus aureus (S. aureus)*. As a result, cucs may be used in combination with antibiotics for the treatment of staphylococcal infections.[23] Currently, cucs are being investigated for their anticancer activity in different cancer cell lines. Moreover, many *in-vivo* studies demonstrate the antiproliverative activity of cucs in combination with other drugs, as well as in monotherapy.

1.3.3. Cucurbitacins Anti-proliferative Activities

The anticancer activity of cucs have been investigated in many cancer cell lines, including lung, leukemia, hepatocellular carcinoma, breast, ovarian, colon, brain, and pancreatic cancers.[23] Generally, cucs as antiproliferative activity can be divided into four mechanisms: proapoptosis, induction of autophagy, cell cycle arrest, and inhibition of cancer invasion

and migration.[24] Cucs have been demonstrated to interfere with important signaling pathways involved in tumor growth, such as EGFR, PI3K/Akt, mTOR, STAT3 and ERK signaling.[25] Epidermal growth factor receptor (EGFR) is a transmembrane protein that has extracellular and intracellular domains.[26] Two mechanisms are used to inhibit EFGR activity. One mechanism competitively inhibits the extracellular binding site of EGF, prevents the dimerization of two EGFR monomers and inhibits the initiation of the downstream cascade. The second mechanism involves the inhibition of kinase activity by which EGFR can phosphorylate the downstream proteins. EGFR is found to be overexpressed in many cancer types, such as breast, lung, pancreatic and liver cancers.[27] The inhibition of EGFR can restrain the pathways of (Ras/Raf/MEK/ERK) that are significant in many cancer types. Another important target for cucs is signal transducer and activator of transcription 3 (STAT3), which is phosphorylated by receptor-associated Janus Kinases (JAK).[28] Moreover, cuc B was reported to inhibit the PI3K/Akt/mTOR pathway. Through inducing p53, p21, and caspase-3, cucs inhibit the growth of tumors through apoptosis[29] and interact with the microtubules and cycloskeleton of the cell, which leads to cell cycle arrest at the G2/M phase.[30]

Upon investigation of the structure activity relationship (SAR) of cucs, studies proofed that the α-β-unsaturated C_{22}-C_{24} enone side chain is the main pharmacophore for cuc anticancer activity. This was demonstrated by decreasing the antiproliferative activity of dihydro-cucs B and D. Moreover, the glycosylated cucs showed less cytotoxic activity than the non-glycosylated cucs. Also, the acetylation of C_{25} of cuc B increased its antiproliferative activity by 1000 fold, compared to cuc D.[31]

Cuc D also demonstrated antiproliferative activity against the PrCa prostate cancer cell line, with an IC_{50} of 0.1 μM to 1μM. This was accomplished by decreasing the GLUT1 expression, which led to a decrease in glucose uptake and lactate secretion. Cuc D affect cell cycle arrest in the G2/M phase, and upon treatment using a PrCa xenograft mouse model, it inhibited tumor growth.[32]

Upon investigation against the gemcitabine-resistant AsPC-I pancreatic cell line, cuc D displayed antiproliferative activity by inhibiting the Muc13 expression, EGFR, and AKT activation, along with enhancing miR-145 expression. Compared to a control group, cuc D reduced tumor size in SCID mice injected with pancreatic cells.

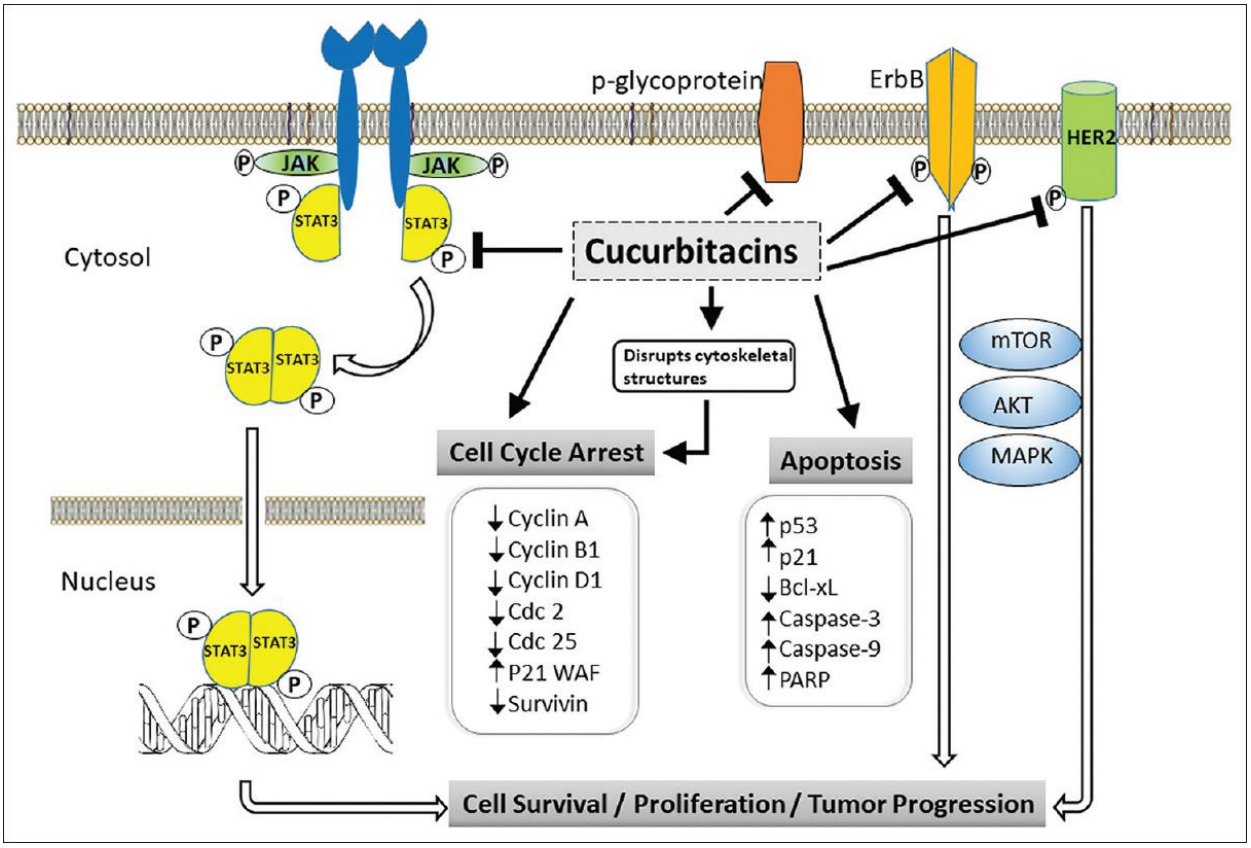

Figure 1.4. Anticancer activity mechanism of cucurbitacin on different pathways.

1.3.4. Mechanism of Antiproliferative Activity of Cucurbitacins

1.3.4.1. Inhibition of MAPK/ERK pathway

The MAPK/ERK (or Ras/B-Raf/MEK/ERK) (Figure 1.5.) pathway is a group of proteins that act as a chain when the receptor, which is the transmembrane protein (EGFR), is activated. This initiates and activate a cascade that ends in the nuclear DNA and regulates vital biological functions such as cell division, differentiation, survival and cell death. This pathway has been considered as one of the successful strategies to treat cancer, although resistance is created by mutation, mainly in the proteins of this pathway.[33]

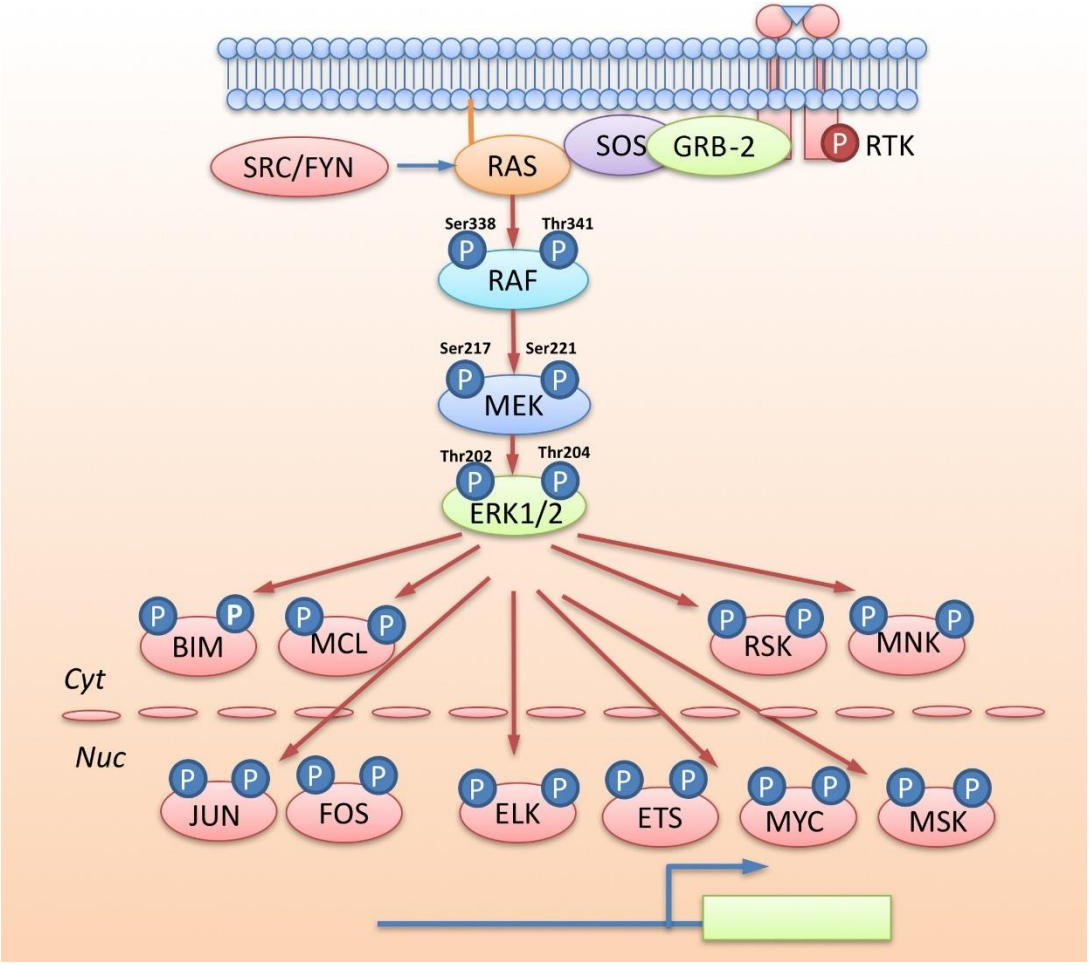

Figure 1.5. ***The*** **major downstream targets of ERK1/2 in the MAPK pathway.**

1.3.4.2. Epidermal Growth Factor Receptors (EGFR) and Cancer

EGFR (ERB1) is one of the four types of the ErbB receptor family. This tyrosine receptor kinase consists of an extracellular binding domain, a hydrophobic transmembrane domain, and a cytosolic domain that causes kinase (phosphorylation) activity for the downstream proteins.[34] When the growth factors, such as transforming growth factor α (TGF- α), binds to the extracellular domain of EGFR, the dimerization or activation of the receptor occurs, resulting in phosphorylation of specific tyrosine residues in the intracellular cytosolic domain of EGFR. This leads to a subsequent activation of the downstream proteins.[34, 35] Liovet *et al.* showed that the deactivation of EGFR increased the survival rate of patients

in the late stages of hepatocellular carcinoma.[36] This occurs through the inhibition of EGFR phosphorylation in pancreatic cancer cells.[25]

1.3.4.3. Rat Sarcoma (RAS) Protein Family and Cancer

Ras gene was discovered in the 1960's in a study that was focused on Harvey sarcoma and Kristen sarcoma viruses originally found in rats, thus named Rat sarcoma.[37] Ras proteins consist of six beta strands and five α-helices, which form GTP, a GDP-binding domain and a C-terminal region. Ras proteins are activated when GTP is bound to it, and deactivated after phosphorylation of the downstream proteins with GDP bound to it.[38] Mutations of RAS proteins, mainly K-RAS mutation, have recently been identified in many cancer cells, such as small intestine, colon, pancreatic, and biliary tract cancers.[39] Due to the ability of phosphorylated RAS to rewire and activate different pathways, it is challenging to inhibit its downstream activity.[40] For example, one of these important pathways is the posttranslational modification of C-MYC, which results in the increased activity of MYC, which is one of the critical pathways of RAS-driven activity.[40] Shukla *et al.* reported that cuc B downregulated C-MYC/K-RAS at the protein level.[41]

1.3.4.4 Rapidly Accelerated Fibrosarcoma (RAF) and Cancer

RAF proteins are activated by RAS-GTPases and consist of three family members. This family of receptors are characterized by the presence of serine/threonine-specific kinases. After phosphorylation by RAS proteins, the A-C proteins phosphorylate the downstream MEK1/2 proteins.[42]

1.3.4.5. Mitogen-Activated Protein Kinase and Cancer (MEK1/2)

Currently, seven types of MAP kinases have been identified; however, MEK1 and 2 are the only known substrates of RAF kinases. These consist of C- and N- terminal domains and an ERK-binding region. RAF phosphorylates MEK/2 at tandem serine residues at a site called an activation loop. Phosphorylated MEK1/2 regulates different cell functions, such as the ERK activation.[43]

1.3.4.6. Extracellular Signal–Regulated Kinases (ERKs)

ERK proteins are involved in the regulation of many cellular functions, such as cell division. The mechanism of activating ERK1/2 by RAF kinases involves phosphorylation. Evidence has been found to show that the phosphorylated ERK2 activated by MEK1 is transferred to the nucleus where it activates the proliferation process, while ERK2 activated by MEK2 is transferred to the cytosol and promotes cell survival.[44] The inhibition of ERK proteins is an important mechanism by which anti-cancer agents act.

1.3.4.7. Cucurbitacins Effect on Filamentous-Actin

Actins are protein components found in all eukaryotic cells and have many important functions. These structures are either globular (G-actin) or filamentous (F-actin). F-actin type maintain many functions in eukaryotic cells, such as maintaining the cytoskeleton and facilitating cell migration.[45] It has been reported that cuc E selectively inhibits F-actin depolymerization (without inhibiting the monomeric globular G-actin) by covalently binding with CYS 257 amino acid residue.[46] Another study proved that cuc E stimulates the actin cytoskeleton disturbance in the prostate cancer cell line.[47]

1.3.4.8. Cucurbitacins' Effect on STAT3 Signaling Pathway

Signal transducers and activators of transcription are a family of cytosolic transcription activators that stimulate the biosynthesis of cell surface receptors and transmit the signal into the nucleus. Several reports indicate that this pathway is key to tumor growth. The most important of the seven member family is STAT3, which promotes the initiation and progression of cancer by several mechanisms, including inhibiting apoptosis and inducing cell proliferation.[48] Activation of STAT3 is carried out by IL-6 and EGF proteins using several mechanisms.[49] After the activation of STAT3, dimerization occurs in the cytoplasm, and subsequently activates the Janus-kinase (JAK) phosphorylation, which leads to phosphorylation of other STAT3 monomers. Phosphorylated STAT3 also induces transcription by binding to DNA.[50]

The activity of cucs in inhibiting the STAT3/JAK pathway has been studied and the structure activity relationship has been demonstrated according to the different functionalities of cucs compounds. For example, cuc I acts by inhibiting the phosphorylation of STAT3 in lung cancer,[51] while cuc A inhibits the activation of JAK2, and cucs B and E act by inhibiting both STAT3 and JAK2.[52]

1.3.4.9. Cucurbitacins' Effect on mammalian target of rapamycin (mTOR) Pathway

mTOR is one of the downstream proteins in PI3K/AKT/mTOR that affects the cell proliferation cycle.[53] The up regulation of this pathway has been observed in cancer cells such as osteosarcoma. Cuc B has been shown to inhibit mTOR directly as a single agent, as well as in combination with methotrexate, although the authors suggest that the exact mechanism by which cuc B inhibits mTOR needs further investigation.[54]

1.3.4.10. Hepatoprotective activity of cucurbitacins

Interestingly, cuc D and dihydrocuc D at lower than the antiproliferative dose indicate a hepatoprotective effect against carbon tetrachloride-induced toxicity on HepG2 cell line. An investigation of the underlying mechanism indicates that cuc D and its dihydro form decrease the production of tumor necrosis factor-alpha and interleukin-6 in hepatocellular carcinoma cell line HSC-T6.[55]

1.4. Pancreatic Cancer

1.4.1 Background

Cancer is a disease that is characterized by abnormal growth of cells. These uncontrolled cells have the ability to invade surrounding tissues when the disease reaches the metastasis stage.[56] Pancreatic ductal adenocarcinoma (PDAC) is the most malignant tumor among pancreatic cancer types and represents about 85% of the diagnosed pancreatic cancer cases.[57] Anatomically, the pancreas, which is about 6 inches long in a normal adult, is characterized by three main parts. The first part is the head, which is located on the right side of the abdomen in front of the small intestine where the duodenum and stomach meet. The larger part of the pancreas, the body, is behind the stomach, while the tail lies on the left site of the abdomen beside the spleen.[58] Histologically, the pancreas contains two types of cells: endocrine and exocrine cells. Exocrine cells excrete digestive enzymes into ducts that merge with bile ducts, then secrete fluid into the duodenum. The endocrine ducts, which secrete less than the exocrine ducts, biosynthesize important hormones such as insulin and glucagon.[58] The tumors that occur with exocrine cells, acinar cells, is called pancreatic ductal adenocarcinoma, which represent the majority of pancreatic cancer types.

The mortality statistics on pancreatic ductal carcinoma (pancreatic cancer) cases indicate it has the fourth highest mortality among cancer types in United States.[59]

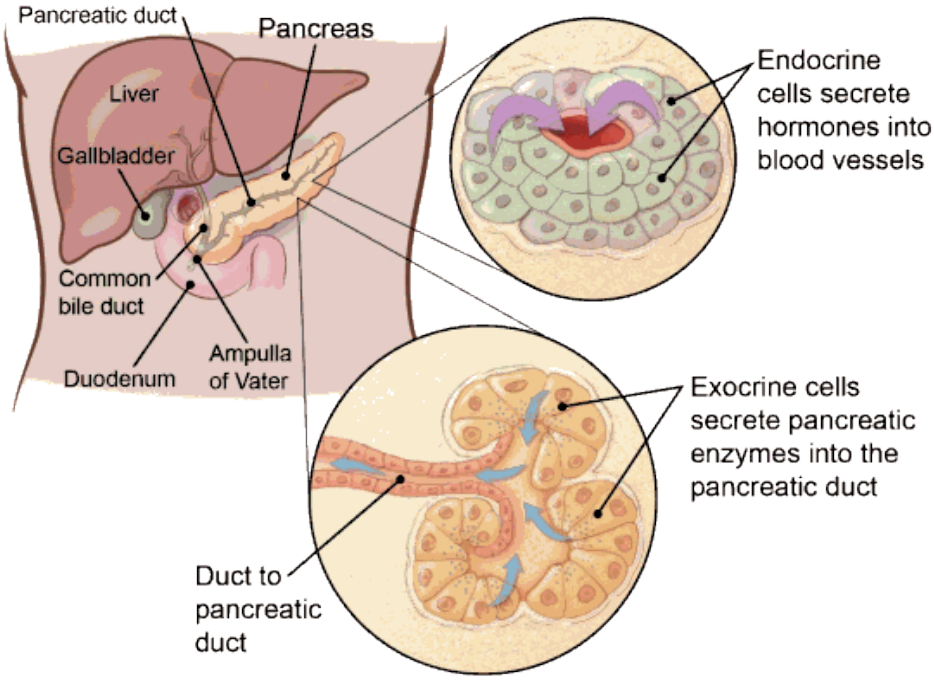

Figure 1.6. Anatomy and histology of the pancreas.[60]

Pancreatic cancer mortality data indicates an increasing number of deaths,[61] and it is expected to be ranked as the second cause of death among cancer types in the near future.[62] The estimate for the number of patients with pancreatic cancer in 2016 is 53,070, and according to the current mortality rate, most of them will have a survival period of 5 years or less.[63] Of the previous cases, 75% of the pancreatic ductal adenocarcinoma patients were between the ages of 55 and 84 years and the majority of them were men. This indicates that the age of 55 is one of the risk factors.[64] Other risk factors are related to lifestyle, including smoking, alcohol usage, and a high cholesterol diet.[65] Based on its pathology, PDAC can be divided into three main stages. The initiation stage begins when the mutation occurs due to the environment effect or a failure in DNA repair after cell division. It is estimated that

the first cell that has the mutation of the drive gene for PDAC occurs 20 years before the disease can be diagnosed.[66] In the second stage, the mutated cell begins to divide and proliferate until it reaches the third stage, where the mutated population of cells spread to the surrounding cells and break the basement membrane.[67]

Molecular biology and genetic sequencing indicate that four common types of mutations occur in PDAC. Mostly KRAS mutation, which encodes the RAS family of GTP-binding proteins, are responsible for cell proliferation and cell survival.[68] Of the analyzed PDAC cases, the KRAS mutation is found in about 95% of the cases.[69] Other mutations include the tumor gene suppressor CDKN2A, the transcription factor TP53, and the co-transcription factor SMAD4.[69]

The symptoms of PDAC include jaundice, dark urine, greasy stool, itchy skin and back pain. The reason for the high mortality rate with pancreatic cancer is the absence of biomarkers that can be detected in the early stages.[70] Moreover, the progress in developing pancreatic anticancer agents is very slow.[71]

The treatment of PDAC differs according to the stage of the disease and the health of the patient. The surgical option is the first choice of treatment if the patient is diagnosed to have stage I, II, or III PDAC. In stage I, the tumor is restricted to the pancreas, while in stage II, the tumor is 2-4 cm in size. By stage III, the tumor has spread to the major blood vessels or nerves close to the pancreas.[59] However, if the patient is diagnosed to have stage IV PDAC, where the cancer has spread to other organs, chemotherapy is the best option. The current standard treatment for pancreatic cancer is gemcitabine; it has an 18% 1-year survival rate, which is much better than the former standard treatment, 5-fluorouracil (5-

FU), that had only a 2% 1-year survival rate. The six-month survival rates for gemcitabine and 5-FU are 23.8% and 4.8%, respectively, which indicates that there is an urgent need to find novel agents for pancreatic cancer treatment.

1.4.2. Current Treatment of Pancreatic Ductal Adenocarcinoma

1) Surgical Resection

Because PDAC is usually diagnosed in the late stages in more than 95% of the patients, the surgical option is only used in 10-15% of the patients. However, several cases have been found in which the surgical resection cannot be performed. These cases include the presence of metastasis on the liver, distant metastasis or lymph node enlargement. Moreover, the mortality rate is approximately 3-5% in the cases in which surgery was performed.[72] Also, the statistical studies indicate that the survival rate after surgery is 3-16% of patients for 5 or more years.[73]

2) Radiotherapy

Applied radiotherapy has been used alone or in combination with surgery or chemotherapy. A Gastrointestinal Tumor Study Group (GITSG) indicated that the survival rate increased to 19% after 10 years of radio chemotherapy.[74]

3) Chemotherapy:

Since the majority of pancreatic cancer patients are diagnosed in the late stage of the disease, chemotherapy is the first option used. Administration of gemcitabine chemotherapy as a single agent is tried first.[75] Gemcitabine has an 18% one-year survival rate compared to the former standard 5-fluorouracil (5-FU) that has only a 2% 1-year

survival rate. The six-month survival rates for gemcitabine and 5-FU are 23.8% and 4.8%, respectively.[76] Several studies have been conducted in which gemcitabine is combined with other drugs, such as cisplatin. In this combination, cisplatin induced DNA lesions, while gemcitabine enhanced this effect by inhibiting DNA repair, resulting in apoptosis of the cells.[77] Colucci *et al.* conducted a clinical study in which two groups of pancreatic ductal adenocarcinoma patients were administered either gemcitabine or the gemcitabine/cisplatin combination weekly for 7 weeks, followed by 1 week rest, then interrupted doses for a period of 4 weeks at days 1, 8, and 15. In this study, no improvement was seen in the combination treatment group. Rather, hematologic toxicity cases were observed in the group administered combination therapy.[75]

After its uptake by human nucleoside transporters (hNTs), gemcitabine is metabolized to 2′, 2′-difluoro-2′-deoxycytidine triphosphate before it is phosphorylated by deoxycytidine kinase and pyrimidine nucleoside monophosphate kinase to produce gemcitabine diphosphate (dFdCDP). At this point, it is incorporated into DNA chain biosynthesis by the DNA polymerase, which results in its termination.[78] However, due to the steps needed for gemcitabine to reach its target, several mechanisms of resistance are adopted by cancer cells to avoid DNA termination. These mechanisms include lack of transporters and phosphorylation enzymes, along with overexpression of gemcitabine deactivating enzymes, such as cytidine deaminase, that convert gemcitabine into its inactive metabolite dFdU.[79] The low survival rate of PDAC patients compared to other cancer types has inspired researchers to investigate novel, more effective anti-pancreatic cancer drugs.

1.5. Cucurbitacin-Inspired Estrone (CIE) Analogs

Chemically, cucurbitacins are characterized by the presence of a cucurbitane nucleus and an α,β-unsaturated ketone side chain that is responsible for the anticancer activity of cucurbitacin.[80] Cuc B was the first cuc that was made biosynthetically. From a biosynthetic point of view, cucs E and B are considered the precursors of all cucs compounds, based on the studies of their biosynthetic gene cluster. For instance, cucurbitacins A, D, C, F, G and H can be synthesized via biotransformation of cuc B, whereas cucs I, K, J and L can be biosynthesized from cuc E.[81] However, due to the low yield of cucs from their natural sources and the challenge of total chemical synthesis, cucs could not be advanced to clinical studies. However, the core of the cucurbitacins was synthesized via a highly regio- and stereoselective Diels-Alder Reaction. [82] Moreover, chemical modifications of cuc B were carried out to study the anticancer activity of cuc B derivatives.[83]

In order to overcome this obstacle, we developed a molecular-modeling dependent novel strategy with cucs pharmacophores, using the triterpenoid four-membered rings estrone as a scaffold. One important pharmacophore of cucs is 23, 24 α, β- unsaturated ketone side chain that is responsible for the anticancer activity of cucs. Interestingly, when we installed this side chain on estrone, it showed comparable anticancer activity to that of cucurbitacin.[84] These cucurbitacin-inspired estrone analogues (CIEA's) opened the door to more investigations regarding the functionalization of this compound at different positions. We searched for more potent anticancer compounds through *in-silico* molecular modeling of these analogs against known cucurbitacin molecular targets. Currently, we have proven that the functionalization of rings A, C and D of CIE analogs can lead to more potent anticancer agents than the currently available standard treatments. Previously, we reported

that the dehydrogenation of C_9-C_{11} and C_{16}-C_{17} generally increased the potency of this group of compounds.[85] Moreover, methylation and sulfamoylation of C_3 increased the potency relative to the originally found phenol.[86] One of the recent modification strategies for the anticancer drugs which currently induce resistance from cancer cells is the introduction of a nitric oxide releasing group, such as NCX-1000, that shows effective hepatoprotective activity. Recently, our investigation shows promising anticancer activity for NO-CIE analogs containing nitric oxide releasing functional groups, such as the furoxan moiety. In this instance, a furoxan moiety was installed at ring C_3 through an ether linker. The IC_{50} of the hybrid with phenyl *para*-trifluoromethyl side chain against HepG2 cell line was 4.69μM. [87] Another modification included the introduction of many functional groups instead of a cucurbitacin side chain through aldol condensation; one such group was phenyl *para*-trifluoromethyl, which showed potent anticancer activity.

One of the arguments regarding CIE analogs is the presence of an aromatic ring instead of ring A in the cucurbitacins. However, the aromatic ring at this position did not decrease the anticancer activity, as previous studies mentioned. Moreover, fevicordin A is an anti-cancer agent that has an aromatic ring as an estrone scaffold and the cucs general structure as well, indicating that the presence of an aromatic ring is not a drawback for CIE analogs.[88]

1.6. Project Objectives

Based on the previous studies that were conducted in our lab and the molecular docking studies, this project focuses on the modification of cucurbitacin-inspired estrone analogs (CIEA's) that target pancreatic cancer. Based on molecular docking data a library of virtual compounds will be designed and the candidates with high binding affinity to the molecular targets will be chemically synthesized and their inhibitory effects will be investigated on EGFR and downstream signaling pathways, including Mitogen Activated Protein Kinase (MAPK) pathway comprised of RAS/ RAF/ MEK/ ERK proteins and PI3K/Akt/mTOR pathway. Moreover, a structure activity relationship study will be conducted in order to sum up the data obtained over 5 years of work on the development and optimization of CIEA's as promising anticancer agents for the treatment of different cancer types.

The main objectives of this project are:

- Molecular modeling study of different CIE analogs modified in rings A, C and D on potential molecular targets of pancreatic cancer cells.
- Synthesis of CIE analogs that have a promising calculated binding affinity to the used molecular targets, according to the molecular modeling study.
- Biological evaluation of the synthesized CIE analogs against three pancreatic cancer cell lines using 2D and 3D cell viability assay using 2D and 3D models.
- Study the cell cycle arrest of CIE analogs that have promising IC_{50} value compared to the currently available drug of choice for pancreatic cancer (gemcitabine).
- Study the effect of these compounds in caspas-3 activity and inducing cell apoptosis.

- Study the inhibitory effect of the promising analogs using the potential molecular targets that were used in the first objective to the rank the virtually designed CIE analogs using In-Cell Western (ICW) assay.

1.7. References

1. Drews, J. J. s., Drug discovery: a historical perspective. **2000,** *287* (5460), 1960-1964.

2. Dickson, M.; Gagnon, J. P. J. N. r. D. d., Key factors in the rising cost of new drug discovery and development. **2004,** *3* (5), 417.

3. U.S. Department of Health & Human Services, About New Therapeutic Uses. **10-30-2018**

4. U.S. Department of Health and Human Services The Drug Development Process. (accessed Jan-23).

5. Advances in Biological Sciences, Guided Tool for Virtual Drug Discovery. **2017**.

6. Gibbs, J. B. J. S., Mechanism-based target identification and drug discovery in cancer research. **2000,** *287* (5460), 1969-1973.

7. Ferreira, L.; dos Santos, R.; Oliva, G.; Andricopulo, A. J. M., Molecular docking and structure-based drug design strategies. **2015,** *20* (7), 13384-13421.

8. Acharya, C.; Coop, A.; E Polli, J.; D MacKerell, A. J. C. c.-a. d. d., Recent advances in ligand-based drug design: relevance and utility of the conformationally sampled pharmacophore approach. **2011,** *7* (1), 10-22.

9. Halgren, T. A. J. J. o. c. c., Merck molecular force field. I. Basis, form, scope, parameterization, and performance of MMFF94. **1996,** *17* (5-6), 490-519.

10. López-Vallejo, F.; Caulfield, T.; Martínez-Mayorga, K.; A Giulianotti, M.; Nefzi, A.; A Houghten, R.; L Medina-Franco, J. J. C. C.; Screening, H. T., Integrating virtual screening and combinatorial chemistry for accelerated drug discovery. **2011,** *14* (6), 475-487.

11. Lipinski, C. A.; Lombardo, F.; Dominy, B. W.; Feeney, P. J. J. A. d. d. r., Experimental and computational approaches to estimate solubility and permeability in drug discovery and development settings. **1997,** *23* (1-3), 3-25.

12. Brown, N. J. B. i. M. C., Bioisosterism in medicinal chemistry. **2012**, 1-14.

13. Faivre, S.; Kroemer, G.; Raymond, E. J. N. r. D. d., Current development of mTOR inhibitors as anticancer agents. **2006,** *5* (8), 671.

14. Samedan LTD Pharmaceutical Publisher, The Roots of Innovation. **2011**.

15. Miro, M. J. P. r., Cucurbitacins and their pharmacological effects. **1995,** *9* (3), 159-168.

16. Fuller, R. W.; Cardellina, J. H.; Cragg, G. M.; Boyd, M. R. J. J. o. n. P., Cucurbitacins: differential cytotoxicity, dereplication and first isolation from Gonystylus keithii. **1994,** *57* (10), 1442-1445.

17. Gry, J.; Søborg, I.; Andersson, H. C., *Cucurbitacins in plant food*. Nordic Council of Ministers: 2006.

18. Alghasham, A. A., Cucurbitacins–a promising target for cancer therapy. *International journal of health sciences* **2013,** *7* (1).

19. Molavi, O.; Ma, Z.; Mahmud, A.; Alshamsan, A.; Samuel, J.; Lai, R.; Kwon, G. S.; Lavasanifar, A., Polymeric micelles for the solubilization and delivery of STAT3 inhibitor cucurbitacins in solid tumors. *International journal of pharmaceutics* **2008,** *347* (1), 118-127.

20. Doskotch, R. W.; Hufford, C. D. J. C. J. o. C., Hexanor–cucurbitacin D, a degraded cucurbitacin from Begonia tuberhybrida var. alba. **1970,** *48* (11), 1787-1788.

21. Chawech, R.; Jarraya, R.; Girardi, C.; Vansteelandt, M.; Marti, G.; Nasri, I.; Racaud-Sultan, C.; Fabre, N. J. M., Cucurbitacins from the leaves of Citrullus colocynthis (L.) Schrad. **2015,** *20* (10), 18001-18015.

22. Bernard, S. A.; Olayinka, O. A., Search for a novel antioxidant, anti-inflammatory/analgesic or anti-proliferative drug: Cucurbitacins hold the ace. *Journal of Medicinal Plants Research* **2010,** *4* (25), 2821-2826.

23. Alghasham, A. A. J. I. j. o. h. s., Cucurbitacins–a promising target for cancer therapy. **2013,** *7* (1), 77.

24. Zhou, Y.; Ma, Y.; Zeng, J.; Duan, L.; Xue, X.; Wang, H.; Lin, T.; Liu, Z.; Zeng, K.; Zhong, Y. J. N. p., Convergence and divergence of bitterness biosynthesis and regulation in Cucurbitaceae. **2016,** *2* (12), 16183.

25. Kaushik, U.; Aeri, V.; Mir, S. R. J. P. r., Cucurbitacins–an insight into medicinal leads from nature. **2015,** *9* (17), 12.

26. Alsayari, A. S., Anticancer and Antiviral Activities of Cucurbitacins Isolated From Cucumis Prophetarum var. Prophetarum Growing in the Southwestern Region of Saudi Arabia. **2014**.

27. Willoughby, D. A.; Moore, A. R.; Colville-Nash, P. R. J. T. L., COX-1, COX-2, and COX-3 and the future treatment of chronic inflammatory disease. **2000,** *355* (9204), 646-648.

28. Recio, M. C.; Prieto, M.; Bonucelli, M.; Orsi, C.; Máñez, S.; Giner, R. M.; Cerda-Nicolas, M.; Ríos, J.-L., Anti-inflammatory activity of two cucurbitacins isolated from Cayaponia tayuya roots. *Planta medica* **2004,** *70* (05), 414-420.

29. Wang, Y.; Zhao, G.-X.; Xu, L.-H.; Liu, K.-P.; Pan, H.; He, J.; Cai, J.-Y.; Ouyang, D.-Y.; He, X.-H. J. P. o., Cucurbitacin IIb exhibits anti-inflammatory activity through modulating multiple cellular behaviors of mouse lymphocytes. **2014,** *9* (2), e89751.

30. Hassan, S.; Berchová-Bímová, K.; Petráš, J.; Hassan, K. J. S. A. J. o. B., Cucurbitacin B interacts synergistically with antibiotics against Staphylococcus aureus clinical isolates and exhibits antiviral activity against HSV-1. **2017,** *108*, 90-94.

31. Cai, Y.; Fang, X.; He, C.; Li, P.; Xiao, F.; Wang, Y.; Chen, M. J. T. A. j. o. C. m., Cucurbitacins: A systematic review of the phytochemistry and anticancer activity. **2015,** *43* (07), 1331-1350.

32. Zhou, J.; Zhao, T.; Ma, L.; Liang, M.; Guo, Y.-J.; Zhao, L.-M. J. O., Cucurbitacin B and SCH772984 exhibit synergistic anti-pancreatic cancer activities by suppressing EGFR, PI3K/Akt/mTOR, STAT3 and ERK signaling. **2017,** *8* (61), 103167.

33. Herbst, R. S. J. I. J. o. R. O. B. P., Review of epidermal growth factor receptor biology. **2004,** *59* (2), S21-S26.

34. Seshacharyulu, P.; Ponnusamy, M. P.; Haridas, D.; Jain, M.; Ganti, A. K.; Batra, S. K. J. E. o. o. t. t., Targeting the EGFR signaling pathway in cancer therapy. **2012,** *16* (1), 15-31.

35. Yuan, Z.-l.; Guan, Y.-j.; Wang, L.; Wei, W.; Kane, A. B.; Chin, Y. E. J. M.; biology, c., Central role of the threonine residue within the p+ 1 loop of receptor tyrosine kinase in STAT3 constitutive phosphorylation in metastatic cancer cells. **2004,** *24* (21), 9390-9400.

36. Alsayari, A.; Halaweish, F. T.; Gurusamy, N. J. P. R., The role of cucurbitacins in combating cancers: A mechanistic review. **2018,** *12* (24), 157.

37. Wang, X.; Tanaka, M.; Peixoto, H. S.; Wink, M. J. P., Cucurbitacins: Elucidation of their interactions with the cytoskeleton. **2017,** *5*, e3357.

38. Matsuda, H.; Nakashima, S.; Abdel-Halim, O. B.; Morikawa, T.; Yoshikawa, M., Cucurbitane-type triterpenes with anti-proliferative effects on U937 cells from an egyptian natural medicine, Bryonia cretica: structures of new triterpene glycosides, bryoniaosides A and B. *Chemical and Pharmaceutical Bulletin* **2010,** *58* (5), 747-751.

39. Liu, F.; Yang, X.; Geng, M.; Huang, M. J. A. p. s. B., Targeting ERK, an Achilles' Heel of the MAPK pathway, in cancer therapy. **2018**.

40. Olayioye, M. A.; Neve, R. M.; Lane, H. A.; Hynes, N. E. J. T. E. j., The ErbB signaling network: receptor heterodimerization in development and cancer. **2000,** *19* (13), 3159-3167.

41. Gullick, W. J. J. E.-R. C., The Type 1 growth factor receptors and their ligands considered as a complex system. **2001,** *8* (2), 75-82.

42. Llovet, J. M.; Bruix, J., Molecular targeted therapies in hepatocellular carcinoma. *Hepatology* **2008,** *48* (4), 1312-1327.

43. Malumbres, M.; Barbacid, M. J. N. R. C., RAS oncogenes: the first 30 years. **2003,** *3* (6), 459.

44. Vetter, I. R.; Wittinghofer, A. J. S., The guanine nucleotide-binding switch in three dimensions. **2001,** *294* (5545), 1299-1304.

45. Prior, I. A.; Lewis, P. D.; Mattos, C. J. C. r., A comprehensive survey of Ras mutations in cancer. **2012,** *72* (10), 2457-2467.

46. National Cancer Institute, N., RAS and MYC: Co-conspirators in Cancer. **2017**, https://www.cancer.gov/research/key-initiatives/ras/ras-central/blog/2017/myc-ras.

47. Shukla, S.; Khan, S.; Kumar, S.; Sinha, S.; Farhan, M.; Bora, H. K.; Maurya, R.; Meeran, S. M. J. C. p. r., Cucurbitacin B alters the expression of tumor-related genes by epigenetic modifications in NSCLC and inhibits NNK-induced lung tumorigenesis. **2015**, canprevres. 0286.2014.

48. Roskoski Jr, R. J. B.; communications, b. r., RAF protein-serine/threonine kinases: structure and regulation. **2010,** *399* (3), 313-317.

49. Johnson, G. L.; Lapadat, R. J. S., Mitogen-activated protein kinase pathways mediated by ERK, JNK, and p38 protein kinases. **2002,** *298* (5600), 1911-1912.

50. Gentry, L.; Samatar, A. A.; Der, C. J., Inhibitors of the ERK mitogen-activated protein kinase cascade for targeting RAS mutant cancers. In *The Enzymes*, Elsevier: 2013; Vol. 34, pp 67-106.

51. Stricker, J.; Falzone, T.; Gardel, M. L. J. J. o. b., Mechanics of the F-actin cytoskeleton. **2010,** *43* (1), 9-14.

52. Sörensen, P. M.; Iacob, R. E.; Fritzsche, M.; Engen, J. R.; Brieher, W. M.; Charras, G.; Eggert, U. S., The natural product cucurbitacin E inhibits depolymerization of actin filaments. *ACS chemical biology* **2012,** *7* (9), 1502-1508.

53. Duncan, K. L.; Duncan, M. D.; Alley, M. C.; Sausville, E. A., Cucurbitacin E-induced disruption of the actin and vimentin cytoskeleton in prostate carcinoma cells. *Biochemical pharmacology* **1996,** *52* (10), 1553-1560.

54. Siveen, K. S.; Sikka, S.; Surana, R.; Dai, X.; Zhang, J.; Kumar, A. P.; Tan, B. K.; Sethi, G.; Bishayee, A. J. B. e. B. A.-r. o. c., Targeting the STAT3 signaling pathway in cancer: role of synthetic and natural inhibitors. **2014,** *1845* (2), 136-154.

55. Hirano, T.; Ishihara, K.; Hibi, M. J. O., Roles of STAT3 in mediating the cell growth, differentiation and survival signals relayed through the IL-6 family of cytokine receptors. **2000,** *19* (21), 2548.

56. Greaves, M.; Maley, C. C. J. N., Clonal evolution in cancer. **2012,** *481* (7381), 306.

57. Ilic, M.; Ilic, I. J. W. j. o. g., Epidemiology of pancreatic cancer. **2016,** *22* (44), 9694.

58. Bockman, D. E. J. T. e. p. b., pathobiology; disease. Raven Press, N. Y., Anatomy of the pancreas. **1993**, 1-8.

59. Hidalgo, M. J. N. E. J. o. M., Pancreatic cancer. **2010,** *362* (17), 1605-1617.

60. Society, A. C., What Is Pancreatic Cancer? **2016**, https://www.cancer.org/cancer/pancreatic-cancer/about/what-is-pancreatic-cancer.html.

61. Malvezzi, M.; Carioli, G.; Bertuccio, P.; Boffetta, P.; Levi, F.; La Vecchia, C.; Negri, E. J. A. o. O., European cancer mortality predictions for the year 2017, with focus on lung cancer. **2017,** *28* (5), 1117-1123.

62. Strimpakos, A.; Saif, M. W.; Syrigos, K. N. J. C.; Reviews, M., Pancreatic cancer: from molecular pathogenesis to targeted therapy. **2008,** *27* (3), 495-522.

63. Siegel, R. L.; Miller, K. D.; Jemal, A. J. C. a. c. j. f. c., Cancer statistics, 2017. **2017,** *67* (1), 7-30.

64. Siegel, R. L.; Miller, K. D.; Jemal, A. J. C. a. c. j. f. c., Cancer statistics, 2015. **2015,** *65* (1), 5-29.

65. National Cancer Institute, N., Pancreatic Cancer Treatment (PDQ®)–Patient Version. **2018**, https://www.cancer.gov/types/pancreatic/patient/pancreatic-treatment-pdq.

66. Yachida, S.; Jones, S.; Bozic, I.; Antal, T.; Leary, R.; Fu, B.; Kamiyama, M.; Hruban, R. H.; Eshleman, J. R.; Nowak, M. A. J. N., Distant metastasis occurs late during the genetic evolution of pancreatic cancer. **2010,** *467* (7319), 1114.

67. Makohon-Moore, A.; Iacobuzio-Donahue, C. A. J. N. r. C., Pancreatic cancer biology and genetics from an evolutionary perspective. **2016,** *16* (9), 553.

68. Biankin, A. V.; Waddell, N.; Kassahn, K. S.; Gingras, M.-C.; Muthuswamy, L. B.; Johns, A. L.; Miller, D. K.; Wilson, P. J.; Patch, A.-M.; Wu, J. J. N., Pancreatic cancer genomes reveal aberrations in axon guidance pathway genes. **2012,** *491* (7424), 399.

69. Yachida, S.; White, C.; Naito, Y.; Zhong, Y.; Brosnan, J. A.; Macgregor-Das, A. M.; Morgan, R. A.; Saunders, T.; Laheru, D.; Herman, J. M. J. C. C. R., Clinical significance of the genetic landscape of pancreatic cancer and implications for identification of potential long term survivors. **2012**, clincanres. 1215.2012.

70. Zhang, X.; Shi, S.; Zhang, B.; Ni, Q.; Yu, X.; Xu, J. J. A. j. o. c. r., Circulating biomarkers for early diagnosis of pancreatic cancer: facts and hopes. **2018,** *8* (3), 332.

71. Goess, R.; Friess, H. J. E. r. o. a. t., A look at the progress of treating pancreatic cancer over the past 20 years. **2018,** *18* (3), 295-304.

72. Beger, H. G.; Rau, B.; Gansauge, F.; Poch, B.; Link, K.-H. J. W. j. o. s., Treatment of pancreatic cancer: challenge of the facts. **2003,** *27* (10), 1075-1084.

73. Yeo, C. J.; Cameron, J. L.; Lillemoe, K. D.; Sohn, T. A.; Campbell, K. A.; Sauter, P. K.; Coleman, J.; Abrams, R. A.; Hruban, R. H. J. A. o. s., Pancreaticoduodenectomy with or without distal gastrectomy and extended retroperitoneal lymphadenectomy for periampullary adenocarcinoma, part 2: randomized controlled trial evaluating survival, morbidity, and mortality. **2002,** *236* (3), 355.

74. Moghanaki, D. J. C., Further evidence of effective adjuvant combined radiation and chemotherapy following curative resection of pancreatic cancer. Gastrointestinal Tumor Study Group. **1987,** *59*, 2006-10.

75. Colucci, G.; Labianca, R.; Di Costanzo, F.; Gebbia, V.; Cartenì, G.; Massidda, B.; Dapretto, E.; Manzione, L.; Piazza, E.; Sannicolo, M. J. J. o. C. O., Randomized phase III trial of gemcitabine plus cisplatin compared with single-agent gemcitabine as first-line treatment of patients with advanced pancreatic cancer: the GIP-1 study. **2010,** *28* (10), 1645-1651.

76. Burris, H. r.; Moore, M. J.; Andersen, J.; Green, M. R.; Rothenberg, M. L.; Modiano, M. R.; Christine Cripps, M.; Portenoy, R. K.; Storniolo, A. M.; Tarassoff, P. J. J. o. c. o., Improvements in survival and clinical benefit with gemcitabine as first-line therapy for patients with advanced pancreas cancer: a randomized trial. **1997,** *15* (6), 2403-2413.

77. Colucci, G.; Giuliani, F.; Gebbia, V.; Biglietto, M.; Rabitti, P.; Uomo, G.; Cigolari, S.; Testa, A.; Maiello, E.; Lopez, M. J. C., Gemcitabine alone or with cisplatin for the treatment of patients with locally advanced and/or metastatic pancreatic

carcinoma: A prospective, randomized phase III study of the Gruppo Oncologico dell'Italia Meridionale. **2002,** *94* (4), 902-910.

78. de Sousa Cavalcante, L.; Monteiro, G. J. E. j. o. p., Gemcitabine: metabolism and molecular mechanisms of action, sensitivity and chemoresistance in pancreatic cancer. **2014,** *741*, 8-16.

79. Gilbert, J. A.; Salavaggione, O. E.; Ji, Y.; Pelleymounter, L. L.; Eckloff, B. W.; Wieben, E. D.; Ames, M. M.; Weinshilboum, R. M. J. C. C. R., Gemcitabine pharmacogenomics: cytidine deaminase and deoxycytidylate deaminase gene resequencing and functional genomics. **2006,** *12* (6), 1794-1803.

80. Chen, J. C.; Chiu, M. H.; Nie, R. L.; Cordell, G. A.; Qiu, S. X. J. N. p. r., Cucurbitacins and cucurbitane glycosides: structures and biological activities. **2005,** *22* (3), 386-399.

81. Chen, X.; Bao, J.; Guo, J.; Ding, Q.; Lu, J.; Huang, M.; Wang, Y., Biological activities and potential molecular targets of cucurbitacins: a focus on cancer. *Anti-cancer drugs* **2012,** *23* (8), 777-787.

82. Jung, M. E.; Lui, R. M. J. T. J. o. o. c., Studies toward the Total Syntheses of Cucurbitacins B and D. **2010,** *75* (21), 7146-7158.

83. Lang, K. L.; Silva, I. T.; Zimmermann, L. A.; Machado, V. R.; Teixeira, M. R.; Lapuh, M. I.; Galetti, M. A.; Palermo, J. A.; Cabrera, G. M.; Bernardes, L. S. C. J. B.; chemistry, m., Synthesis and cytotoxic activity evaluation of dihydrocucurbitacin B and cucurbitacin B derivatives. **2012,** *20* (9), 3016-3030.

84. Ahmed, M. S.; El-Senduny, F.; Taylor, J.; Halaweish, F. T. J. C. b.; design, d., Biological screening of cucurbitacin inspired estrone analogs targeting mitogen-activated protein kinase (MAPK) pathway. **2017,** *90* (3), 478-484.

85. Ahmed, M. S.; Kopel, L. C.; Halaweish, F. T. J. C., Structural Optimization and Biological Screening of a Steroidal Scaffold Possessing Cucurbitacin-Like Functionalities as B-Raf Inhibitors. **2014,** *9* (7), 1361-1367.

86. Mahnashi, M. H., Design, Synthesis and Biological Screening of Novel Cucsinspired Estrone Analogues Towards Treatment of Hepatocellular Carcinoma. **2017**.

87. Achenbach, H.; Hefter-Bübl, U.; Constenla, M. A., Fevicordin A and fevicordin A glucoside, novel norcucurbitacins from Fevillea cordifolia. *Journal of the Chemical Society, Chemical Communications* **1987,** (6), 441-442.

88. Valente, L. M.; Gunatilaka, A. L.; Glass, T. E.; Kingston, D. G.; Pinto, A. C., New norcucurbitacin and heptanorcucurbitacin glucosides from Fevillea trilobata. *Journal of natural products* **1993,** *56* (10), 1772-1778.

Chapter two

Molecular Modeling of Novel Cucurbitacin-Inspired Estrone Analogs Against Molecular Targets of Pancreatic Adenocarcinoma

2.1. Introduction

Computer-based drug design is one of the fundamental tools in modern drug discovery due to the time, effort and cost minimization facilitated by computational drug design programs.[1] The main purpose of the docking study is to predict the binding of a ligand towards an active site of a molecular target based on the most stable conformer of a designed ligand and a 3-D structure of a crystalized molecular target using a computational docking tool.[2]

There are many approaches in drug discovery focusing in investigation for novel potent drugs. Among these approaches is pharmacophore approach which include linking the active pharmacophores in small molecules to result in one entity that have most or similar potency to that of the parent molecule.[3] Based on the kind of the modification, two strategies are adopted in pharmacophore approach.[4] The first approach where the modification of the ligand is hypothesized based on the active compound and is called ligand-based approach. On the other hand, the receptor-based modification utilize the binding pocket for the agonist and the antagonist in order to modify novel ligands.[4] However, each strategy has its challenges and drawbacks. For example, ligand flexibility represents a challenge in ligand-based drug discovery because based on the predicted conformation the molecular docking against the target pocket will be conducted. In order to minimize the error caused by the variations exist in 3D conformation prediction, two

strategies have been used. The first strategy is creating different conformers of each ligand and screen them against the target pocket or conducting an extensive modeling process to each ligand to calculate the most stable conformer against specific pocket which is time consuming.[5] One of the challenges that limit the use of receptor-based drug discovery approach is availability of 3D structure of the macromolecule crystallized with its ligand which is fundamental to build the modified ligands based on the features of the original ligand and the arrangement of the amino acids in the binding pocket.[5]

An example of a drug developed using computational drug design is the development of carbonic anhydrase II inhibitor, dozolamide that is used for treatment of glaucoma. Based on cone-shape pocket of X-ray crystallography of carbonic anhydrase II, dorzolamide was developed by introducing sulfamoyl moiety that show a significant coordination with zinc.[6]

Another example of rational drug design is neuraminidase (NA) enzymes inhibitors used as antiviral agents. NA enzymes are essential macromolecules of influenza virus envelops that catalyze the breakdown of glycosidic linkage between the virus sialic acid and hemagglutinin residues and the host cell wall followed by spreading the virus all around the body. Inhibition of this enzyme will restrict the virus and force it to remain connected to the cells and prevent its spread.[95] After reporting the crystal structure of neuraminidase II, antiviral agents were developed based on the conservative sites in NA II enzyme using GRID software and utilizing NA II inhibitor 2-deoxy-2, 3-dehydro-*N*-acetylneuraminic acid (DANA). Subsituting 4-hydroxy group in DANA with amine led to a potent inhibitor for NA which was called zanamivir.[8]

Nolatrexed dihydrochloride is a phase I anticancer agent showed anticancer activity against hepatocellular carcinoma was developed based on the crystal structure of *E.coli* thymidylate synthase that catalyze the conversion of deoxyuridine monophosphate to deoxy thymidylate by methylation and reduction of thymidyl ring which is an essential in DNA synthesis.[8, 9]

Molecular modeling programs are used in many aspects to improve drug design including pharmacodynamics data such as potency, affinity, and efficacy along with pharmacokinetic properties, which are absorption, distribution, metabolism, and excretion which lead eventually to structure activity relationship (SAR) for different groups of compounds.[1] Generally, there are three main approaches of conducting molecular dockings including flexible ligand docking where the molecular target is rigid and a library of different conformers of ligands are docked against that rigid target. In rigid docking, both the target and ligands are rigid molecules which is opposite to the flexible docking where both the screened ligands and the target molecules are flexible.[10] The molecular modeling that we utilized in our investigation is a semiflexible modeling, meaning that the pocket of the molecule is fixed while different conformers of the designed compound that were designed using ChemBio3D Ultra 12.0 [11] are screened against the pocket of the protein that was downloaded from protein data bank[12] and processed using Make Receptor® software. This approach led to decrease the cost and effort of the medicinal chemists in drug discovery and result in increasing discovery of huge number of small molecules to be used pharmacologically in treatment of different diseases.[2]

OpenEye® Scientific Software is one of the molecular docking software that uses FRED software which docks multi-conformers database of molecules against a putative binding

pocket of a rigid receptor using exhaustive search algorithm.[13] Our molecular modeling studies was carried out using two OpenEye Softwares, (Omega) that generates the conformers of the compounds and rigid exhaustive docking (FRED). The targets for the previously mentioned proteins were processed and generated using Make Receptor® software.

ChemBio3D Ultra 12.0 utilizes two force fields to predict the bond angles, MM2 and MMFF94, where the later uses different equations to estimate the intramolecular Van der Waals interactions and contain more parameters.[14] Calculating the most minimized form of the compound based on its total energy is conducted following the equation:

$$\text{Esteric energy} = \text{Estr} + \text{Ebend} + \text{Estr-bend} + \text{Eoop} + \text{Etor} + \text{EVdW} + \text{Eqq}$$

Where Estr is the energy needed to stretch or compress the bond between two atoms and Ebend is the energy required to bend a bond from its equilibrium angle, θ^o. Estr is the energy needed to stretch or compress the bond when the bond is bent because the energy required at this case is affected by that bent. Eoop estimates the energy required for an atom to move of that angle of planar plane. While Eoop is used with the atoms that form planar geometry such as in sp^2 hybridized carbons and is called improper torsion, Etor is used to calculate the energy required to torsion rotate bonds, which means that this calculation is used in single bonds but not the double or the triple rigid bonds. EVdW and Eqq are the two interactions that exists between the non-bonded atoms and are important in the formation of the molecule geometry. Eqq are the electrostatic energy which exists when there are polar or partial electrostatic charges bonds in the molecule.[14] The main difference between MM2 (2^{nd} generation Molecular Mechanics) and MMFF94 (Merck

Molecular Force Field) is that the constants used to predict EVdW in MM2 are derived from hydrocarbons and is not reliable in calculating the field force for the compounds that contain oxygen or in compounds containing nitrogen or sulfur.[14]

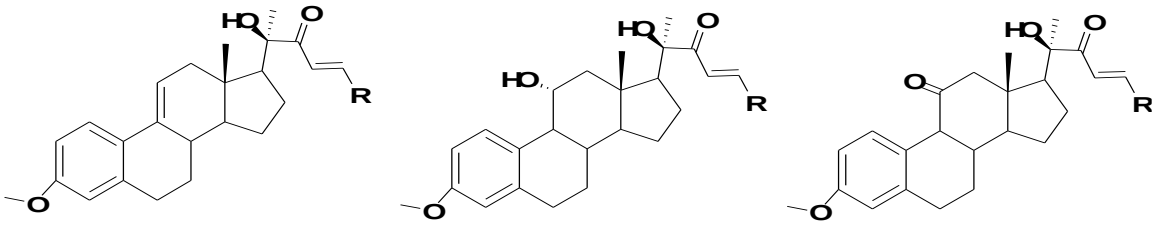

Figure 2.1. The promising C_{11} functionalized CIE analogs.

Previously, utilizing OpenEye® Scientific Software we developed a molecular-modeling strategy to design hybrid antiproliferative compounds consists of estrone as a carrier and cucurbitacin main pharmacophore 23, 24 α, β- unsaturated ketone side chain that is responsible for its anticancer activity. Based on cell viability assays, Cucurbitacin-Inspired Estrone compounds were found to have anticancer activity comparable to that of cucurbitacins.[15] Following that, several modifications have been conducted on these compounds led to increase the antiproliferative potency dramatically against many cancer cell lines. These modifications include dehydrogenation of C_9-C_{11} in ring C, and C_{16}-C_{17} in ring D, [16] and modifications in ring A including methylation, sulfamoylation and the nitric oxide releasing moiety furoxan at C_3 which was proofed to have promising antiproliferative activity against hepatocellular carcinoma.[17,18] The other modifications include introducing of many 23, 24 α, β- unsaturated ketone side chains other that of

cucurbitacin side chain through aldol condensation such as *para*-trifluoromethyl, which dramatically increased the anticancer potency.

These results inspired us to investigate more for novel cucurbitacin-inspired estrone (CIE) analogs modified at C_{11} on ring C of CIE analogs in order to develop more potent antiproliferative compounds. In this study different functional groups were introduced virtually to C_{11} of CIE analogs including halogens, hydroxyl, ketone, amine, amide, ethers, hydrazine, and methyl ketone functional groups. Our molecular-docking study demonstrates that there are three promising functional groups have high calculated affinity to pancreatic ductal adenocarcinoma targets such as EGFR, Erk, STAT3, and JAKI. These modifications include dehydrogenation of C_9-C_{11} in ring C that showed cucurbitacin-like conformation upon docking in Erk active pocket. Another modifications include introducing hydroxyl and ketone groups at C_{11} which show low consensus scores upon docking to EGFR ATP binding site.

2.2. Results and Discussions

More than 400 analogs were generated using Chem3D with different functional groups at rings A, D, and ring C at C_{11} in order to investigate for the effect of functionalization of ring C in binding affinity calculations. Previously, our molecular modeling studies and the biological evaluation of CIE analogs indicated that the functionalization of ring C can lead to increase in the anticancer activity on melanoma cancer cells.[7]

In order to conduct the molecular modeling study, each designed virtual compound was energy minimized using MMFF94 application to calculate the most stable conformer. The target proteins were downloaded from protein data bank using the following codes from

the protein data bank (PDB) database (EGFR PDB ID # 1M17, STAT3 PDB ID # 4ZIA, 3LJ2, RAF PDB ID # 3OMV, MAPK PDB ID # 2YO8, RAS PDB ID # 4DTS, ERK PDB ID # 2OJJ, Akt PDB ID # 3MV5, PI3K PDB ID # 3L54)

The processing of the proteins was achieved by selecting the required pockets with the crystalized original ligand followed by removing of the water molecules and determining the margins of the box where it contains the pocket where the designed compounds will be screened against. In order to conduct the docking experiment, the designed compounds must be compiled onto one file which is achieved by the required command according to OPENEYE® instruction manual.101 The file after that was converted into the required OEB format using OMEGA® software (one of included softwares). FRED® software conduct the exhaustive molecular docking using the required command and VIDA is used to analyze the final results where the tested ligands are arranged from the ligand that has the highest affinity or the lower consensus score followed by the lower affinity, while the compounds that cannot be fitted in the pocket are excluded. The scoring function that are mathematical calculations used to predict the binding affinity of the pocket toward certain molecule are different from software to another. Generally, the binding affinity are calculated by different functions which calculate the difference the total energy of the protein-ligand complex and the free energy of each of the compound and the protein separately. The scoring functions initially was optimized based on the known ligand erlotinib that was crystalized with EGFR ATP binding pocket. Using the following scoring functions shapegauss, chemgauss3, oechemscore, screenscore and PLP optimization of the docking for erlotinib in its binding pocket was conducted and compared to the published data. These scoring functions differ from each other in certain functions while they are

similar in some. **Table 2.1** indicates the various intermolecular interactions that the scoring functions available in FRED® use to rank the compounds during the docking experiment. The used scoring functions differ in the used parameters to rank the compounds. For example, screenscore and PLP scoring functions show similar parameters which indicate that their results are close to each other, while Chemgauss3 is assumed to calculate different results due to the presence of the algorithm of desolvation calculation. [16] Based on these values, VIDA rank the compounds using the consensus score which represents the total energy difference of the complex compared to the binding free energy of the protein and ligand before binding. The negative free energy is preferable because it means that the protein has a good affinity to the binding pocket of the protein.

After conducting the molecular docking against EGFR, we used the reported data for erlotinib on its crystallization with EGFR that is available in protein data bank to confirm the validity of the docking study where it has a hydrogen bonding with methionine MET:769: A as it has been reported (**figure 2.2**).

Molecular modeling results against EGFR, JAK, STAT3, Raf, Ras, Erk, Akt and PI3K proteins, indicate that the dehydrogenation of C_9 and C_{11} and introducing of hydroxyl, carbonyl functional groups at C_{11} with methylation of ring A at C_3 lead to high consensus scores compared to erlotinib cucurbitacin B, and D which were used as standards for the molecular docking. introducing of hydroxyl, carbonyl functional groups at C_{11} with methylation of ring A at C_3 Show promising virtual binding affinity towards molecular targets such as EGFR and STAT3, while dehydrogenation of C_9 and C_{11} showed a better binding affinity to ERK binding pocket compared to the C-11 functionalized analogs (**Figure 2.1**).

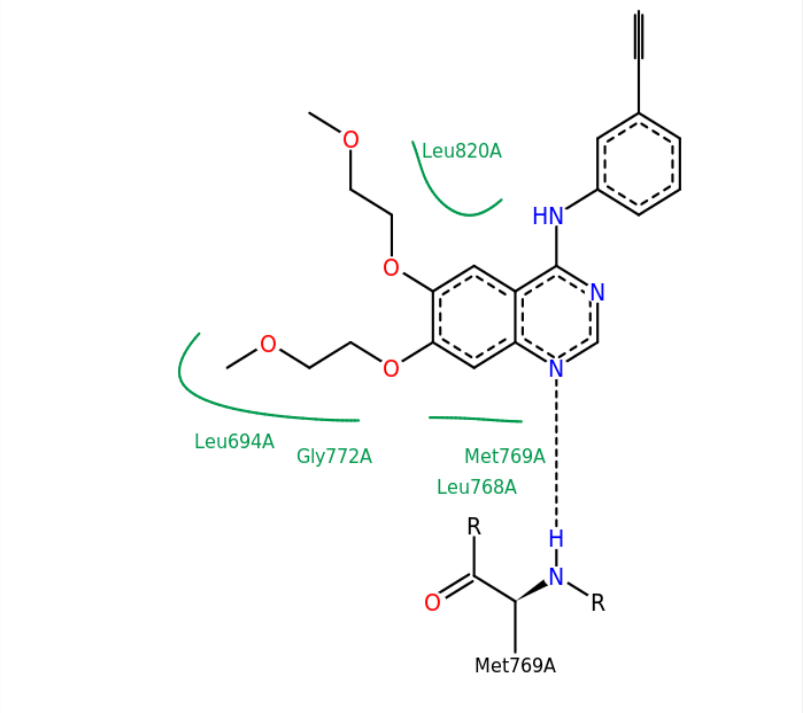

A. A diagram indicates the amino acid binding to erlotinib through hydrogen bonding.

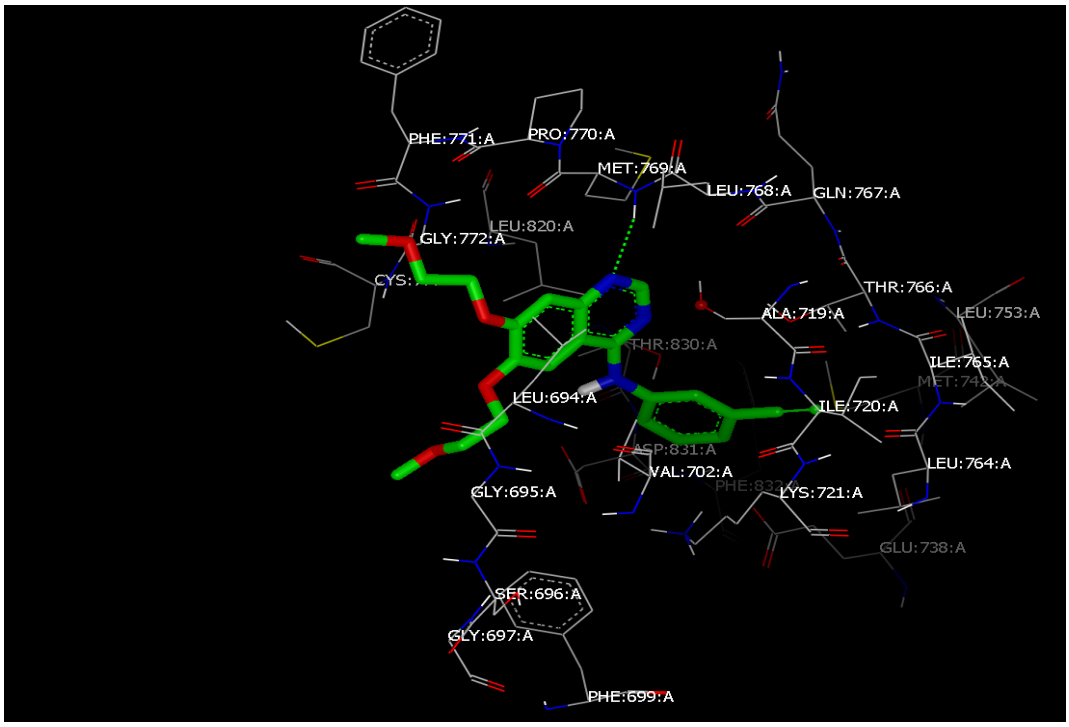

B. Docking of erlotinib to ATP binding site of EGFR mimic the crystallization reported data.

Figure 2.2. Comparison between the reported crystallization data and the molecular modeling results for erlotinib in EGFR validate the conducted molecular docking experiment and the used docking scores.

Table 2.1. The interactions that scoring functions of FRED® calculate.[16]

Scoring Function	Shape	H Bonds	Metal	Aromatic	Desolvation
Shapegauss	Yes	No	No	No	No
Chemgauss3	Yes	Yes	Yes	No	Yes
Chemscore	Yes	Yes	Yes	No	No
Screenscore	Yes	Yes	Yes	No	No
PLP	Yes	Yes	Yes	No	No

The molecular modeling study shows that most of these compounds are ranked high in other molecular targets that are inhibited by previously synthesized CIE analogs such as ERK.

The molecular docking experiment indicate that there are 3 set of compounds functionalized at C_{11} CIE. The first group of compounds which include KA20, KA22, KA19, KA23, and KA21 are dehydrogenated at C_9 and C_{11}, where the other analogs with hydroxyl group and ketone groups which show good binding affinities in ATP binding site of EGFR, while the desaturated compounds show a better binding affinity to ERK biding pocket.

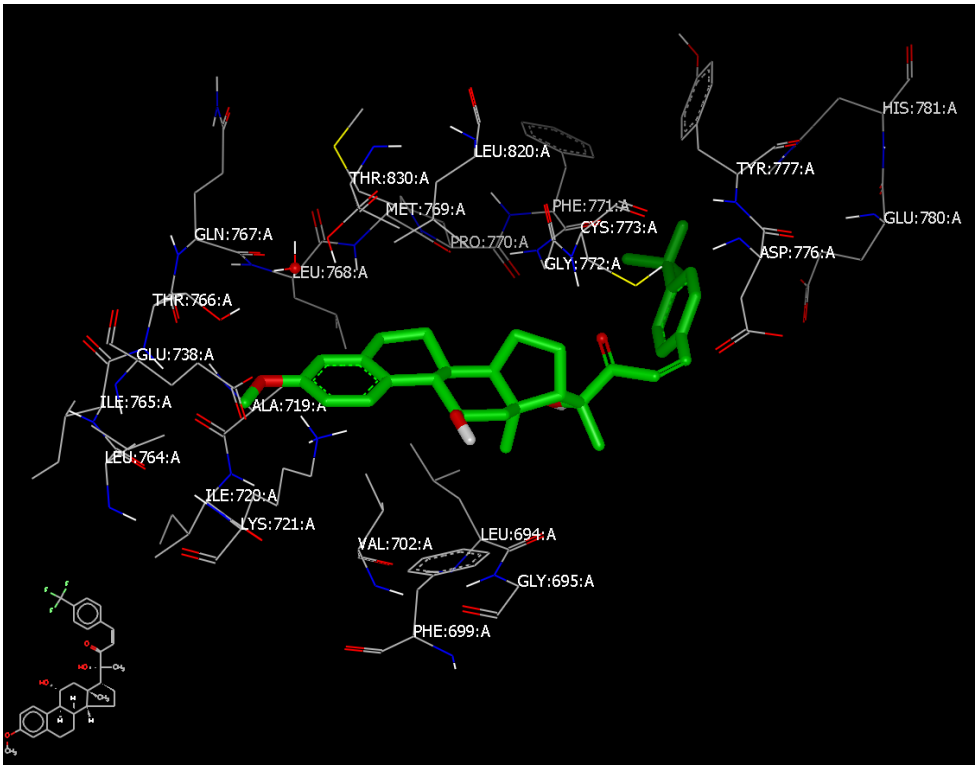

A. The docking of KA2 in ATP binding site of EGFR.

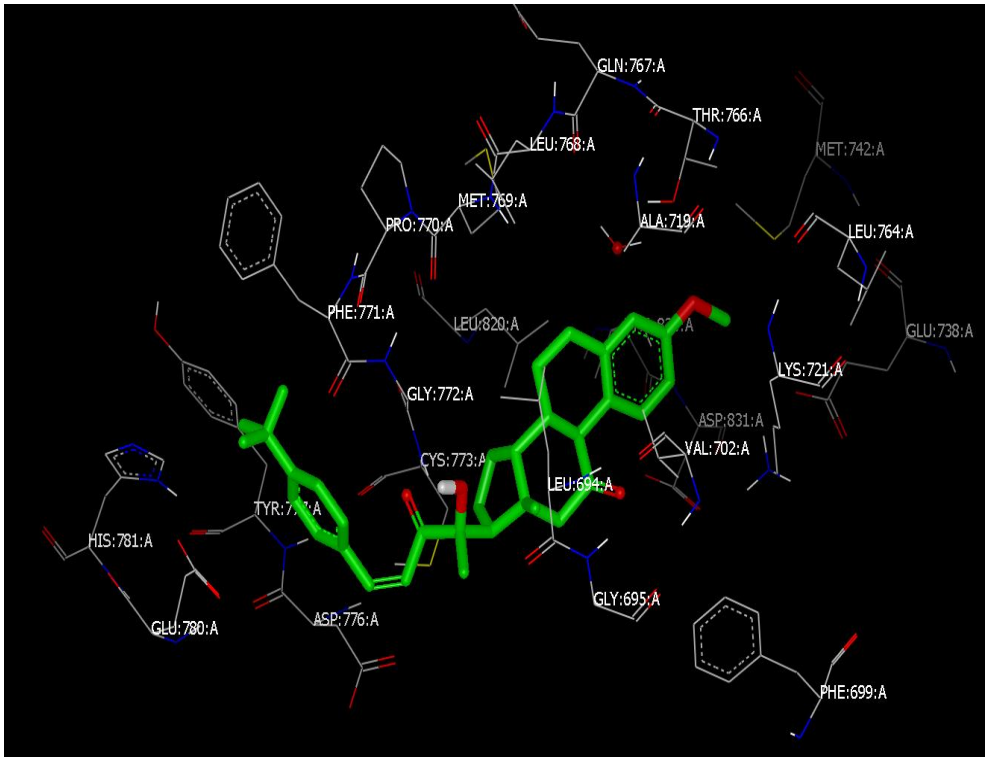

B. The binding of KA9 in ATP Binding pocket of EGFR.

Figure 2.3. The binding of KA2 and KA9 in ATP binding site of EGFR.

An example of C_{11}-hydroxyl compounds are KA1 and KA2, containing *para*-trifluoromethyl and cucurbitacin side chains, respectively, which show high binding affinities toward ATP binding site of EGFR binding pocket (Figure 2.3A and 2.4). KA2 shows a hydrogen bonding with proline 770 in chain A of EGFR which occurs with the hydroxyl group of the side chain.

Generally, *para*-trifluoro side chain indicate a good binding affinity such as KA1 and KA9 with C_{11} hydroxyl and ketone, respectively as it is indicated in **Figure 2.3**.

From the indicated results, the docking profiles of the two compounds are close to each other; however, KA9 show a better fitting in the pocket compared KA1 which show a space between the compound and the amino acids.

One the other hand the third modification that show constant pattern is the desaturated C_9-C_{11} compounds where they score better than the other compounds including C_{11} oxygenated-CIE analogs in Erk and RAS proteins which indicate the importance of this modification to be investigated more by modifying it with different side chains. In terms of functional groups, hydroxyl group containing compounds score more higher than the compounds desaturated at C_9 and C_{11} and C_{11}-ketone containing analogs.

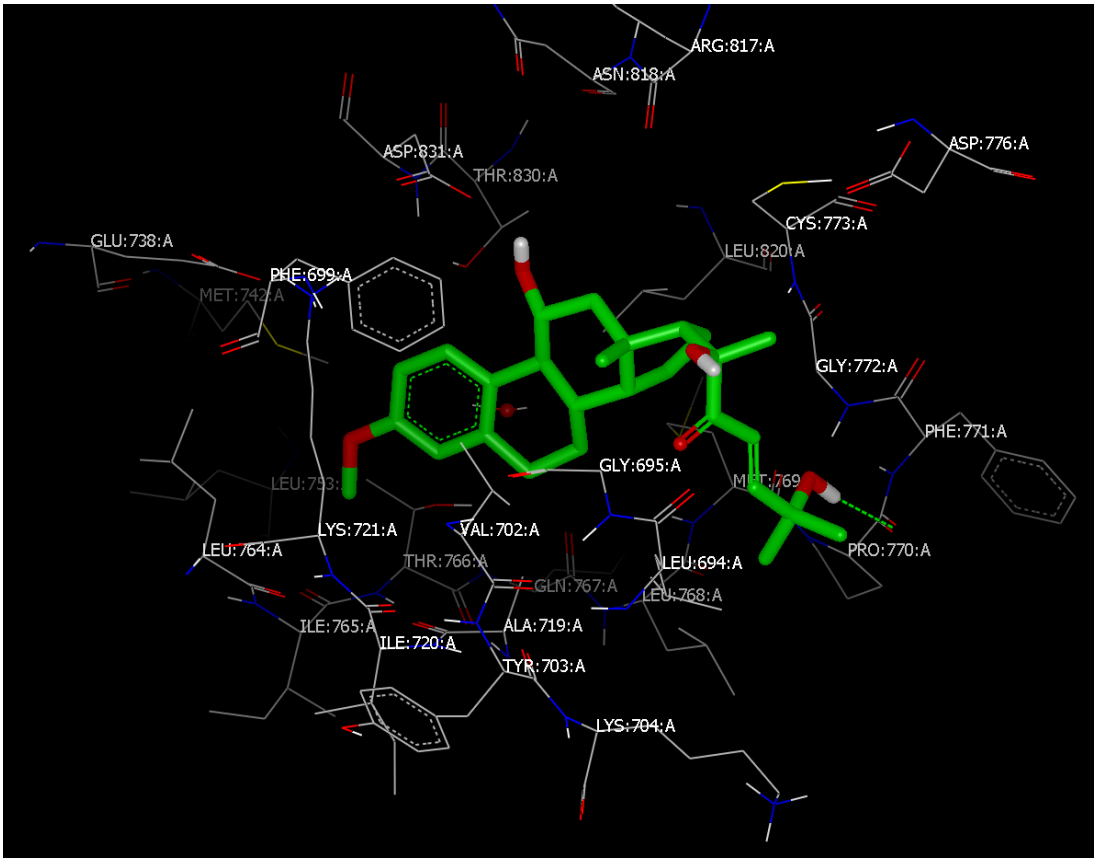

Figure 2.4. The hydrogen bonding of hydroxyl group of isopropyl alcohol side chain of KA2 to proline 770: A in ATP binding site of EGFR.

The docking results of the same library against ERK binding pocket indicate the importance of the double bond introduced in C_9 and C_{11} which lead to change the conformation of the whole molecule to adopt the structure of cucurbitacin D as indicated from **figure 2.5** (A and B). For example, phenyl *para*-nitro side chain adopts the similar binding conformation of cuc D in ERK binding pocket as it was indicated previously. This conformation is one of the modifications that led to increase the calculated binding affinity of CIE analogs in Erk binding pocket.

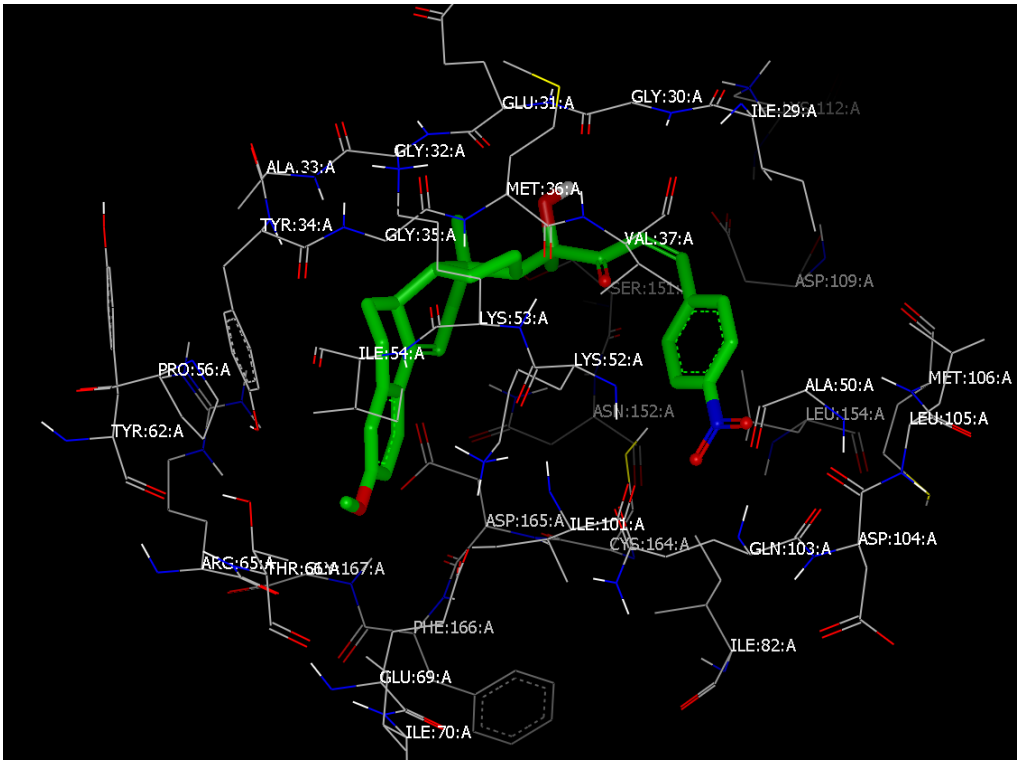

A. The curve-like structure of KA19 in ERK binding pocket.

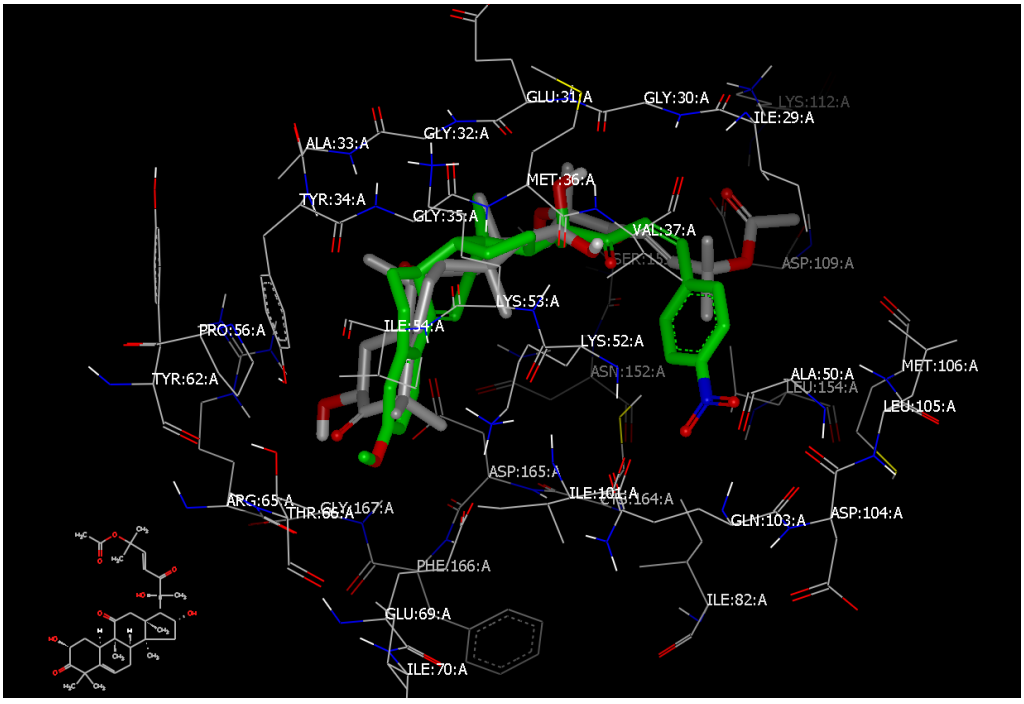

B. Similarity of KA19 with cuc D structure in fitting into ERK binding pocket.

Figure 2.5. The similarity of KA19 and cuc D binding in ERK pocket.

Table 2.2. The consensus scores obtained from VIDA software for the virtually designed CIE analogs docked in different potential molecular targets.

VIDA Name	EGFR	STAT3	RAF	RAS	ERK	PI3K
KA9_57	18	0	183	59	84	41
KA13_53	25	31	97	49	82	84
KA11_43	26	19		93	28	60
KA8_153	31	13	22	56	54	55
KA3_126	32	60		35	47	87
KA6_73	35	111	150	47	50	111
KA1_72	36	79	62	77	37	72
KA7_143	37	1	162	33	37	68
KA4_156	42	61	99	82	31	53
KA14_3	51	78	53	45	98	49
KA5_62	52	23	78	74	63	84
KA12_127	54	52	50	58	72	88
KA20_31	57	75	37	14	44	123
KA22_55	59	42	15	17	17	126
KA19_112	60	42	37	9	9	17
CucD_197	67	100	99	98	106	59
Iso B_113	73	303	116	80	94	135
KA10_64	74	62	55	26	75	67
KA23_55	76	50	70	36	36	32
IsoCucD	82	100	99	108	82	96
KA21_29	83	54	252	83	7	104
Erl_38	126	63	30	100	162	89

2.3. Methods of Molecular Modeling

All computer works were conducted on Gateway Computer with Windows XP and OpenEye.[6]

2.3.1. Preparation of the virtual ligands

A virtual library of 400 CIE analogs containing 23, 24 α, β- unsaturated ketone side chain assembled in C_{17} of estrone and different functional groups at C_{11} with hydroxy-, methoxy-, at C_3 skeleton with cucurbiracins B and D and the inhibitors of the used receptors as standards were generated and energy minimized utilizing Chem3D office 2012, using MMFF94 force field function for energy minimization process in order to acquire similar structural confirmation mimic that of the existed 3-D structure adopted by the designed molecules.

The energy minimized compounds were compiled in one folder and through OMEGA software were converted from .pdb format to .oeb format which is compatible with FRED software. Omega produce different conformers of each single compound in the virtual library. Some of Omega settings were modified from the default settings such as highest number of output conformers 400 (GP-NUM-OUT-CONFS), rejecting conformers that has energy differences compare to standards minimum > 0.5 Kcal/mole (GP-ENERGY-WINDO) and choosing the conformers with lowest energy from the final calculations (GP-SELECT-RANDOM false). Furthermore, increase the number of free rotatable bonds in each ligand to be 30 (GP-MAX-ROTORS) to create different conformers for all molecules in our library.

2.3.2. Preparation of the molecular targets

Receptor preparation started by choosing the receptor of interest and processing it using make receptor application which convert the .pdb file into 3-D view of the receptor chains including its binding ligands and co-factors. Then the next step is pointing to the binding pocket that the co-crystalized ligand binds to. Then mode selection window of the application will allow the generation of the grid box which should be in specific size of 60,000 A^o or lower. However, if a large grid box needed to be form (larger than 60.000 A^o), the box can be divided to two sites, otherwise the docking process will not be conducted smoothly. Final step is specifying the pocket shape so the docking program can recognize the inner and outer contour. After conducting all the previous steps, the protein will be ready for executive molecular docking.

2.3. 3. Conducting Molecular Docking Process Using FRED

FRED program locates the 3D area where the algorithmic search conducted and recognize the possible shape for docking calculations that is called shape fitting step. The shape fitting step determines the 3D area for the ligand best binding pocket avoiding unnecessary binding with other components of the protein and at the same time reserving the area for optimal interactions. In the last step, both files of the combined ligands and the files of the prepared receptor are put into FRED to conduct the molecular docking simulations. Scoring functions perspective can be optimized by different available optimization steps including torsion optimization, rigid skeleton optimization and hydroxyl group rotamers optimization. Consensus scores of the docking study can be acquired by various scoring functions at the final stage such as shapegauss, chemgauss3, oechemscore, screenscore and PLP. All the functional commands for OpenEye® FRED can be found in electronic manual

(link www.eyesopen.com/products). 3D structure of the docked ligands with protein can be visualized utilizing OpenEye® VIDA application where 3D picture of the ligand-protein complex can be taken.

2.4. Conclusion

Theoretical modification conducted in C_{11} indicates the importance of investigation of this position experimentally. Different groups show different affinities to the MAPK signaling pathway. For instance, C_9-C_{11} unsaturated CIE analogs score better in Erk and RAS proteins compared to the other modifications. One of the important challenges in treatment of pancreatic ductal adenocarcinoma is KRAS mutation which is responsible about 90% of the resistance against gemcitabine. Moreover, Ketone containing compound KA9 is the highest scoring compound among CIE analogs in EGFR. However, the hydroxyl containing compounds generally score in all the used proteins better than any other C_{11} functionalized compounds except Erk and RAS.

2.5. References

1. Gibbs, J. B. J. S., Mechanism-based target identification and drug discovery in cancer research. **2000,** *287* (5460), 1969-1973.

2. Dar, A.; Mir, S. J. J. A. B. T., Molecular docking: approaches, types, applications and basic challenges. **2017,** *8*, 2.

3. Cui, F.; Yang, K.; Li, Y. J. P. O., Investigate the binding of catechins to trypsin using docking and molecular dynamics simulation. **2015,** *10* (5), e0125848.

4. Mills, N., ChemDraw Ultra 10.0 CambridgeSoft, 100 CambridgePark Drive, Cambridge, MA 02140. www. cambridgesoft. com. Commercial Price: 1910fordownload, 2150 for CD-ROM; Academic Price: 710fordownload, 800 for CD-ROM. ACS Publications: 2006.

5. Berman, H. M.; Westbrook, J.; Feng, Z.; Gilliland, G.; Bhat, T. N.; Weissig, H.; Shindyalov, I. N.; Bourne, P. E. J. N. a. r., The protein data bank. **2000,** *28* (1), 235-242.

6. SCINTIFIC, O., **2018**, https://www.eyesopen.com/.

7. Ahmed, M. S.; Halaweish, F. T. J. J. o. e. i.; chemistry, m., Cucurbitacins: potential candidates targeting mitogen-activated protein kinase pathway for treatment of melanoma. **2014,** *29* (2), 162-167.

8. Alsayari, A.; Kopel, L.; Ahmed, M. S.; Pay, A.; Carlson, T.; Halaweish, F. T. J. S., Design, synthesis, and biological evaluation of steroidal analogs as estrogenic/anti-estrogenic agents. **2017,** *118*, 32-40.

9. Ahmed, M. S.; Kopel, L. C.; Halaweish, F. T. J. C., Structural optimization and biological screening of a steroidal scaffold possessing cucurbitacin-like functionalities as B-raf inhibitors. **2014,** *9* (7), 1361-1367.

10. Cousins, K. R., Computer review of ChemDraw Ultra 12.0. ACS Publications: 2011.

11. Stéphan, E.; Zen, R.; Authier, L.; Jaouen, G. J. S., Improved synthesis of a protected 11-oxoestrone. **1995,** *60* (12), 809-811.

12. Shattuck, T. W. J. D. o. C., Colby College, Waterville, Maine, Colby College Molecular Mechanics Tutorial. **2008,** *4901*.

13. Lensink, M. F.; Méndez, R.; Wodak, S. J. J. P. S., Function,; Bioinformatics, Docking and scoring protein complexes: CAPRI 3rd Edition. **2007,** *69* (4), 704-718.

14. Du, X.; Li, Y.; Xia, Y.-L.; Ai, S.-M.; Liang, J.; Sang, P.; Ji, X.-L.; Liu, S.-Q. J. I. j. o. m. s., Insights into protein–ligand interactions: mechanisms, models, and methods. **2016,** *17* (2), 144.

15. Ahmed, M. S.; Kopel, L. C.; Halaweish, F. T. J. C., Structural Optimization and Biological Screening of a Steroidal Scaffold Possessing Cucurbitacin-Like Functionalities as B-Raf Inhibitors. **2014,** *9* (7), 1361-1367.

16. OpenEye Scientific Software, I., *FRED Fast Rigid Exhaustive Docking* OpenEye Scientific Software, Inc. : 9 Bisbee Ct, Suite D Santa Fe, NM 87508 2008

17. Ahmed, M. S.; Kopel, L. C.; Halaweish, F. T. J. C., Structural Optimization and Biological Screening of a Steroidal Scaffold Possessing Cucurbitacin-Like Functionalities as B-Raf Inhibitors. **2014,** *9* (7), 1361-1367.

18. Mahnashi, M. H., Design, Synthesis and Biological Screening of Novel Cucsinspired Estrone Analogues Towards Treatment of Hepatocellular Carcinoma. **2017**.

CHAPTER THREE

Synthesis and Biological Activity of 9, 11 dehydrogenated Cucurbitacin Inspired Estrone Analogs Targeting Pancreatic Cancer

Abstract

Pancreatic cancer is expected to be the second leading cause of death in Untied States by 2030. The standard treatment is Gemcitabine as a mono-chemotherapy; this is currently used in combination with other anticancer drugs. However, the survival rate range after treatment is low compared to other cancer types, which suggests an urgent need to search for new treatment agents. Recently, the triterpenoid natural product, cucurbitacin B, showed promising antiproliferative activity against human pancreatic cancer cells. This activity involved decreasing the expression levels of pSTAT3 and pEGFR in a dose- and time-dependent manner by inducing cell apoptosis via inhibition of STAT3 phosphorylation. Additionally, in an in vivo study, it decreased the pancreatic tumor size in combination with gemcitabine. Due to the low yield of cucurbitacin from its natural sources and the challenging chemical synthesis of its highly stereochemical complexity, we developed a novel strategy that facilitates the use of cucurbitacin pharmacophores with estrone as a scaffold. We virtually installed the cucurbitacin pharmacophores on estrone, then used molecular modeling software to identify the best candidates for chemical synthesis and in-vivo study. The molecular docking study showed promising binding affinity for the cucurbitacin-inspired estrone analogues (CIEAs) unsaturated in C_9 and C_{11}; this group of compounds show better calculated affinity than the saturated analogs, due to cis conformation at the juncture of rings B and C. Moreover, the molecular docking study displayed similar conformation for all the analogs upon docking in the EGFR and Erk

binding sites. Based on that result, 8 analogs were synthesized and biologically screened against PANC-I and AsPC-I pancreatic cancer cell lines. Two analogs showed promising IC_{50} values compared to cucurbitacin B, so they were further studied through in-cell western analysis to confirm the inhibition of pErk overexpression as the mechanism of action. KA19 and KA20 inhibited the phosphorylation of Erk and the inhibition increase up on increasing the treatment concentration, which confirmed the theoretical result obtained from the previously conducted molecular modeling study.

3.1. Introduction

Pancreatic adenocarcinoma (PDAC) is one of the leading causes of death in both men and women. The understanding of its pathology is advancing, since more cases are now found in Europe, North America and Australia. In the United States PDAC is expected to be the second leading cause of death by 2030.[1,2] Pancreatic cancer is the only cancer type that has a stable rate of mortality in both men and women, reported to be 3.5% for women in 2017.[3] The reason for the high mortality rate for pancreatic cancer is the absence of biomarkers with to detect the disease in its earlier stages.[4] The risk factors for pancreatic cancer include type II diabetes mellitus, smoking, and obesity.[5,6] Studies have reported that an increase in the waist to hip ratio increases the risk of PDAC by 70%. Inversely, a decrease in weight and exercise can reduce the PDAC risk.[7] In addition to the late diagnosis for pancreatic cancer, the anti-pancreatic cancer drug discovery process has been slow compared to other cancer types.[8] The nucleoside analog gemcitabine is the drug of choice for the treatment of PDAC, either as a monotherapy or in combination with other anticancer drugs such as cisplatin. The one-year survival rate is 18% for patients treated with gemcitabine, compared with 2% for the previously used anti-pancreatic cancer drug 5-fluorouracil (5-FU).[9] Recently, it was reported that a combination of gemcitabine and capecitabine increased the 25-month survival rate from 22.7-27.9 to 95% in terms of 28 months.[10] After its uptake by human nucleoside transporters (hNTs), gemcitabine is metabolized to 2′,2′-difluoro-2′-deoxycytidine triphosphate before it is phosphorylated by deoxycytidine kinase and pyrimidine nucleoside monophosphate kinase to produce gemcitabine diphosphate (dFdCDP). At this point, it is incorporated into the DNA chain biosynthesis by DNA polymerase and results in its termination.[11] However, due to the numerous steps that

gemcitabine has to pass through to reach its target, several mechanisms of resistance have been adopted by cancer cells to avoid DNA termination. These mechanisms include lack of transporters and phosphorylation enzymes, along with overexpression of gemcitabine deactivating enzymes, such as cytidine deaminase, that converts gemcitabine into its inactive metabolite, dFdU.[12]

The low patient survival rate compared to other cancer types has inspired researchers to search for novel, more effective anti-pancreatic cancer drugs. Overexpressed proteins such as pEGFR and pERK, which leads to effects such as tumor growth, overexpression of fatty acid synthase enzyme and a disturbance in lipid metabolism and cell migration have been reported in pancreatic cancer patients.[13]

The natural anticancer triterpenoid, cucurbitacin B, in combination with gemcitabine at low doses, led to the inhibition of pancreatic tumor growth.[14] Recent studies have indicated that cucurbitacin works mainly by inhibiting the JAK-STAT and MAPK pathways, which play an important role in tumor growth and survival.[14]

Among the promising, new compounds that demonstrate significant inhibition of cancer growth and the MAPK pathway are the semisynthetic estrone analogs that mimic cucurbitacin compounds. Cucurbitacin-inspired estrone (CIE) analogs were initially designed based on molecular modeling against cucurbitacin's potential targets, such as EGFR and ERK proteins.[15]One of the reported targets for CIE analogs is epidermal growth factor receptor (EGFR), where CIE analogs inhibit its phosphorylation, along with that of extracellular signal-regulated kinase (ERK).[16]

A recent target-based drug discovery has developed more potent CIE analogs targeting different cancer types. Molecular modeling studies have been utilized to synthesize three major groups of compounds so far. The first group contain a 23, 24 α, β- unsaturated ketone side chain that mimics cuc compounds.[17] Additional compounds were designed based on molecular modeling results and verified biologically by replacing the cuc side chain with different side chains that improved the activity of these compounds against hepatocellular carcinomas, both resistant and non-resistant HepG2.[18,19] The second group included the dehydrogenation of C_{16} and C_{17}, which dramatically increased its activity compared to the previously synthesized analogs. The third modification to this group was the synthesis of CIE analogs that contain a sulfamoyl moiety instead of methyl at C_3; that modification showed promising anticancer activity.[20] The dramatically increased activity of this group was attributed to the ability of sulfamoyl-modified compounds to bypass the first phase metabolism, as noted in a study that showed anticancer activity on a 3-sulfamoyl estrone.[21]

3.2. Molecular Modeling Design Strategy

A molecular modeling study using the biological screening data of the first group of compounds indicated that the dehydrogenation of C_9 and C_{11} cucurbitacin-inspired estrone analogs (CIEA's) increased the anticancer activity of MSA-8 to 12.2 μM, compared to that of MSA-7, which is saturated at the previously mentioned positions[22] (Figure 3.1). Thus, this modification shows great promise for improving the activity of CIE analogs. This increase in anticancer activity is attributed to the configuration of the compound, changing ring B from the chair to half-chair configuration. Moreover, the substitution of a 23, 24 α, β- unsaturated ketone side chain was reported to increase anticancer activity; however, the

effect of substituting this side chain with a different side chain is yet to be investigated in depth. The modification of ring A resulted in blocking the estrogenic activity of the CIE analogs.[22]

Considering the findings from the biological studies, as well as the molecular docking studies, different CIE analogs were virtually designed with various substituted side chains and modeled against CIE potential analogs using OpenEye® scientific software. The study used novel designed CIE analogs with an alkene group at C_9 and C_{11} and various 23, 24 α, β- unsaturated ketone side chains with lower consensus scores and show promising binding calculations against potential molecular targets of pancreatic cancer, including EGFR, ERK, STAT3, JAK2, P53, B-RAF.

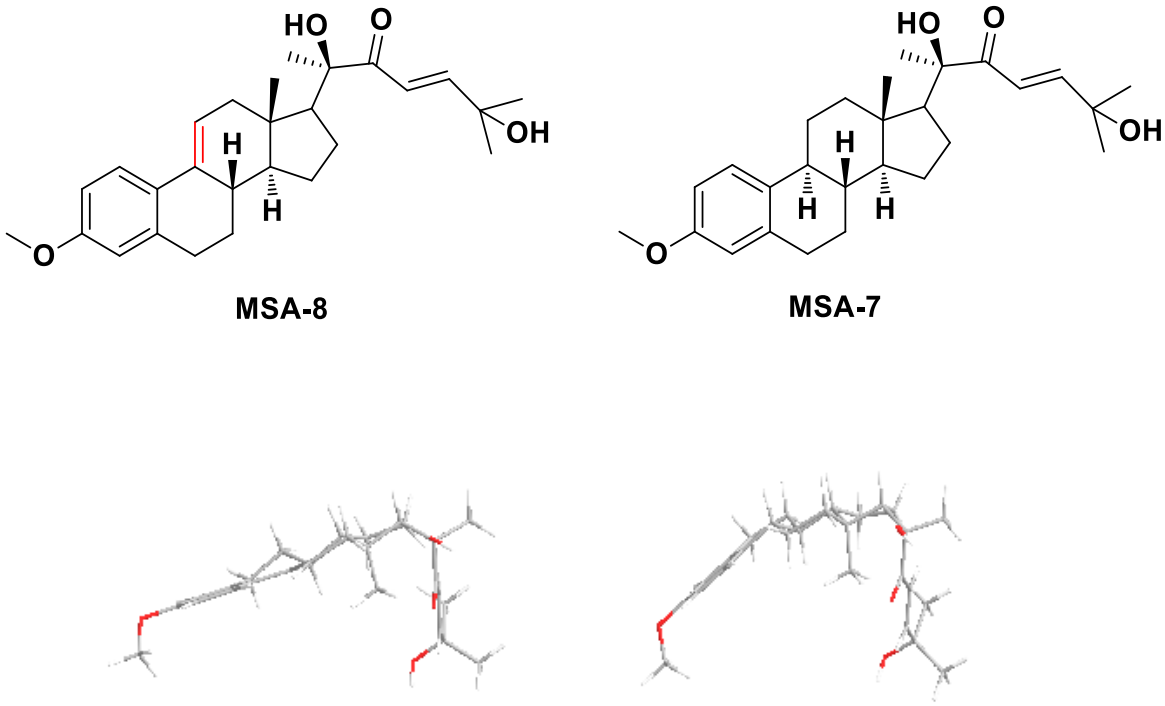

Figure 3.1. The dehydrogenation of MSA-8 at C_9 and C_{11} increased the anticancer activity of MSA-7 due to a change in the configuration of the molecule.[20]

3.3. Results and Discussions

3.3.1. *In-silico* molecular modeling

A virtual library of CIE analogs was designed to mimic cucurbitacin compounds with different functional groups in positions 9 and 11, and different enon side chains at position 17. Cucurbitacins B and D, with erlotinib and NCX-1000 were used as standards and designed through in ChemDraw software, followed by energy minimization by Chem3D using the force field MMFF94. The catalytic domains for EGFR and ERK proteins were downloaded from the protein data bank using their PDB codes, 1M17 and 2OJJ, respectively.[23] Various OpenEye® software applications were used to perform the molecular modeling experiment. OMEGA application generated different conformers, while the docking was conducted using FRED software. The output of the molecular modeling process was visualized using VIDA application, which ranked the compounds based on their consensus scores, where the lower score indicates a better binding affinity of the compound toward an active site of the protein that was processed and determined using MAKE RECEPTOR®. Based on this process, 8 compounds were selected to be synthesized and biologically tested against PANC-I and AsPC-I pancreatic cancer cell lines. All the selected ligands **(Figure 3.3)** showed better binding than the previously mentioned standards, based on consensus score calculations, **(Table 3.1)**. The molecular modeling process was validated by using the binding profile of the standard erlotinib to EGFR. Among the high scoring ligands, KA19 showed promising binding affinity to ERK binding site where it adopts the same profile as cuc D binding to the same pocket. This explains the increased anticancer potency of this group compared to the previously synthesized CIE analogs **(Figure 2.3 A, B)**.

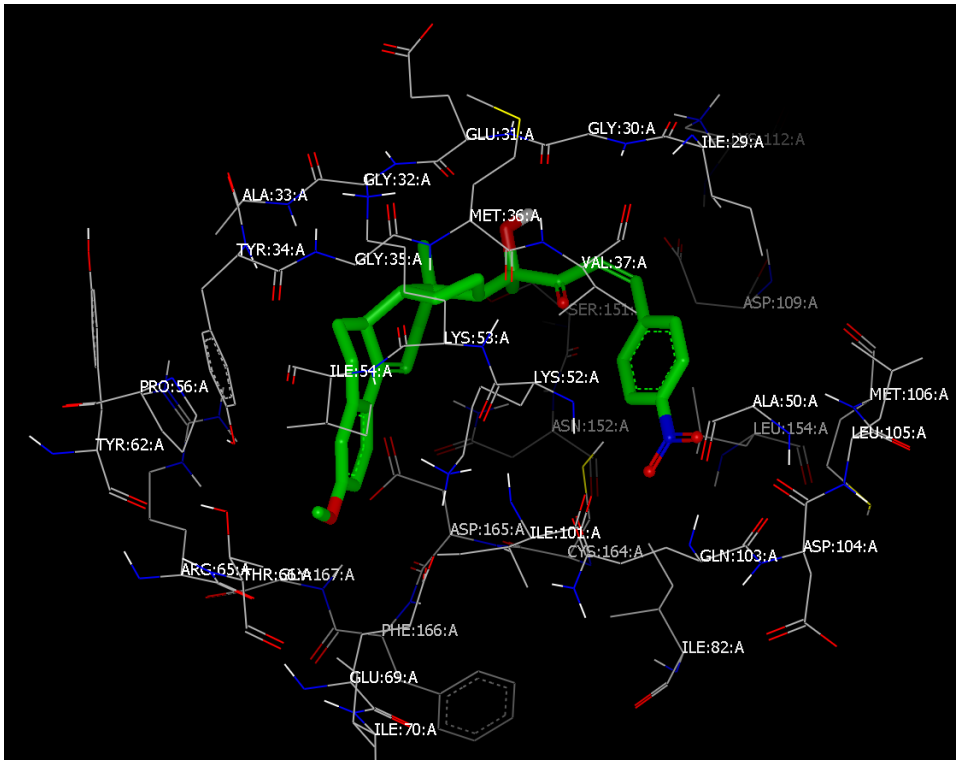

A. KA19 docking profile in ERK binding pocket.

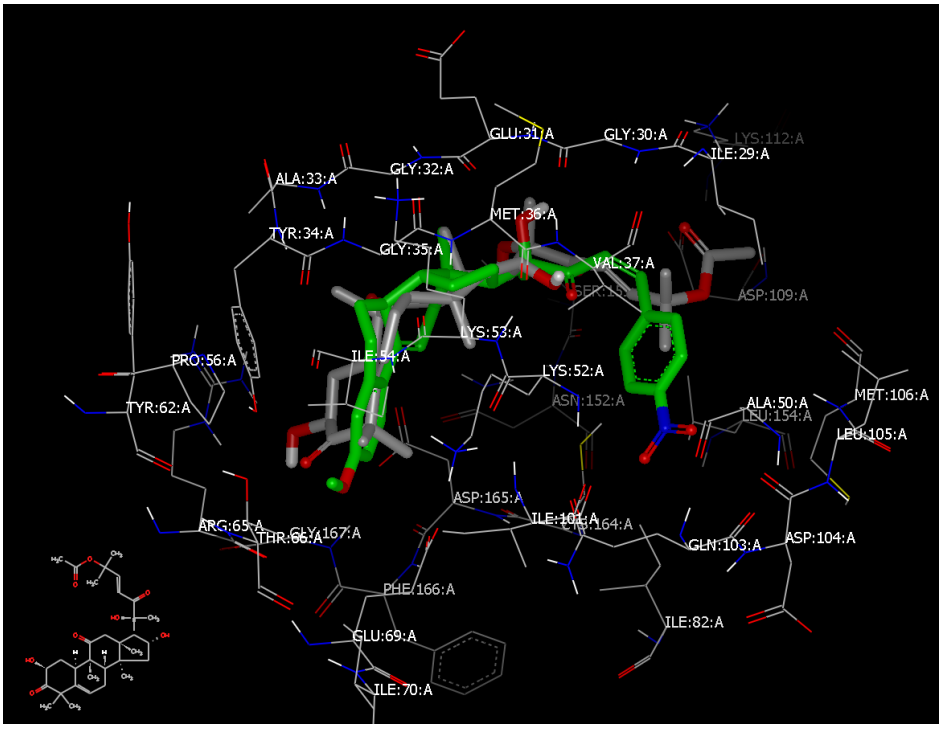

B. KA19 shows a cuc-like docking profile in the Erk binding pocket.

Figure 2.3. The docking profile of the highest scoring CIE analog in Erk docking.

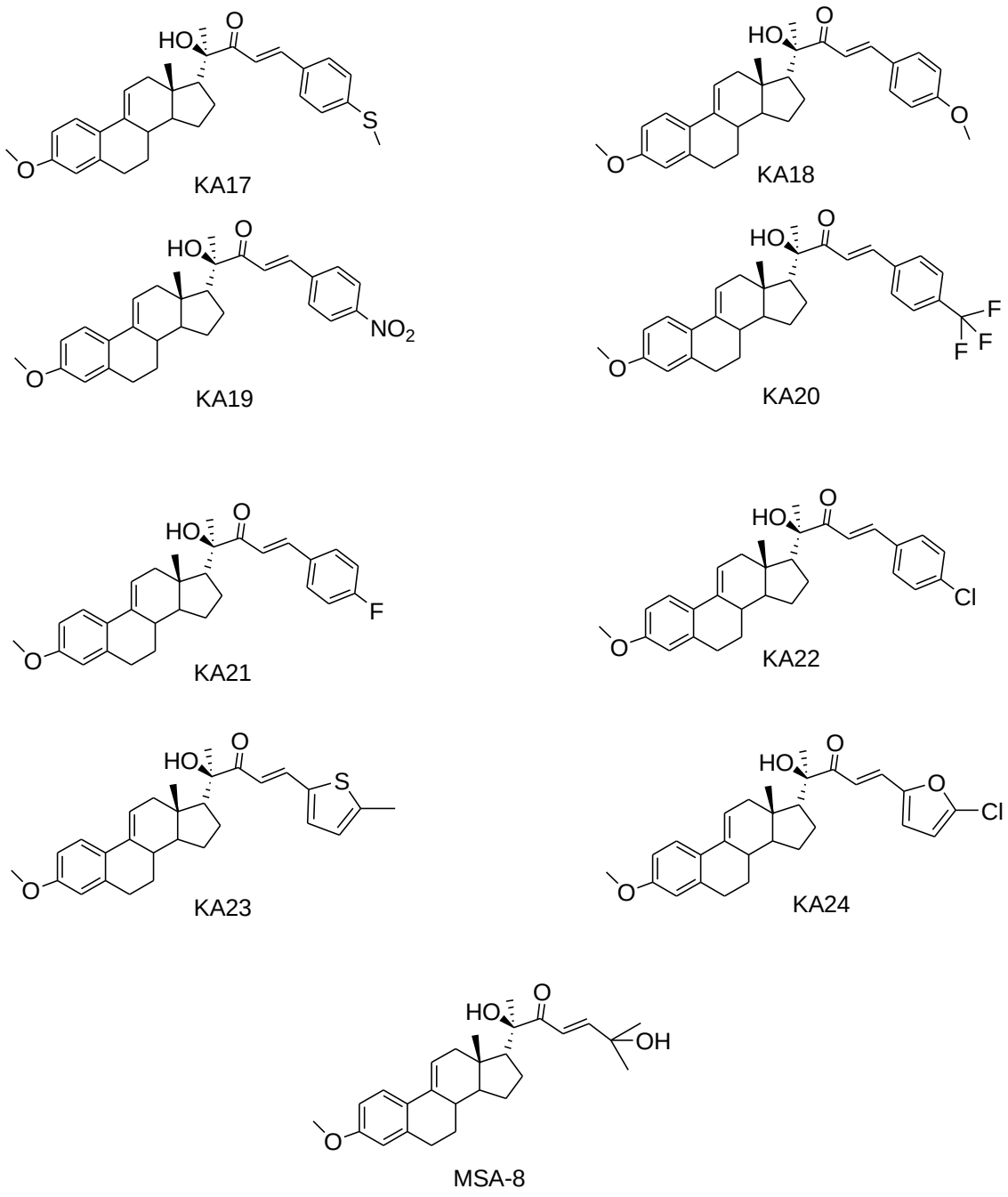

Figure 3.3. The structures of the promising C_9-C_{11} dehydrogenated cucurbitacin-inspired analogs.

Table 3.1. The consensus scores of the docked C_9-C_{11} dehydrogenated CIE analogs on Erk binding pocket.

VIDA Name	PLP	Chemgauss3	OEChemscore	Screenscore	Consensus Score
KA19_59	-57.9087	-64.6093	-46.7819	-140.123	9
KA17_117	-61.5173	-60.1572	-44.8431	-143.464	14
KA22_64	-53.9205	-62.8396	-44.9295	-126.344	17
KA23_66	-52.4111	-57.3973	-44.7099	-117.968	36
KA20_37	-55.5477	-51.1163	-41.5947	-125.192	44
KA18_182	-45.3341	-59.6018	-45.5775	-104.68	47
ISo D_68	-38.3577	-61.9525	-42.9418	-87.7898	70
Cucurbitacin I_22	-35.6603	-58.9337	-41.6845	-99.3021	76
KA21_37	-41.3433	-37.2141	-42.7684	-105.011	76
Iso B_88	-39.4889	-28.2737	-43.2004	-104.984	80
KA26_9	-38.9837	-39.097	-33.543	-114.729	90
KA25_28	-29.1705	-42.2166	-35.7163	-101.308	97
CucD_53	-36.6245	-36.1404	-39.0127	-97.0475	98
CucurbitacinE_21	-25.1026	-42.2368	-33.4445	-83.312	108

3.3.2. Chemical synthesis

As described in **Scheme 1**, the key intermediate C_9-C_{11} desaturated α-hydroxy methyl ketone **(KI9)** was synthesized from estrone in 10 steps. Intermediate KI9 was used to synthesize the target compounds by installing the required side chains at C_{21}. The key intermediate synthesis began by protecting the estrone phenolic ring A at C_3 with *tert*-butyldimethylsilyl chloride (TBSCl). Wittig reaction was carried out on the estrone TBS ether (KI1) on ring D to produce alkene intermediate (KI2). Hydroboration oxidation was used to obtain KI3 using 9-borabicyclo [3.3.1] nonane (9-BBN) at 60 ℃, followed by oxidation using PCC to produce intermediate KI4.

The reaction of (KI4) with TMSCN in DCM, in the presence of a catalytic amount of zinc iodide, resulted in nitrile intermediate KI5 at an 84% yield. Intermediate KI5 was moved to the next reaction where the nucleophilic addition of MeLi was carried out in ether at 0 ℃ to generate imine, which was converted into α-hydroxy methyl ketones by the addition of glacial acetic acid. After the separation of intermediate KI6, it was deprotected using TBAF to yield (KI7). The desaturation of C_9 and C_{11} was carried out at 45℃ in the presence of DDQ in methanol. This was followed by the methylation of crude extract KI8 by MeI in acetonitrile in the presence of $CsCO_3$ to produce the key intermediate (KI9).

In order to synthesize the required product at C_{21}, the key intermediate was reacted with a suitable aldehyde, as indicated in **Scheme 1,** by conducting aldol condensation in THF in the presence of NaOH. The synthesized analogs include aromatic aldehydes with different substituents at the *para* position of the benzene ring. Moreover, the CIE analogs, KA23 and KA24, contained the heterocyclic rings 4-chloro-furan and 4-methylthiophen.

Although the yield of the DDQ reaction with intermediate KI8 was 53%, which is lower than that of estrone (80%), Reaction DDQ with KI8 was preferred to avoid the side reaction that occurred upon the reaction of C_9-C_{11} dehydrogenated estrone with 9-BBN after Wittig product. One of the challenges is the separation of the final products, as they have an R_f value close to key intermediate KI9.

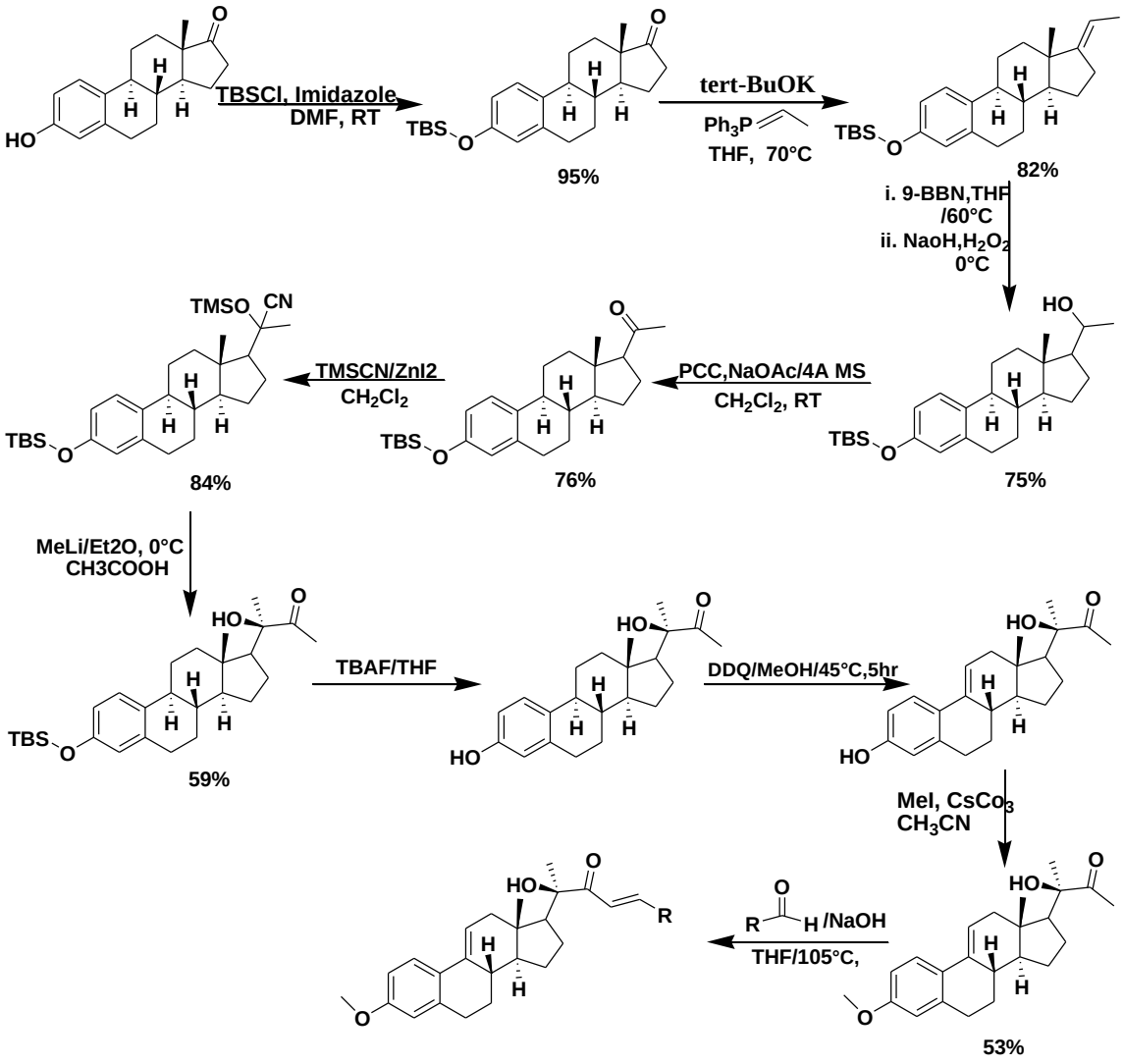

Scheme 1. The synthetic route for KA17-KA24.

3.3.3. Biological evaluation

In order to evaluate the antiproliferative activity against pancreatic ductal adenocarcinoma, MTT assay was conducted against two pancreatic cancer cell lines PANC-I and AsPC-1. Five concentrations ranging from 3.125 μM to 50 μM quadruplicate was treated from each compounds in 10,000 cells/ well with –ve control wells that contain 0.05 % of DMSO. Based on the absorbance, the percent of the viable cells was calculated after normalization by the number of cells in the wells containing the –ve control. After treatment of each compounds for 48 hrs., KA19 and KA20 containing phenyl *para*-nitro and *para*-trifluoro side chains showed promising antiproliferative activities with IC_{50}s of 11.23 and 7.674 μM, respectively, upon treatment of PANC-I and with IC_{50} values of 11.68 and 9.67 μM upon treatment against AsPC-I (**Table 2.3**).

Table 3.2. IC_{50} values of the synthesized CIE analogs on PANC-1 and AsPC-I cell lines.

Compound	PANC-I (μM)	AsPC-I (μM)
KA17	NA	NA
KA18	NA	NA
KA19	11.22±0.38	11.68±1.1
KA20	7.674 ±1.34	9.674±0.68
KA21	NA	NA
KA23	NA	NA
KA24	NA	NA
Gemcitabine	>100	>100

These promising results are correlated to some extent with the molecular docking data in which *Para-trifluoromethyl* and *para*-nitro scored higher than various side chains, as well as the cucurbitacin compounds previously mentioned in the docking experiments. In Erk molecular modeling, KA19 showed a lower consensus score than KA20. However, when focusing on molecular docking against multiple targets, such as EGFR, STAT3, RAF, RAS, and PI3K, KA20 scored higher than KA19 (**Table 2.2 in chapter 2**), which can be correlated with the results obtained by MTT cell viability assay.

Previous published results by our group indicate that Erk phosphorylation is inhibited by CIE analogs. In order to confirm whether this is the same mechanism of action adopted by KA19 and KA20 on pancreatic cancer cells, in-cell western analysis was conducted on PANC-I cells. During this test, the cells were treated with four different concentrations of each compound (¼, ½, 1, and 2 of IC_{50} values). In the case of KA19, significant inhibition of Erk phosphorylation was noted, compared to the negative control and the lower concentrations of the same compound. Similar results were obtained with KA20, although less inhibition was noted than with KA19. The anticancer activity of KA19 and KA20 act through inhibition of the pErk activation, as indicated in **Figures 3.4 and 3.5**, based on in-cell western analysis.

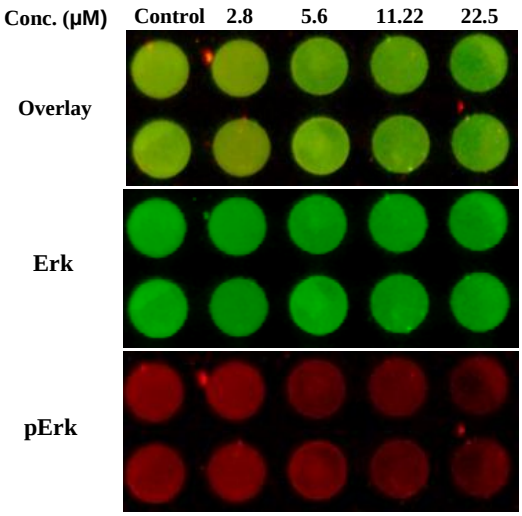

A.

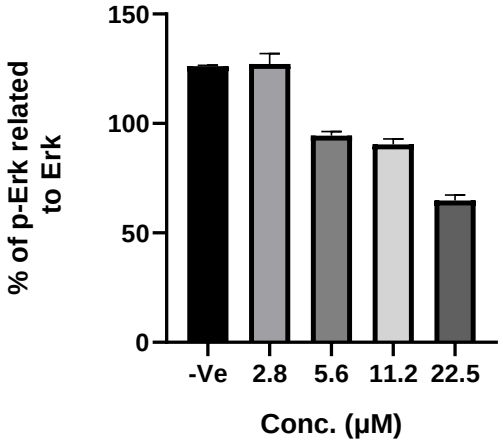

B.

Figure 3.4. In-Cell Western analysis of potential KA19 targets. (A) ICW plate image (p-Erk intensity in 800 channels was normalized to total Erk intensity in 700channel) (B) Analysis of Erk phosphorylation in PANC-I cells.

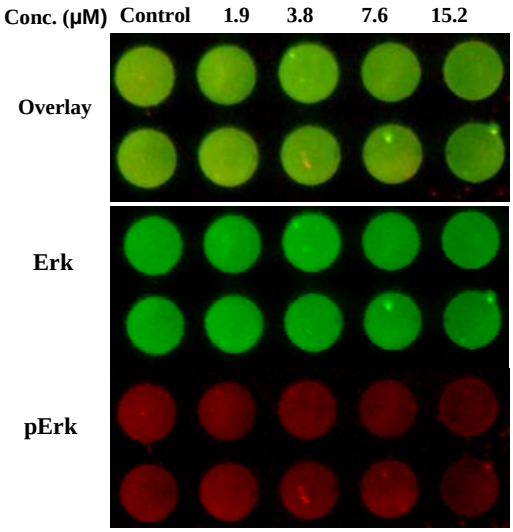

A.

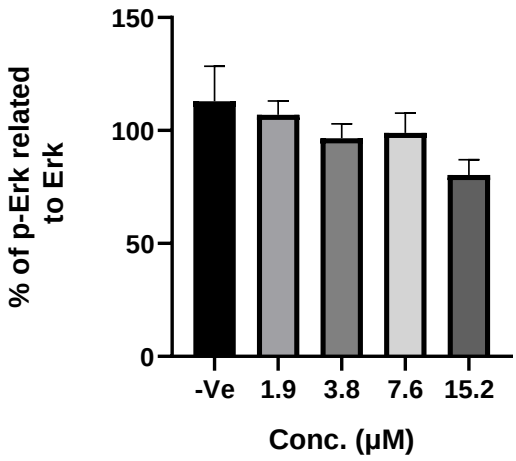

B.

Figure 3.5. In-Cell Western analysis of potential KA20 targets. (A) ICW plate image (p-Erk intensity in 800 channels was normalized to total Erk intensity in 700channel) (B) Analysis of Erk phosphorylation in PANC-I cells.

3.4. MATERIAL AND METHODS

3.4.1 Chemistry experiment section

General

All chemicals and solvents (ACS grades) were purchased from Fisher Scientific or Sigma Aldrich and used without any additional treatment. Before conducting the experiments, all the glassware and tools were cleaned, washed and dried in a 120 °C oven, and before conducting the reaction according to the mentioned conditions, closing and introducing nitrogen gas to the reaction vessel for all the reaction period was performed, except when mentioned during the experiment. TLC plates (Silica gel, 0.2-mm thick, polyester backed, Sorbtech) were used to analyze the reaction conditions under UV254. All synthetic intermediates and final compounds were purified using column chromatography packed with silica gel 60A, 40-63 μm. ^{1}H and ^{13}C NMR spectra were carried out using Bruker AVANCE-400 MHZ and 600 MHZ NMR spectrometers, while the solvents used for the compounds are $CDCl_3$. NMR chemical shifts were presented in δ(PPM) using residual solvent peaks as standards ($CDCl_3$, 7.26 (^{1}H), 77.16 (^{13}C)). High resolution mass (HRMS) was performed using a Thermofinnigan MAT 95XL mass spectrometer at the Buffalo mass spectroscopy facility. X-ray crystallography was conducted at the University of South Dakota on KI 9 using a Bruker APEX^{II} diffractometer.

KII

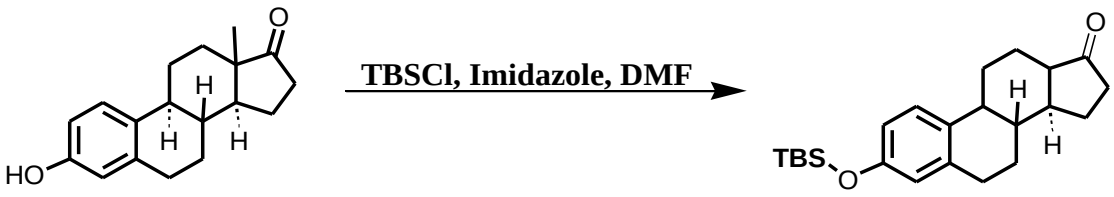

To a stirred solution of estrone (5 g, 18.5 mmol) in DMF (75 ml), imidazole (3.5 g, 50.85 mmol) and tert-butyldimethylsilyl chloride (TBSCl) (4.2 g, 27.75 mmol) were added. The reaction was stirred overnight at room temperature. The result mixture were evaporated to provide the crude extract that was purified using column chromatography and eluted using 80 % hexane: ethyl acetate produce the white solid estrone tert-butyldimethylsilyl ether KI1 (6.75 g, 95%).[18]

^{1}H NMR (400 MHz, Chloroform-*d*) δ 6.91 (dd, *J* = 8.6, 1.0 Hz, 1H), 6.47 – 6.33 (m, 2H), 2.72 – 2.59 (m, 3H), 2.28 (dd, *J* = 18.7, 8.7 Hz, 1H), 2.16 (dt, *J* = 14.0, 3.7 Hz, 1H), 2.08 – 1.65 (m, 5H), 1.48 – 1.14 (m, 7H), 0.79 (s, 9H), 0.75 – 0.65 (m, 4H), 0.00 (s, 6H).

^{13}C NMR (101 MHz, Chloroform-*d*) δ 219.97, 153.47, 137.57, 132.47, 126.17, 120.02, 117.35, 50.44, 47.98, 44.04, 38.34, 35.87, 31.65, 29.54, 26.62, 25.85 21.63, 18.20, 13.90, -4.30.

KI 2

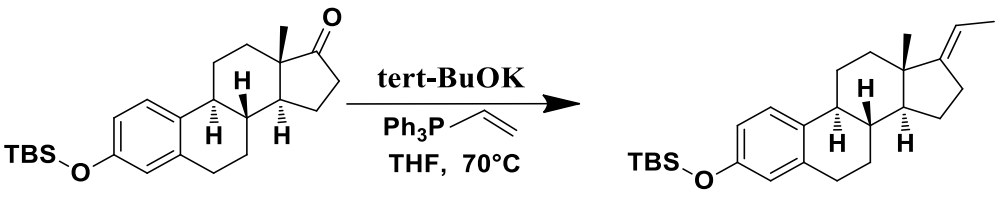

To prepare the ylide, (4 g, 35.9 mmol) of potassium tert-butoxide was added to a solution of ethyl triphenylphosphonium bromide (18 g, 38.52 mmol) in THF (33.83 ml) at room temperature to result in an orange mixture that was stirred for 1 hr. A solution of KI 1 (6.5g, 16.9 mmol) in THF (15 ml) was added to the prepared ylide and the orange mixture was stirred for 6 hrs. at 70 ^{0}C. After that, the reaction mixture was allowed to cool to room temperature and quenched with saturated ammonium chloride (NH_4Cl) solution, followed by extraction of the aqueous layer by ethyl acetate (3×100 ml), dried over sodium sulfate anhydrous (Na_2SO_4), filtrated and concentrated. The crude extract was purified by silica gel column chromatography 80 % hexane: ethyl acetate) to obtain KI 2 (4.8 g, 82%).[18]

1H NMR (400 MHz, CDCl3) δ 7.06 (d, J = 8.4 Hz, 1H), 6.56 (dd, J = 8.4, 2.5 Hz, 1H), 6.50 (d, J = 2.4 Hz, 1H), 5.10 (dtd, J = 7.1, 5.1, 2.1 Hz, 1H), 2.87 – 2.69 (m, 2H), 2.45 – 2.11 (m, 6H), 1.93 – 1.81 (m, 1H), 1.57 – 1.16 (m, 9H), 0.93 (s, 10H), 0.13 (d, J = 3.1 Hz, 6H).

^{13}C NMR (101 MHz, Chloroform-*d*) δ 153.33, 150.30, 137.87, 133.32, 126.11, 126.11, 119.99, 117.18, 113.45, 55.33, 44.63, 43.93, 38.40, 37.32, 31.51, 29.77, 27.66, 26.96, 25.80, 24.24, 18.24, 17.03, 13.23, -4.31.

KI3

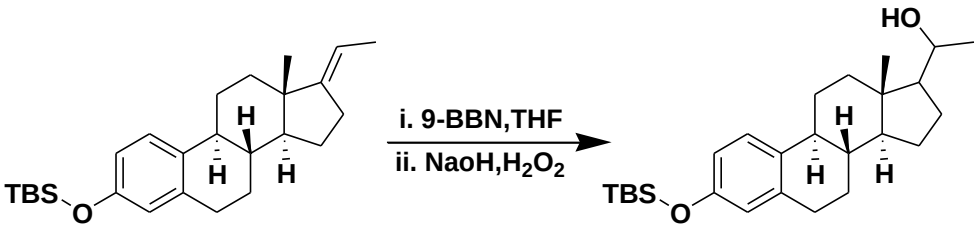

To the purified mixture of KI 2 (4.8 g, 12.184 mmol), 9-BBN (0.5 M in THF, 107.4 ml, 53.72 mmol) was added at room temperature. The reaction mixture was stirred for 18 hrs., then cooled down to 0 ^{0}C and 200 ml of 10%NaOH and 200 ml of 30% H_2O_2 were added drop wisely. The reaction mixture was stirred for 1 hr. at 0 ^{0}C followed by extraction by ethyl acetate (3×100 ml) and the mixture was washed with 100 ml of saturated sodium thiosulfate, dried over sodium sulfate anhydrous (Na_2SO_4) and concentrated. Column chromatography was used to purify the crude extract with 70 % hexane: ethyl acetate to provide alcohol KI 3 (3.7 g, 75 %).[18]

1H NMR (400 MHz, CDCl3) δ 6.92 (t, J = 6.9 Hz, 1H), 6.41 (dd, J = 8.4, 2.5 Hz, 1H), 6.36 (d, J = 2.3 Hz, 1H), 3.63 (ddd, J = 12.0, 8.2, 3.8 Hz, 1H), 3.52 (tt, J = 12.3, 6.3 Hz, 1H), 2.73 – 2.54 (m, 2H), 2.25 – 1.93 (m, 5H), 1.79 (ddd, J = 15.0, 11.4, 7.7 Hz, 3H), 1.71 – 1.58 (m, 5H), 1.50 (dddd, J = 15.6, 11.1, 4.9, 2.0 Hz, 7H), 1.11 – 1.02 (m, 5H), 0.79 (s, 9H), 0.51 (s, 17H), -0.00 (s, 6H).

^{13}C NMR (101 MHz, Chloroform-*d*) δ 153.25, 137.82, 133.23, 126.03, 119.95, 117.12, 72.01, 58.59, 55.38, 43.79, 42.03, 38.41, 34.66, 27.47, 26.42, 25.75, 23.59, 22.76, 18.17, 12.60, -4.36.

KI 4

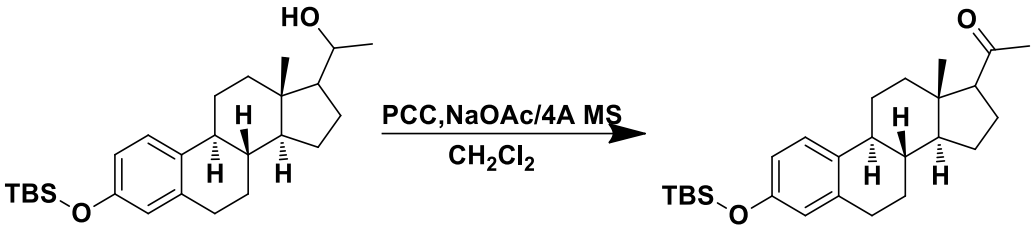

KI 3 (3.7 g, 9 mmol) was dissolved in 50 ml of dried DCM, followed by addition of 4^0 A powdered molecular sieves (3.5 g), and 2.9 g, 43 mmol of sodium acetate (NaOAc) and pyridinium chlorochromate (PCC) (3.87 g, 17.8 mmol). The reaction mixture was stirred at room temperature for 5 hrs. The crude extract was filtered over a silica gel pad using ethyl acetate to elute the material and trap the pyridinium. The collected material was then concentrated and the crude extract was purified by column chromatography (80 % hexane: ethyl acetate) to yield ketone KI 4 (2.85 g, 76 %).[18]

1H NMR (400 MHz, CDCl3) δ 6.92 (t, J = 6.9 Hz, 8H), 6.41 (dd, J = 8.4, 2.5 Hz, 9H), 6.36 (d, J = 2.3 Hz, 8H), 3.63 (ddd, J = 12.0, 8.2, 3.8 Hz, 10H), 3.52 (tt, J = 12.3, 6.3 Hz, 9H), 2.62 (t, J = 7.9 Hz, 15H), 2.23 – 1.94 (m, 44H), 1.79 (ddd, J = 15.0, 11.4, 7.7 Hz, 21H), 1.71 – 1.59 (m, 38H), 1.55 – 1.42 (m, 62H), 1.06 (t, J = 4.9 Hz, 33H), 0.79 (s, 72H), 0.51 (s, 20H), -0.00 (s, 51H), -0.10 (d, J = 3.0 Hz, 6H)

^{13}C NMR (101 MHz, Chloroform-*d*) δ 209.31, 153.36, 137.72, 132.80, 126.05, 119.99, 117.20, 67.01, 63.81, 55.69, 44.38, 43.71, 39.01, 38.70, 31.49, 29.64, 27.74, 26.62, 25.75, 24.16, 22.88, 18.17, 13.45, -4.35.

KI5

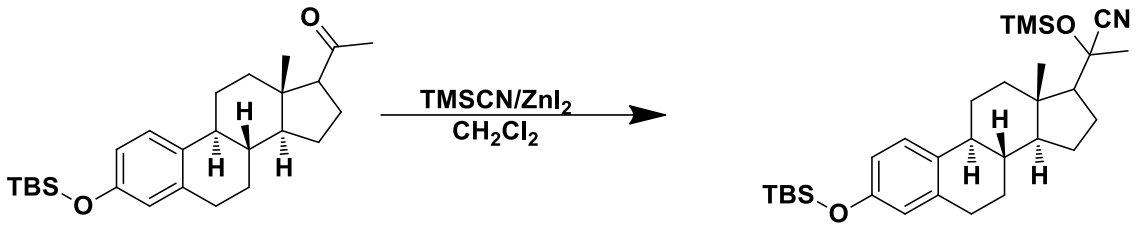

To a stirred solution of KI 4 (2.85 g, 6.8 mmol) in DCM (20 ml), zinc iodide (ZnI_2) (0.07 g, 0.2 mmol) was added, followed by addition of (0.85 g, 8.8 mmole) of trimethylsilyl cyanide (TMSCN) and the mixture was stirred at room temperature for 2 hrs. The reaction was quenched with water and extracted with DCM (3 X 30 ml), dried over sodium sulfate anhydrous (Na_2SO_4) and concentrated. Column chromatography was used to purify the crude material (90 % hexane :ethyl acetate) to yield KI 5 (2.8 g, 84 %).[18]

1H NMR (400 MHz, CDCl3) δ 6.95 (d, J = 8.5 Hz, 8H), 6.45 (dd, J = 8.3, 2.3 Hz, 10H), 6.40 (s, 8H), 2.80 – 2.58 (m, 20H), 2.16 – 1.96 (m, 30H), 1.77 – 1.67 (m, 20H), 1.68 – 1.55 (m, 41H), 1.39 – 1.24 (m, 32H), 1.25 – 1.11 (m, 43H), 1.11 – 1.02 (m, 15H), 0.84 (s, 82H), 0.13 (s, 49H), 0.05 (s, 33H).

^{13}C NMR (101 MHz, Chloroform-*d*) δ 151.69, 136.09, 131.52, 124.45, 120.47, 120.47, 118.33, 115.57, 70.79, 58.92, 53.30, 42.25, 42.16, 38.41, 36.52, 29.21, 28.02, 26.13, 24.87, 24.16, 23.26, 22.26, 16.58, 11.23, 0.00, 0.23, -5.95.

KI 6

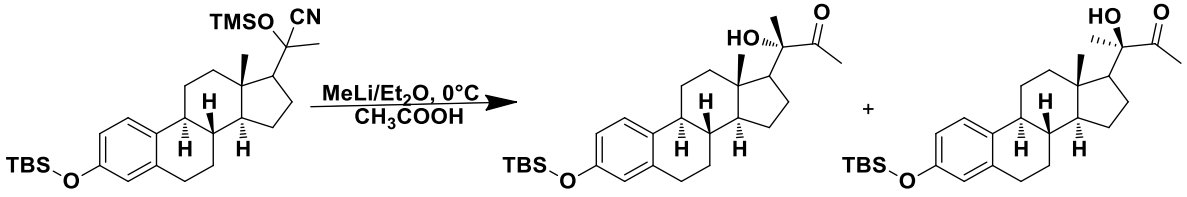

A solution of KI 5 (5.6 g, 11.2 mmole) in ether (34 ml) was stirred at 0^0 C, and (1.6 M in ether, 21 ml, 34 mmole) of methyl lithium (MeLi) was added in drop wisely and the reaction mixture was stirred for 2 hrs. at 0 ^{0}C. After that, reaction was quenched by adding glacial acetic acid (4.2 ml) at 0 ^{0}C and stirred for 30 min. Saturated sodium bicarbonate solution was added to neutralize the acidic mixture. The mixture was extracted with ethyl acetate (3X50ml) and dried with sodium sulfate anhydrous (Na_2SO_4) and concentrated. The resulting mixture were purified by silica gel column chromatography using 95 % hexane: ethyl acetate to result in α-hydroxyl ketone 6 (3.07 g, 59 %).[18]

1H NMR (400 MHz, CDCl3) δ 6.92 (d, J = 8.5 Hz, 1H), 6.42 (dd, J = 8.4, 2.6 Hz, 1H), 6.36 (d, J = 2.5 Hz, 1H), 3.79 (s, 1H), 2.69 – 2.54 (m, 2H), 2.12 – 2.05 (m, 2H), 2.02 (s, 3H), 1.71 – 1.59 (m, 2H), 1.53 (ddd, J = 14.6, 8.6, 4.6 Hz, 2H), 1.45 – 1.33 (m, 4H), 1.28 (s, 3H), 0.81 – 0.79 (m, 8H), 0.75 (s, 3H), 0.08 – -0.04 (m, 6H).

^{13}C NMR (101 MHz, Chloroform-*d*) δ 211.69, 153.32, 137.78, 133.10, 126.05, 119.99, 117.18, 80.10, 55.79, 55.15, 44.25, 43.88, 40.73, 38.08, 31.65 , 25.74, 24.62, 23.73, 23.24, 22.70, 18.18, 13.54, -4.38.

KI7 and KI8

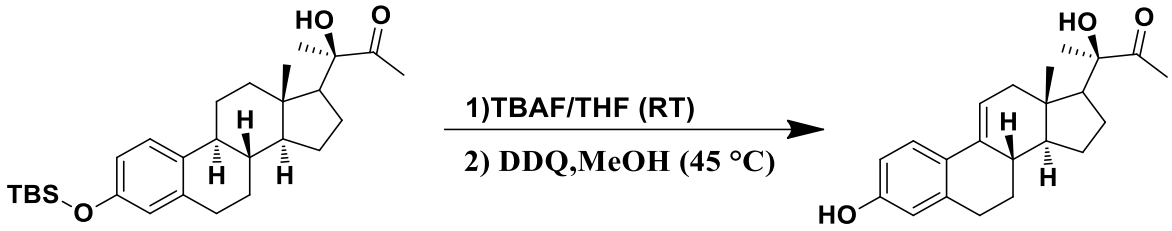

Tetra-butyl ammonium fluoride (TBAF) (14.3 ml, 14.13 mmol) was added to a stirred solution of KI 6 (2.08 g, 4.56 mmol) in 70.7 THF and stirred for 48 hrs. before the reaction was quenched by the addition of an NH_4Cl solution. The aqueous layer was extracted by ethyl acetate (3 X 50 ml). The organic layer was dried using Na_2SO_4, concentrated *in vacuo.*

The crude extract was dissolved in 152 ml of methanol at a temperature of 45 ^{0}C, followed by addition of 2, 3-Dichloro-5, 6-dicyano-1, 4-benzoquinone (DDQ) (1.6 g, 6.83 mmol). The reaction was stirred for 5 hrs. followed by evaporation of methanol using *vacuu*. The crude extract was moved to the next reaction.

KI9

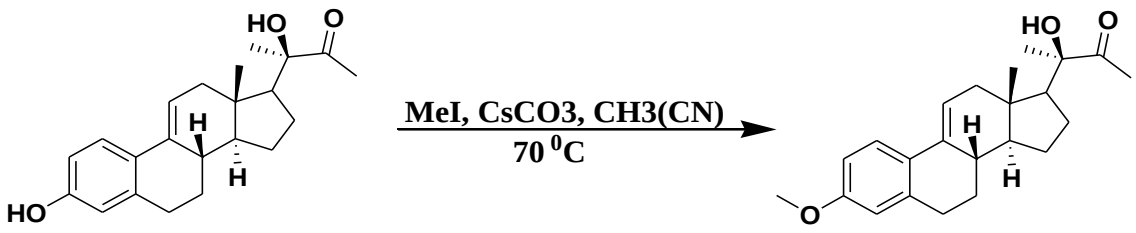

The crude material was dissolved in acetonitrile (90 ml), followed by the addition of crushed granulate potassium hydroxide (4.032 g, 86.46 mmole). Then, methyl iodide (2.24 g, 35.94 mmole) was added to the reaction mixture. The reaction was stirred at room temperature for 2h and quenched by the addition of water (400 ml) and stirred for 15 minutes. Ethyl Acetate (3 x100 ml) was used to extract the aqueous layer, and the organic layer was dried over sodium sulfate anhydrous and concentrated in vacuo to obtain the dry organic portion. Next, a silica gel column was used to purify the crude material using 9:1 (hexane: ethyl acetate) to provide KI 9 (4.3 g, 71.33 %) as a white material.

^{1}H NMR (400 MHz, CDCl3) δ 7.53 (d, J= 8.81 Hz, 1H, -CH (1)), 6.72 (dd, J= 8.8 Hz, 2.7, 1H), 6.59 (d, J= 2.77 Hz, 1H), 6.09 (m, 1H), 4 (s, 1H), 3.79 (s, 3H), 2.95-2.75 (m, 2H), 2.36-2.11 (m, 2H), 2.23 (s,2H), 1.94-1.15 (m,10H), 1.48 (s,3H), 0.94 (s,3H)

^{13}C NMR (101 MHz, Chloroform-*d*) δ 211.8, 158.3, 137.5, 134.9, 127.3, 125.1, 117.5, 113.2,112.6,80.0, 55.2, 52.7, 43.06, 42.3, 38.1, 30.0, 28.6, 24.7, 24.3, 23.3, 22.2, 13.6.

KA17

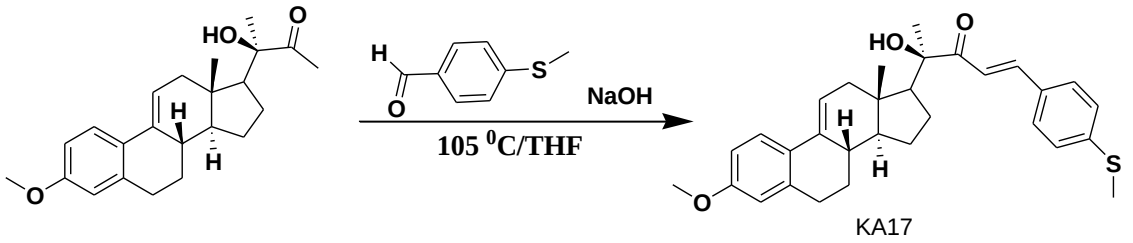

KA17

1H NMR (600 MHz, CDCl3) δ 7.84 (d, J = 15.5 Hz, 1H), 7.56 (dd, J = 12.5, 8.7 Hz, 3H), 7.28 (d, J = 8.4 Hz, 2H), 7.01 (d, J = 15.6 Hz, 1H), 6.76 (dd, J = 8.8, 2.7 Hz, 1H), 6.63 (d, J = 2.4 Hz, 1H), 6.14 (s, 1H), 3.82 (s, 3H), 2.90 (d, J = 13.2 Hz, 1H), 2.84 (d, J = 17.2 Hz, 1H), 2.60 (d, J = 16.8 Hz, 1H), 2.55 (s, 3H), 2.48 (d, J = 17.8 Hz, 1H), 2.36 (s, 1H), 2.20 (s, 1H), 2.09 (s, 1H), 2.03 (s, 1H), 2.00 – 1.96 (m, 1H), 1.84 (s, 1H), 1.70 (s, 2H), 1.59 (s, 3H), 1.54 – 1.47 (m, 2H), 1.01 (s, 3H).

13C NMR (151 MHz, CDCl3) δ 201.88, 158.35, 145.30, 143.16, 137.56, 134.99, 130.67, 129.05, 127.41, 125.89, 125.13, 117.62, 117.12, 113.27, 112.68, 78.98, 55.26, 52.75, 43.11, 42.37, 38.21, 31.95, 30.09, 29.73, 29.39, 28.63, 24.75, 24.12, 22.72, 22.20, 15.08, 14.15, 13.78.

KA18

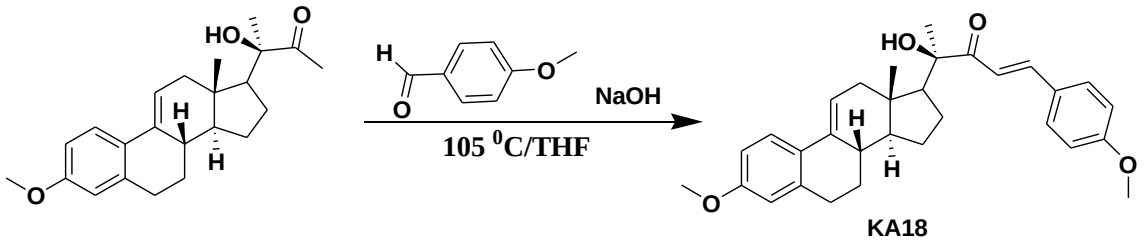

1H NMR (600 MHz, CDCl3) δ 7.86 (d, J = 15.5 Hz, 1H), 7.60 (t, J = 5.8 Hz, 2H), 7.58 (d, J = 8.8 Hz, 1H), 6.97 (d, J = 1.9 Hz, 1H), 6.96 (d, J = 1.8 Hz, 1H), 6.95 – 6.92 (m, 1H), 6.76 (dd, J = 8.7, 2.7 Hz, 1H), 6.63 (d, J = 2.5 Hz, 1H), 6.16 – 6.13 (m, 1H), 4.32 (s, 1H), 3.89 (s, 3H), 3.82 (s, 3H), 2.95 – 2.81 (m, 2H), 2.61 (ddd, J = 17.4, 5.4, 1.7 Hz, 1H), 2.48 (d, J = 17.6 Hz, 1H), 2.13 – 1.96 (m, 3H), 1.84 (ddd, J = 19.4, 11.8, 5.2 Hz, 1H), 1.70 (ddd, J = 16.0, 12.9, 4.0 Hz, 1H), 1.63 (d, J = 8.4 Hz, 2H), 1.58 (d, J = 8.3 Hz, 3H), 1.54 – 1.48 (m, 1H), 1.37 (dddd, J = 19.7, 13.8, 11.8, 4.6 Hz, 4H), 1.01 (d, J = 6.8 Hz, 3H).

13C NMR (151 MHz, $CDCl_3$) δ 201.88, 162.06, 158.34, 145.64, 137.56, 134.98, 130.55, 127.43, 126.99, 125.13, 117.67, 115.84, 114.48, 113.28, 112.67, 78.89, 55.48, 55.32, 55.26, 52.76, 43.12, 42.35, 38.22, 30.10, 28.63, 24.75, 24.17, 22.19, 13.77.

KA19

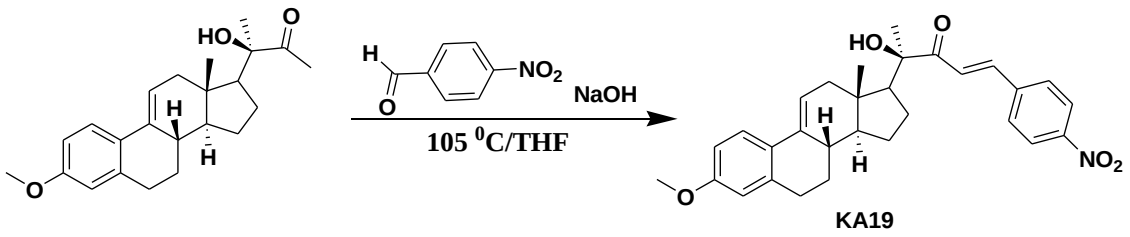

KA19

1H NMR (600 MHz, Acetone) δ 8.32 – 8.29 (m, 20H), 8.11 – 8.07 (m, 21H), 7.85 (dd, J = 15.7, 7.4 Hz, 11H), 7.81 – 7.77 (m, 10H), 7.56 (d, J = 8.8 Hz, 7H), 6.73 (dd, J = 8.6, 2.7 Hz, 10H), 6.64 (d, J = 2.7 Hz, 7H), 6.14 (td, J = 3.9, 1.7 Hz, 7H), 3.78 (s, 28H), 2.90 (s, 28H), 2.87 – 2.78 (m, 21H), 2.69 (dt, J = 20.0, 7.6 Hz, 6H), 2.55 – 2.52 (m, 16H), 2.43 (ddd, J = 19.2, 14.5, 6.5 Hz, 8H), 2.27 – 2.21 (m, 11H), 2.17 (dtd, J = 13.8, 7.1, 2.1 Hz, 5H), 2.07 (dt, J = 4.4, 2.2 Hz, 24H), 2.05 – 2.00 (m, 14H), 1.87 – 1.74 (m, 24H), 1.60 (d, J = 4.1 Hz, 29H), 1.52 – 1.44 (m, 12H), 1.37 – 1.27 (m, 32H), 0.99 (s, 21H).

13C NMR (151 MHz, Acetone) δ 203.21, 159.46, 149.56, 142.26, 142.01, 138.25, 135.77, 130.56, 125.97, 125.69, 124.82, 124.68, 118.31, 114.18, 113.94, 113.48, 111.58, 80.34, 67.48, 55.60, 55.42, 53.45, 43.39, 42.95, 39.15, 30.68, 30.26, 30.13, 30.01, 29.88, 29.75, 29.62, 29.49, 25.45, 24.45, 22.95, 14.35.

KA20

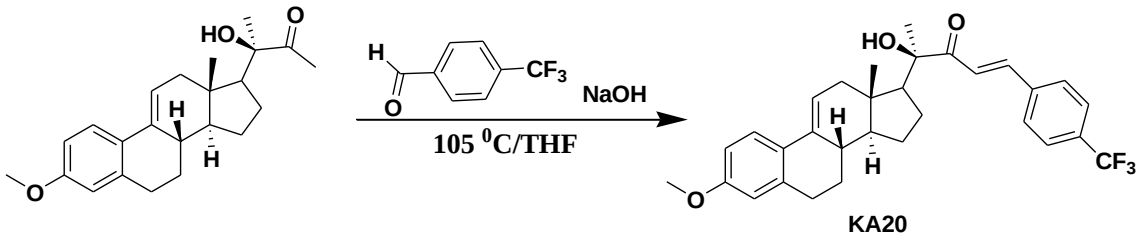

KA20

1H NMR (600 MHz, CDCl3) δ 8.29 (dd, J = 9.1, 2.0 Hz, 2H), 7.88 (d, J = 15.7 Hz, 1H), 7.78 (t, J = 5.5 Hz, 2H), 7.57 (d, J = 8.8 Hz, 1H), 7.22 – 7.18 (m, 1H), 6.76 (dd, J = 8.8, 2.7 Hz, 1H), 6.63 (d, J = 2.6 Hz, 1H), 6.14 – 6.12 (m, 1H), 3.82 (s, 3H), 2.95 – 2.88 (m, 1H), 2.86 – 2.81 (m, 1H), 2.61 (ddd, J = 17.3, 5.5, 1.7 Hz, 1H), 2.49 (d, J = 17.6 Hz, 1H), 2.09 (dd, J = 11.2, 9.5 Hz, 1H), 2.06 – 1.97 (m, 2H), 1.90 – 1.83 (m, 1H), 1.76 – 1.68 (m, 1H), 1.63 (d, J = 7.8 Hz, 3H), 1.55 – 1.48 (m, 1H), 1.36 (dddd, J = 11.6, 9.2, 6.4, 4.2 Hz, 3H), 1.01 (s, 3H).

13C NMR (151 MHz, CDCl3) δ 201.63, 158.39, 148.80, 142.55, 140.34, 137.54, 135.00, 129.25, 127.31, 125.14, 124.24, 122.25, 117.45, 113.27, 112.71, 79.42, 55.26, 55.12, 52.72, 43.05, 42.47, 38.18, 30.06, 28.61, 24.75, 23.97, 22.27, 13.82.

KA21

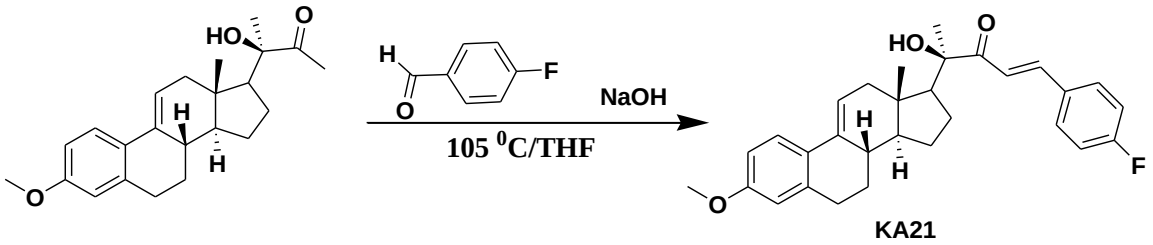

KA21

1H NMR (600 MHz, CDCl3) δ 7.96 – 7.93 (m, 5H), 7.87 – 7.82 (m, 9H), 7.57 (dd, J = 8.7, 5.2 Hz, 8H), 7.27 – 7.23 (m, 5H), 7.01 (s, 6H), 6.76 (dd, J = 8.7, 2.7 Hz, 7H), 6.73 – 6.67 (m, 4H), 6.63 (d, J = 2.6 Hz, 6H), 6.15 – 6.13 (m, 6H), 4.23 (s, 6H), 3.82 (s, 19H), 2.90 (ddd, J = 15.7, 13.8, 5.0 Hz, 11H), 2.86 – 2.76 (m, 12H), 2.61 (ddd, J = 17.3, 5.5, 1.6 Hz, 7H), 2.48 (d, J = 17.6 Hz, 8H), 2.30 (s, 4H), 2.12 – 2.01 (m, 23H), 2.01 – 1.96 (m, 14H), 1.91 – 1.82 (m, 13H), 1.73 – 1.67 (m, 15H), 1.60 (s, 20H), 1.53 – 1.48 (m, 11H), 1.46 (s, 23H), 1.01 (s, 17H).

13C NMR (151 MHz, CDCl3) δ 201.82, 190.55, 158.36, 144.51, 137.55, 134.99, 132.31, 132.24, 130.71, 130.65, 127.38, 125.55, 125.13, 118.01, 117.57, 116.47, 116.31, 116.17, 113.28, 112.69, 79.06, 55.25, 55.22, 52.75, 43.10, 42.39, 38.20, 34.25, 30.34, 30.08, 29.73, 28.63, 24.74, 24.06, 22.21, 13.78.

KA23

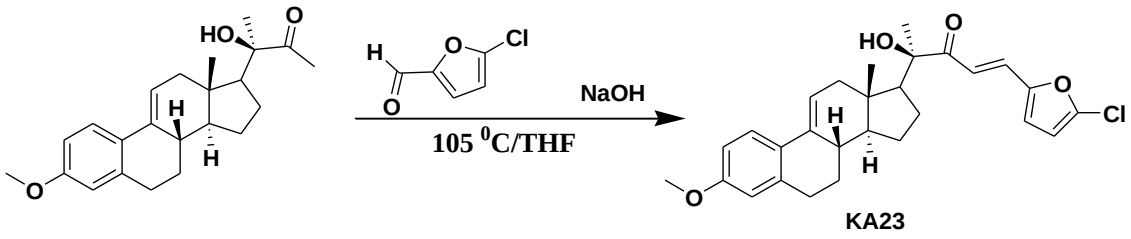

1H NMR (600 MHz, CDCl3) δ 7.39 (d, J = 8.7 Hz, 1H), 7.31 (dd, J = 10.9, 5.8 Hz, 1H), 6.72 – 6.69 (m, 1H), 6.57 (dt, J = 9.3, 3.2 Hz, 2H), 6.54 (d, J = 3.5 Hz, 1H), 6.44 (d, J = 2.7 Hz, 1H), 6.16 (d, J = 3.5 Hz, 1H), 3.63 (s, 4H), 2.76 – 2.68 (m, 2H), 2.67 – 2.65 (m, 1H), 2.39 (dddd, J = 19.6, 17.5, 5.6, 1.9 Hz, 2H), 2.32 (d, J = 17.6 Hz, 1H), 2.23 (dd, J = 15.4, 5.9 Hz, 1H), 2.08 (s, 1H), 1.89 – 1.83 (m, 4H), 1.53 – 1.45 (m, 3H), 1.39 (d, J = 2.5 Hz, 3H), 1.33 (s, 1H), 1.28 (s, 3H).

13C NMR (151 MHz, CDCl3) δ 201.67, 158.33, 150.67, 140.18, 137.53, 134.92, 130.25, 127.45, 125.15, 118.98, 117.69, 116.09, 113.28, 112.66, 109.76, 79.04, 55.25, 55.06, 52.70, 43.03, 42.38, 38.21, 30.33, 30.09, 29.72, 28.62, 24.76, 24.02, 22.19, 13.78.

3.4.2. Biological evaluations

Cytotoxicity assay

Two cell lines were used to carry out the cytotoxicity assay against pancreatic cancer, PANC-I and AsPC-1. In a 96-well plate, a total of $10x10^5$ cells were seeded. After 24 hrs, a serial dilution of the synthesized compounds (from 50 μM down to 3.125 μM as Quadruplicate for each concentration) was added to make the total volume 200 μL /well. 0.05% DMSO (Acros Organics) was used as a negative control and cuc B as a positive control. This was followed by incubation at 37 °C and 5% CO2 for 48 hrs. After 48 hrs, 20 μL of 3-(4, 5-dimethylthiazol-2-yl)-2, 5-diphenyl tetrazolium bromide (MTT) (Sigma Aldrich) (5 mg/mL PBS) was added to each well and the plate was incubated in the same conditions for 2hrs. The solutions were discarded from each well and 200 μL DMSO was added to each well and mixed. The absorbance was measured directly at 570 nm with a Hidex Sense Microplate reader.

In-cell western assay (ICW)

PANC-I cell line was seeded in clear-bottomed, black walled 96-well plates with a density of 1×10^5 cells/well and allowed to grow till confluency. Next, the cells were treated with different concentrations of KA19 or KA20 starting from ¼ to twice IC_{50} for 24 hrs. and DMSO was used as a -ve control. The cells were then fixed with 3.7% formaldehyde in 1X PBS for 30 min, then washed and permeabilized with 0.1% TritonX-100 in 1X PBS. Cells were then blocked with 1X PBS fish gel solution and incubated with an antibody to Erk (cell signaling technology), Phospho-Erk (Santa Cruz Biotechnology), and GAPDH (Santa Cruz Biotechnology) for 2 h with gentle shaking. They were then incubated overnight at 4

°C without shaking (i.e.: stationary). The cells were then washed with 0.1% Tween-20 in 1X PBS four times and incubated with secondary antibodies conjugated to IR dye for 1h with gentle shaking (protected from light). Cells were next washed with 0.1% Tween-20 in 1X PBS four times. After the last wash, any residual liquid was gently pipetted out and the plate was blotted dry using the In-cell Western protocol on an Odyssey® imager (LI-COR®), according to manufacturer's directions. Phospho-proteins were normalized for total protein signals. To correct for well-to-well variation in cell numbers, percent-inhibition was determined relative to control wells. Data are expressed as mean values of at least two runs ± the standard deviation (SD).

3.5. Conclusion

Molecular modeling study against known molecular targets of pancreatic ductal adenocarcinoma has been conducted to filter out the best candidates to be synthesized. The current structure-based drug design approach enabled us to synthesize 9 promising cucurbitacin-inspired analogs modified desaturated at C_9 and C_{11}, followed by cell viability MTT assay against two pancreatic ductal adenocarcinoma cell lines, among which two promising candidates KA19 and KA20 show promising IC_{50} values against pancreatic cancer cell lines PANC-I, 11.2 and 7.7 µM, and ASPC-I , 11.7 and 9.7 µM, compared to the current standard treatment gemcitabine. Furthermore, both compounds show promising inhibition of Erk phosphorylation at the double concentration of $IC_{50's}$,which support the obtained results from the molecular docking study that this group score higher than the other CIE analogs modified at C_{11}. Our results indicate that the modification of C_{11} can increase the antiproliferative activity compared to the non-modified CIE analogs.

3.6. References

1. Bray, F.; Ferlay, J.; Soerjomataram, I.; Siegel, R. L.; Torre, L. A.; Jemal, A. J. C. a. c. j. f. c., Global cancer statistics 2018: GLOBOCAN estimates of incidence and mortality worldwide for 36 cancers in 185 countries. **2018,** *68* (6), 394-424.

2. Rahib, L.; Smith, B. D.; Aizenberg, R.; Rosenzweig, A. B.; Fleshman, J. M.; Matrisian, L. M. J. C. r., Projecting cancer incidence and deaths to 2030: the unexpected burden of thyroid, liver, and pancreas cancers in the United States. **2014,** *74* (11), 2913-2921.

3. Malvezzi, M.; Carioli, G.; Bertuccio, P.; Boffetta, P.; Levi, F.; La Vecchia, C.; Negri, E. J. A. o. O., European cancer mortality predictions for the year 2017, with focus on lung cancer. **2017,** *28* (5), 1117-1123.

4. Zhang, X.; Shi, S.; Zhang, B.; Ni, Q.; Yu, X.; Xu, J. J. A. j. o. c. r., Circulating biomarkers for early diagnosis of pancreatic cancer: facts and hopes. **2018,** *8* (3), 332.

5. Eibl, G.; Cruz-Monserrate, Z.; Korc, M.; Petrov, M. S.; Goodarzi, M. O.; Fisher, W. E.; Habtezion, A.; Lugea, A.; Pandol, S. J.; Hart, P. A. J. J. o. t. A. o. N.; Dietetics, Diabetes mellitus and obesity as risk factors for pancreatic cancer. **2018,** *118* (4), 555-567.

6. Iodice, S.; Gandini, S.; Maisonneuve, P.; Lowenfels, A. B. J. L. s. a. o. s., Tobacco and the risk of pancreatic cancer: a review and meta-analysis. **2008,** *393* (4), 535-545.

7. Birks, S.; Peeters, A.; Backholer, K.; O'brien, P.; Brown, W. J. O. r., A systematic review of the impact of weight loss on cancer incidence and mortality. **2012,** *13* (10), 868-891.

8. Goess, R.; Friess, H. J. E. r. o. a. t., A look at the progress of treating pancreatic cancer over the past 20 years. **2018,** *18* (3), 295-304.

9. Heinemann, V. J. O., Gemcitabine: progress in the treatment of pancreatic cancer. **2001,** *60* (1), 8-18.

10. Neoptolemos, J. P.; Palmer, D. H.; Ghaneh, P.; Psarelli, E. E.; Valle, J. W.; Halloran, C. M.; Faluyi, O.; O'Reilly, D. A.; Cunningham, D.; Wadsley, J. J. T. L., Comparison of adjuvant gemcitabine and capecitabine with gemcitabine monotherapy in patients with resected pancreatic cancer (ESPAC-4): a multicentre, open-label, randomised, phase 3 trial. **2017,** *389* (10073), 1011-1024.

11. de Sousa Cavalcante, L.; Monteiro, G. J. E. j. o. p., Gemcitabine: metabolism and molecular mechanisms of action, sensitivity and chemoresistance in pancreatic cancer. **2014,** *741*, 8-16.

12. Gilbert, J. A.; Salavaggione, O. E.; Ji, Y.; Pelleymounter, L. L.; Eckloff, B. W.; Wieben, E. D.; Ames, M. M.; Weinshilboum, R. M. J. C. C. R., Gemcitabine pharmacogenomics: cytidine deaminase and deoxycytidylate deaminase gene resequencing and functional genomics. **2006,** *12* (6), 1794-1803.

13. Bian, Y.; Yu, Y.; Wang, S.; Li, L. J. B.; communications, b. r., Up-regulation of fatty acid synthase induced by EGFR/ERK activation promotes tumor growth in pancreatic cancer. **2015,** *463* (4), 612-617.

14. Miro, M. J. P. r., Cucurbitacins and their pharmacological effects. **1995,** *9* (3), 159-168.

15. Nakamura, H.; Kawasaki, N.; Taguchi, M.; Kabasawa, K. J. T., Survival impact of epidermal growth factor receptor overexpression in patients with non-small cell lung cancer: a meta-analysis. **2006,** *61* (2), 140-145.

16. Verbeek, B. S.; Adriaansen-Slot, S. S.; Vroom, T. M.; Beckers, T.; Rijksen, G. J. F. l., Overexpression of EGFR and c-erbB2 causes enhanced cell migration in human breast cancer cells and NIH3T3 fibroblasts. **1998,** *425* (1), 145-150.

17. Ahmed, M. S.; Halaweish, F. T. J. J. o. e. i.; chemistry, m., Cucurbitacins: potential candidates targeting mitogen-activated protein kinase pathway for treatment of melanoma. **2014,** *29* (2), 162-167.

18. Mahnashi, M. H., Design, Synthesis and Biological Screening of Novel Cucsinspired Estrone Analogues Towards Treatment of Hepatocellular Carcinoma. **2017**.

19. Abou-Salim, M. A.; Shaaban, M. A.; El Hameid, M. K. A.; Elshaier, Y. A.; Halaweish, F. J. B. c., Design, synthesis and biological study of hybrid drug candidates of nitric oxide releasing cucurbitacin-inspired estrone analogs for treatment of hepatocellular carcinoma. **2019,** *85*, 515-533.

20. Ahmed, M. S.; El-Senduny, F.; Taylor, J.; Halaweish, F. T. J. C. b.; design, d., Biological screening of cucurbitacin inspired estrone analogs targeting mitogen-activated protein kinase (MAPK) pathway. **2017,** *90* (3), 478-484.

21. Ahmed, M. S.; Kopel, L. C.; Halaweish, F. T. J. C., Structural optimization and biological screening of a steroidal scaffold possessing cucurbitacin-like functionalities as B-raf inhibitors. **2014,** *9* (7), 1361-1367.

22. Ahmed, M. S.; Kopel, L. C.; Halaweish, F. T., Structural optimization and biological screening of a steroidal scaffold possessing cucurbitacin-like functionalities as B-raf inhibitors. *ChemMedChem* **2014,** *9* (7), 1361-1367.

23. Stamos, J.; Sliwkowski, M. X.; Eigenbrot, C., Structure of the epidermal growth factor receptor kinase domain alone and in complex with a 4-anilinoquinazoline inhibitor. *Journal of Biological Chemistry* **2002,** *277* (48), 46265-46272.

Chapter Four

Synthesis and Biological Activity of C-11 Hydroxy Cucurbitacin-Inspired Estrone Analogs Targeting Pancreatic Ductal Adenocarcinoma

Abstract

Pancreatic cancer was the fourth leading cause of cancer-related deaths in 2016. However, the long-term survival rate is low, compared to other cancer types, due to poor prognosis and low survival after treatment with the standard drug, gemcitabine. This suggests an urgent need to investigate for new treatment agents. Recently, the triterpenoid natural product, cucurbitacin B, showed promising antiproliferative activity against human pancreatic cancer cells in a dose- and time-dependent manner. However, the low yield of cucurbitacin from its natural sources and the challenging chemical total synthesis due its highly stereochemical complexity hindered its usage in clinical trials. In order to overcome this obstacle, molecular modeling studies were performed against known molecular targets of pancreatic cancer, using a novel strategy that uses estrone as a scaffold with cucurbitacin pharmacophores. More than 400 virtual compounds were designed by installing the cucurbitacin pharmacophores, such as various 23, 24 α, β- unsaturated ketone side chains, on estrone with different functionalizations at C_{11}. This was followed by molecular docking against known pancreatic cancer molecular targets, such as the proteins EGFR, JAK, STAT3, Raf, Ras, Erk, Akt and PI3K. The molecular docking study showed a promising binding affinity for the cucurbitacin-estrone hybrid analogues, substituted with a hydroxy group at C_{11}. Using this approach, 8 analogs were synthesized through 12 steps, followed by an MTT cell viability assay against PANC-I, AsPC-I, and BXPC-3 pancreatic cell lines.

Three C_{11} hydroxyl analogs KA1, KA2, and KA11 containing phenyl *para*-trifluoro, cucurbitacin, and phenyl *para*-methtylthio side chains, showed promising IC_{50} values. The first two were further studied in cell cycle arrest. Also, the cell cycle arrest for KA1 and KA2 was studied at different time points. In order to further investigate the effectiveness of these two analogs, they were evaluated against 2D and 3D pancreatic cancer cell line PANC-I using cell Titer assay. KA1 and KA2 were proven to increase caspase-3 activity and induce cell death. Our results indicate that KA1 and KA2 are promising antiproliferative agents and are possible candidates for clinical study. Moreover, our results indicate that additional modifications to the cucurbitacin-inspired estrone analogs may lead to more potent antiproliferative agents.

4.1. Introduction

Among cancer types, pancreatic cancer is the only type that has demonstrated a stable rate of mortality.[1] Pancreatic cancer is currently the fourth leading cause of death among cancer types[2], and is expected to be the second in the next twenty years.[3] The reason for the high mortality of pancreatic cancer is the absence of biomarkers that can be detected in its early stages.[4] Moreover, the development of pancreatic anticancer agents is still slow.[5]

The current treatments for pancreatic cancer are correlated with the stage of the disease. Only 20% of pancreatic ductal adenocarcinoma patients can be treated with surgery, while the remaining patients are diagnosed after the disease reaches its late stages.[6] The current standard chemotherapy treatment for pancreatic cancer is gemcitabine; however, it has an 18% one-year survival rate, which is significantly better than the former standard, 5-fluorouracil (5-FU) that has only a 2% 1-year survival rate.[7] The six-month survival rates

for gemcitabine and 5-FU are 23.8% and 4.8%, respectively. These data highlights the urgent need to investigate for novel agents for pancreatic cancer treatments.

Epidermal transmembrane factor receptor (EGFR) is a 170 kd glycoprotein and one of tyrosine kinase that is overexpressed in many cancer types, including pancreatic cancer. EGFR overexpression was found to be related to the advancement of the disease, its low survival rate, and metastasis.[8, 9]

Natural products have been the main source for drug discovery until recent times. From 1981 to 2010, statistics indicate that almost two-thirds of the approved drugs were related to natural products, either directly by using the natural products or indirectly through chemical modification and structure replication of the useful compounds.[10] Approximately 47% of the approved anticancer drugs were derived from natural products, which indicates the importance of these products in the discovery of novel anticancer agents.[11] One of these natural products is cucurbitacins (**Figure 4.1**), a group of triterpenoid compounds that contain cucurbitane ring and are characterized by bitterness and toxicity.[12, 13] Currently, more than 18 types of cucurbitacins have been found, among which 9 compounds have been reported to have anticancer activity against lung, breast, colon, and pancreatic cancers.[14,15, 16] Moreover, cucurbitacins also have other biological effects, such anti-inflammatory and antiviral activities.[17]

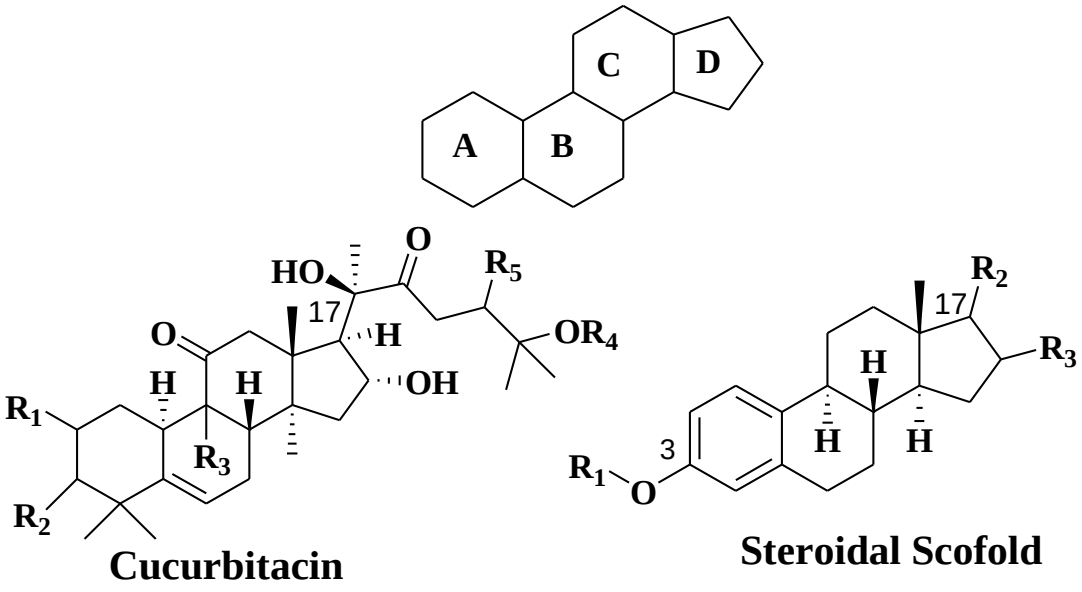

Figure 4.1. General structures of cucurbitacin and steroid

In 2010, Lwanski *et al.* reported that a relatively low dose of cucurbitacin B, in combination with gemcitabine (0.5 mg/Kg and 25 mg/Kg, respectively), resulted in a significant decrease in tumor size.[10] The mechanism of action for cucurbitacin B included inhibition of STAT3 phosphorylation, activation of caspase 3, and upregulation of p53 and p21 expression.[18] Cucurbitacin E showed antiproliverative activity against pancreatic cancer through inhibition of STAT3 phosphorylation and upregulation of the tumor suppressor p53.[19,20] However, one of the challenges that prevents the use of cucurbitacins as anticancer remedies is the difficulty of separating the natural sources due to their polarity and the minute amounts that are obtained after separation. Moreover, the oxygenated A, C, and D and the stereochemistry of cucurbitacin represent a challenge in attempting the total synthesis of cucurbitacins, although successful trials have synthesized rings C and D of

cucurbitacin I.[21] One of the important pharmacophores is the 23, 24 α, β- unsaturated ketone side chain that is responsible for the anticancer activity of cucurbitacin.[22] Interestingly, this side chain was installed in the four membered-rings estrone, and it shows a comparable anticancer activity to that of cucurbitacin.[23] These cucurbitacin-inspired estrone analogues (CIEA's) opened the door for further functionalization of these family of compound in different positions. Molecular modeling was employed to search for more potent anticancer compounds through the modeling of these novel analogs against known cucurbitacin molecular targets.

Up to date, we have proved that the functionalization of rings B and C leads to potent anticancer agents which are more active than the currently available standard treatments. Previously, we reported that the dehydrogenation of C_9-C_{11} and C_{16}-C_{17} generally increased the potency of this group of compounds.[24, 25] Moreover, the methylation of C_3 increased the potency relative to the originally found phenol. The other modifications include the introduction of many functional groups at the cucurbitacin side chain, such as *para*-trifluoromethyl through aldol condensation, which showed potent anticancer activity.[26] Here, we report molecular modeling of more than 400 virtual CIEA's analogs with synthesis of a 8 CIE analogs functionalized at C_{11}, and screening them using MTT cell viability assay against 3 pancreatic cancer cell lines PANC-I, AsPC-I, and BXPC-I followed by flowcytometric analysis of the most potent CIEA's at different time points.

4.2. Results and Discussions

4.2.1. Molecular Modeling Design Strategy

Based on the previously obtained results regarding CIE analogs, it was found that transferring the C_3 OH group into ether can increase the anticancer activity of these

compounds. Also, through molecular modeling studies, we found that the introduction of various side chains, such as phenyl *para*-trifluoromethyl and phenyl *para*-thiomethyl at C_{17} on ring D of estrone can result in high scoring analogs against many molecular targets, such as EGFR. Therefore, to investigate further, we designed additional analogs with a hydroxy group at C_{11} and carried out the molecular modeling analysis on molecular targets reported to be expressed in pancreatic ductal adenocarcinoma.

A virtual library of 400 CIEA compounds were designed to mimic cucurbitacin compounds with various functional groups in positions C_3 and C_{11}, as well as several methyl hydroxy enon side chains at position C_{17}. Also, cucurbitacins B and D were used as standards for the molecular targets. Molecular modeling results indicate that 8 compounds (**Figure 4.2**) show a better binding affinity to EGFR and other molecular targets such as STAT3, Akt, PI3K, than the standards, erlotinib, cucurbitacin B and D. One of the high scoring compounds is KA1, a CIE analog with C_{11} hydroxy and a phenyl *para*-trifluoro enone side chain. This demonstrated hydrogen bonding with Pro: 770: A at EGFR binding site (**Figure 4.3 A**), close to the erlotinib hydrogen binding site with Met: 769: A (**Figure 4.3B**). In addition, KA2 and KA11, containing a cucurbitacin and a phenyl *para*-thiomethyl side chains, respectively, showed promising binding affinity to EGFR compared to the previously mentioned standards. This indicates that the hydroxyl group modification may increase the binding affinity to known pancreatic cancer molecular targets.

Table 4.1. The consensus scores of hydroxylated C_{11} CIE analogs on the EGFR binding pocket.

VIDA Name	PLP	Chemgauss3	OEChemscore	Screenscore	Consensus Score
KA11_43	-51.7283	-66.5209	-39.2823	-116.575	26
KA8_153	-48.7798	-68.3666	-40.7735	-103.059	31
KA3_126	-51.8626	-51.2126	-41.1819	-109.046	32
KA6_73	-55.8415	-47.2346	-42.2838	-104.658	35
KA1_72	-47.2135	-80.9063	-35.1766	-118.451	36
KA7_143	-48.619	-70.2779	-39.9259	-97.2335	37
KA4_156	-45.7753	-68.0197	-40.0748	-99.0202	42
KA5_62	-48.1965	-66.2347	-35.877	-102.4478	52
CucD_197	-40.4721	-54.3241	-38.0069	-92.221	67
Iso B_113	-39.2614	-50.7752	-38.6223	-89.5715	73
KA10_64	-39.3671	-67.012	-33.2958	-89.5334	74
Iso D_37	-35.4754	-44.8475	-41.7118	-80.8827	82
KA15_1	-37.2535	-61.1314	-31.4152	-81.4897	88
Cucurbitacin I	-33.1051	-41.8658	-41.5028	-78.295	89
Cucurbitacin E	-35.7174	-48.0769	-38.0201	-73.3811	90
Erl_38	-39.3291	-53.9956	-33.5598	-84.2492	90

Molecular docking was also carried out against the previously reported targets for cucurbitacin, including the MAPK signaling pathway proteins (EGFR, RAS, RAF, MEK, and ERK proteins. (**Figure 4.4**)

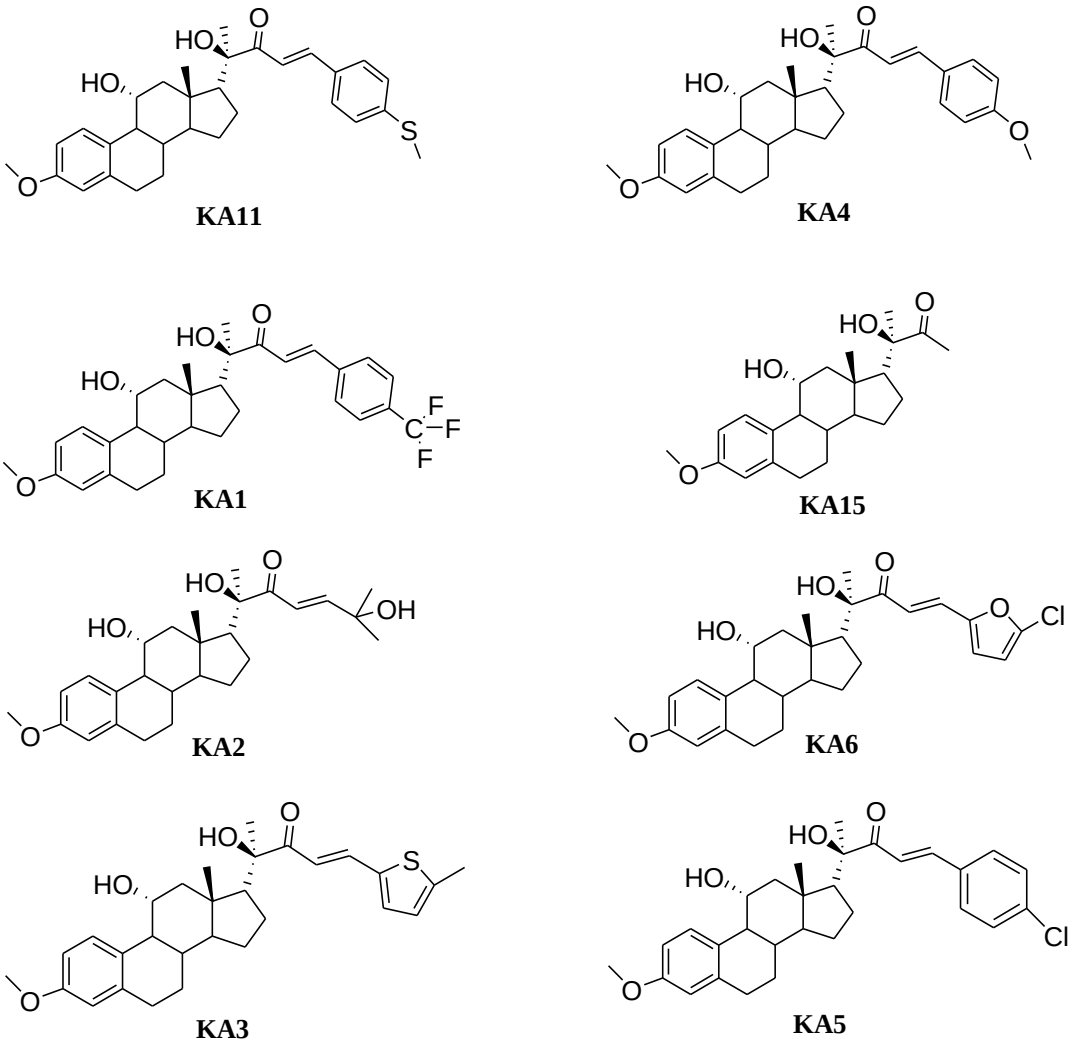

Figure 4.2. The structures of the synthesized oxygenated cucurbitacin-inspired analogs.

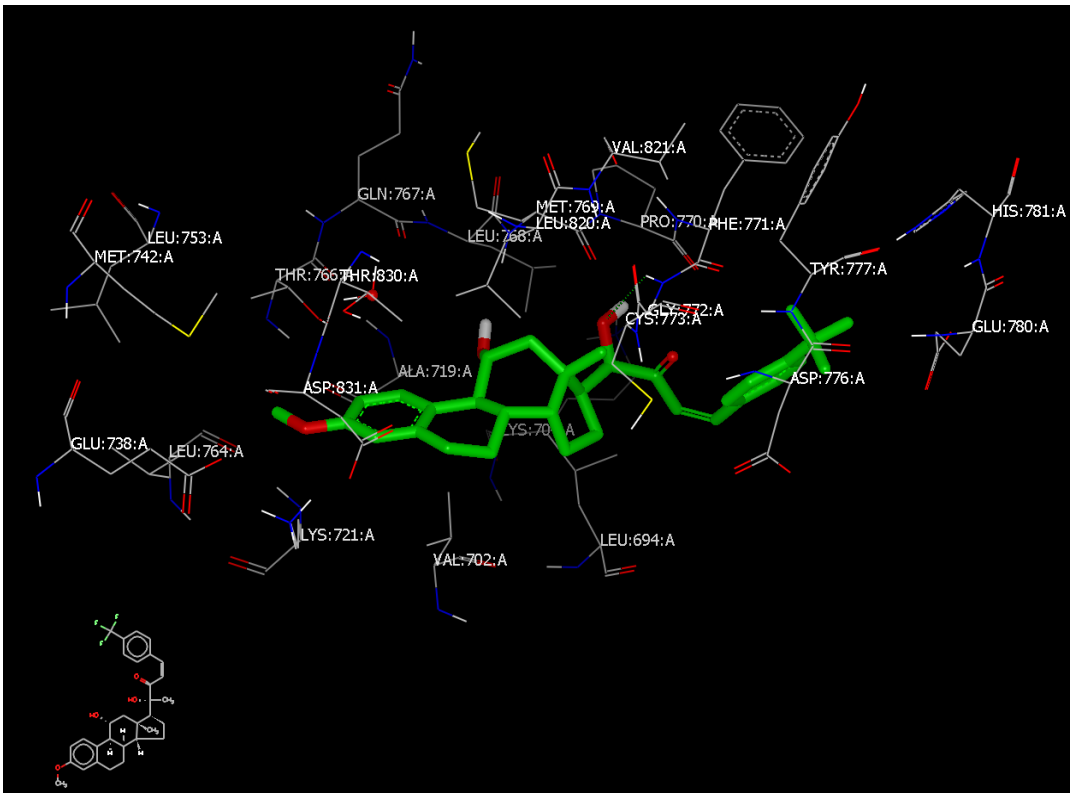

A.

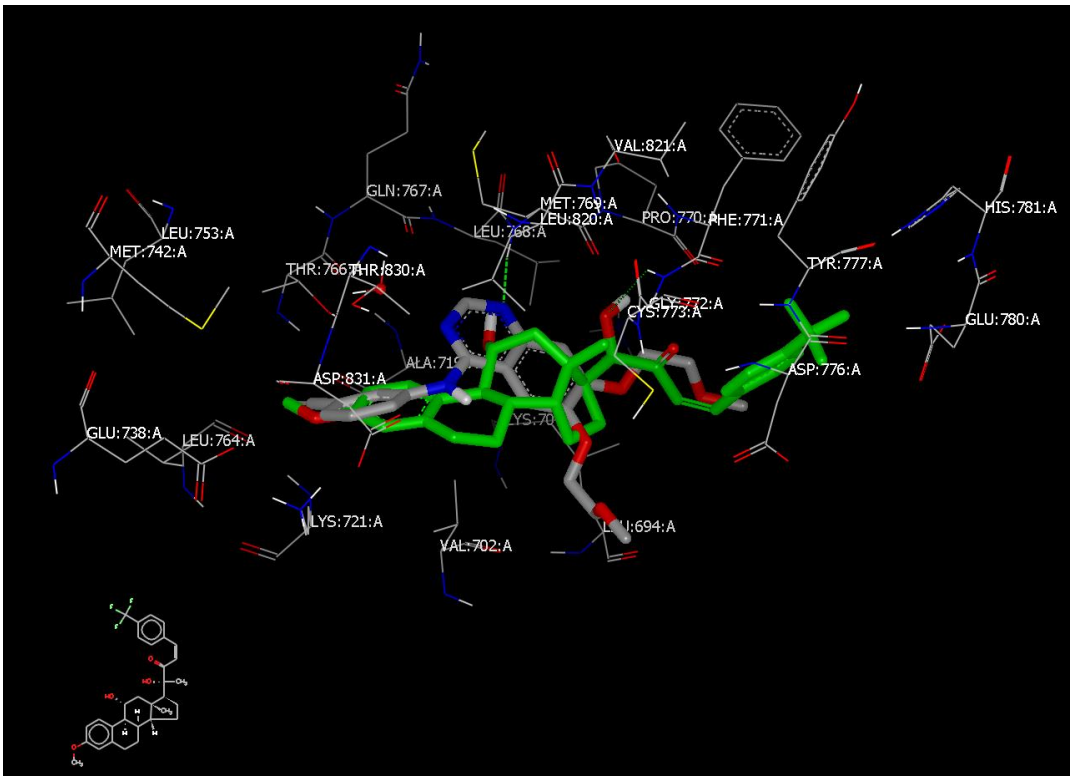

B.

Figure 4.3. A) Binding of KA1 into EGFR ATP binding pocket. B) Overlay with erlotinib binding in the same pocket.

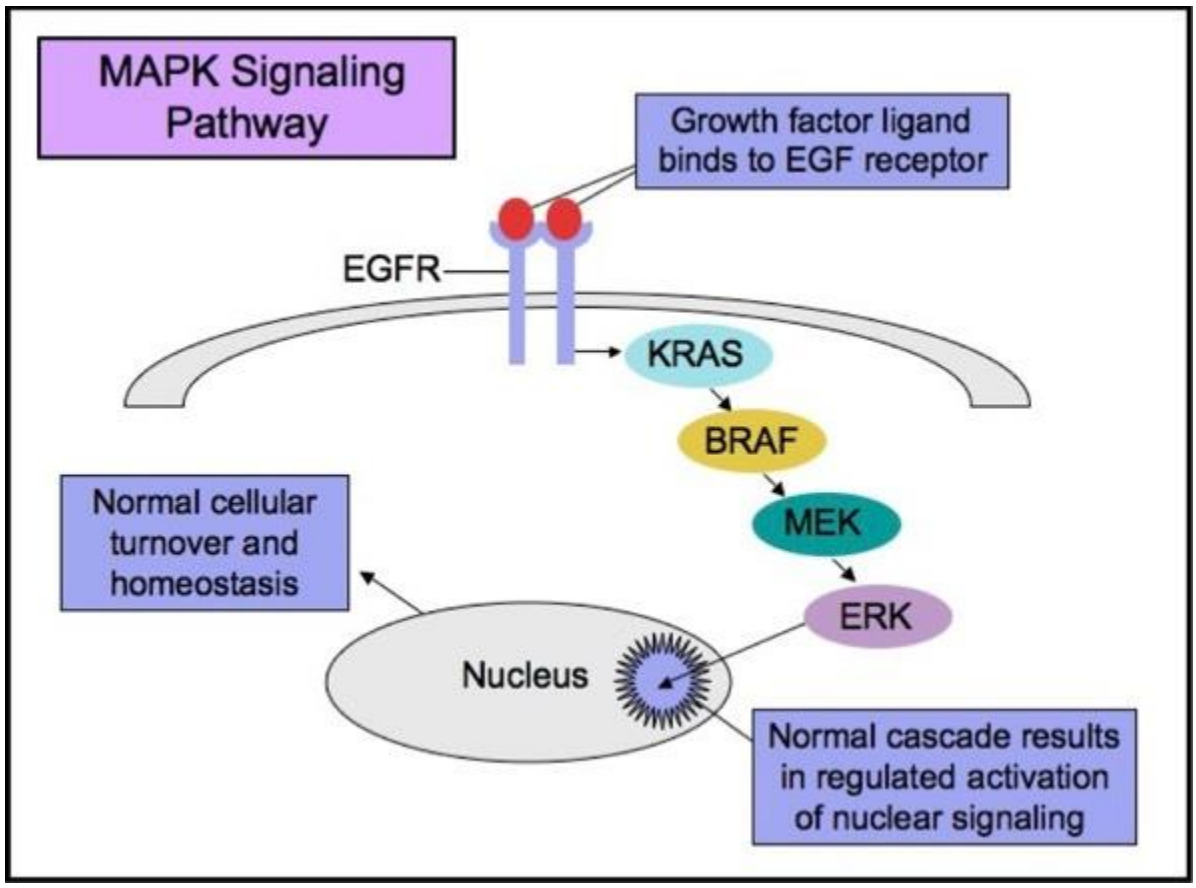

Figure 4.4. The major targets of MAPK signaling pathway.[27]

Generally, up on the docking against EGFR, the best-scoring compounds contained ketone, followed by analogs containing hydroxyl functional groups at C_{11}, which scored better than the analogs desaturated at C_9 and C_{11}.

4.2.2. Chemical Synthesis

Scheme 1 shows the general route for the synthesis of the best scoring compounds. The chemical challenge that prevented the convergent synthesis for the CIEA analogs using Grignard reaction was the stereochemistry product of at C_{20}, where the major product was

S instead of R, as in a cucurbitacin side chain. So, the first step was oxidation of C_9-C_{11} of estrone using DDQ. The best yield for this step was obtained upon its reaction with estrone, rather than with methylated estrone; however, the next step was run on the crude extract due to the poor solubility of the product and, therefore, its purification. Following this, was the formation of a ketal at C_{17} to avoid side reactions upon the hydroboration hydroxylation reaction. One of the chemical challenges for the synthesis of the target analogs was the hindrance of position C_{11}, as will be indicated below. Three reagents were used to carry out the hydroboration. With 9-BBN, no hydroboration was obtained, while hydroboration with BH_3 yielded 28% of the hydroxylated product. However, the highest yield in this reaction was obtained with $(CH_3)_2SBH_3$ at 60%. After the purification of KI3 and its deprotection was carried out using 10% HCl/ acetone mixture to obtain KI4. The protection of the C_{11} hydroxyl group was initially carried out by TBSCl in DMF in presence of imidazole. However, no product was obtained, although it was previously found that this reaction worked with C_3 phenolic OH using the same conditions, which further indicates that this position is hindered by the stereochemistry of the compound. TMS-protection was performed and worked successfully, but it was not stable after Wittig reaction to produce KI6; some of the product was deprotected. This indicates that TBS protection was the only choice to proceed through the synthetic route. A convenience method for protection of the hindered hydroxyl groups, such as tertiary alcohols or secondary alcohols adjacent to a tertiary alcohol was reported, using Mg turnings as a catalyst in DMF with TBSCl. Upon using this condition to protect the C_{11} hydroxyl group, a 90% yield of KI5 was obtained. The installation of the cucurbitacin side chain was gained through the Wittig reaction, followed by hydroboration oxidation using 9-BBN as a hydroboration reagent. The

oxidation of the hydroxyl group and the cyanohydrin formation was performed as indicated in the experimental section. KI10 was obtained after methylation and the formation of a hydroxy-methyl ketone from the imine. In order to indicate the stereochemistry of the hydroxy group in $C_{11\ at}$ the key intermediate hydroxy-methyl ketone KI10, X-ray crystallography for KI10a was carried out (**Figure 4.5**). The aldol condensation reaction was performed using LDA at -78 °C due to the low boiling point of the TBS protected iso-propyl aldehyde compared to the other indicated aldehydes. This boiling point is much lower than the other used aldehydes that were reacted using NaOH at 105 °C.

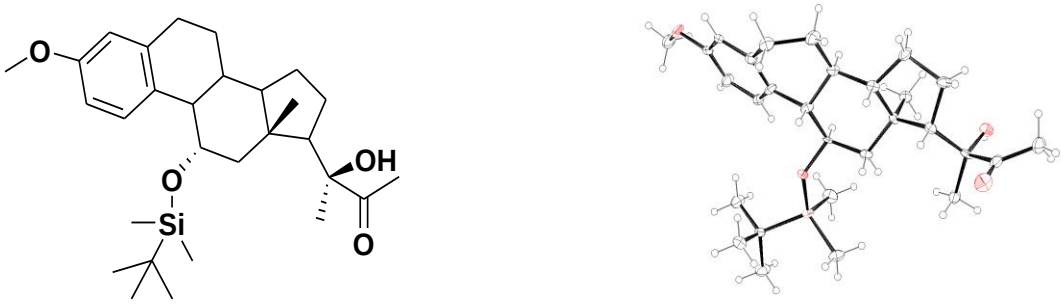

Figure 4.5. X-ray crystal structure of KI10 indicates that the stereochemistry of C_{11} is an R configuration.

The products KI11-KI18 were used to synthesize the target final compounds. The general procedure to deprotect the hydroxylated C_{11} was using 12 equivalence of TBAF and running the reaction for 72 hrs. in order to obtain the products KA1-KA8. The high equivalence of TBAF and the long period of time needed is also proof for the hindrance of this position (**Scheme 2**).

4.2.3. Biological Evaluation

All the synthesized compounds were screened against three pancreatic cell lines: BXPC3, PANC-I, and AsPC-I, as noted in **Table 4.2**. The results indicate that the compounds KA1 and KA2, containing a phenyl *para*-trifluoro side chain and cuc side chain, respectively, are the most potent analogs. Generally, based on MTT results, the presence of a hydroxyl group increases the antiproliferative activity of the synthesized compounds.

Table 4.2. IC_{50} results of the synthesized CIE analogs after treatment with 3 pancreatic cancer cell lines

Compound	PANC-I IC_{50} (µM)	AsPC-I IC_{50} (µM)	BXPC-3 IC_{50} (µM)
KA1	5.52	11.2	4.7
KA2	12.81	16.28	10.89
KA3	>100	NA	85.9
KA4	44.71	49.04	49.04
KA5	NA	NA	NA
KA6	NA	NA	NA
KA11	NA	NA	NA
KA15	NA	NA	NA
Gemcitabine	>100	>100	>100

To further investigate the mechanism of action of KA1 and KA2, cell cycle analysis was carried out in 24, 48, and 72 hrs. periods to investigate the inhibition at different time points. The results confirm that both CIE analogs accumulate cells during the G1 phase in 24 hrs; however, inhibition decreased after this point.

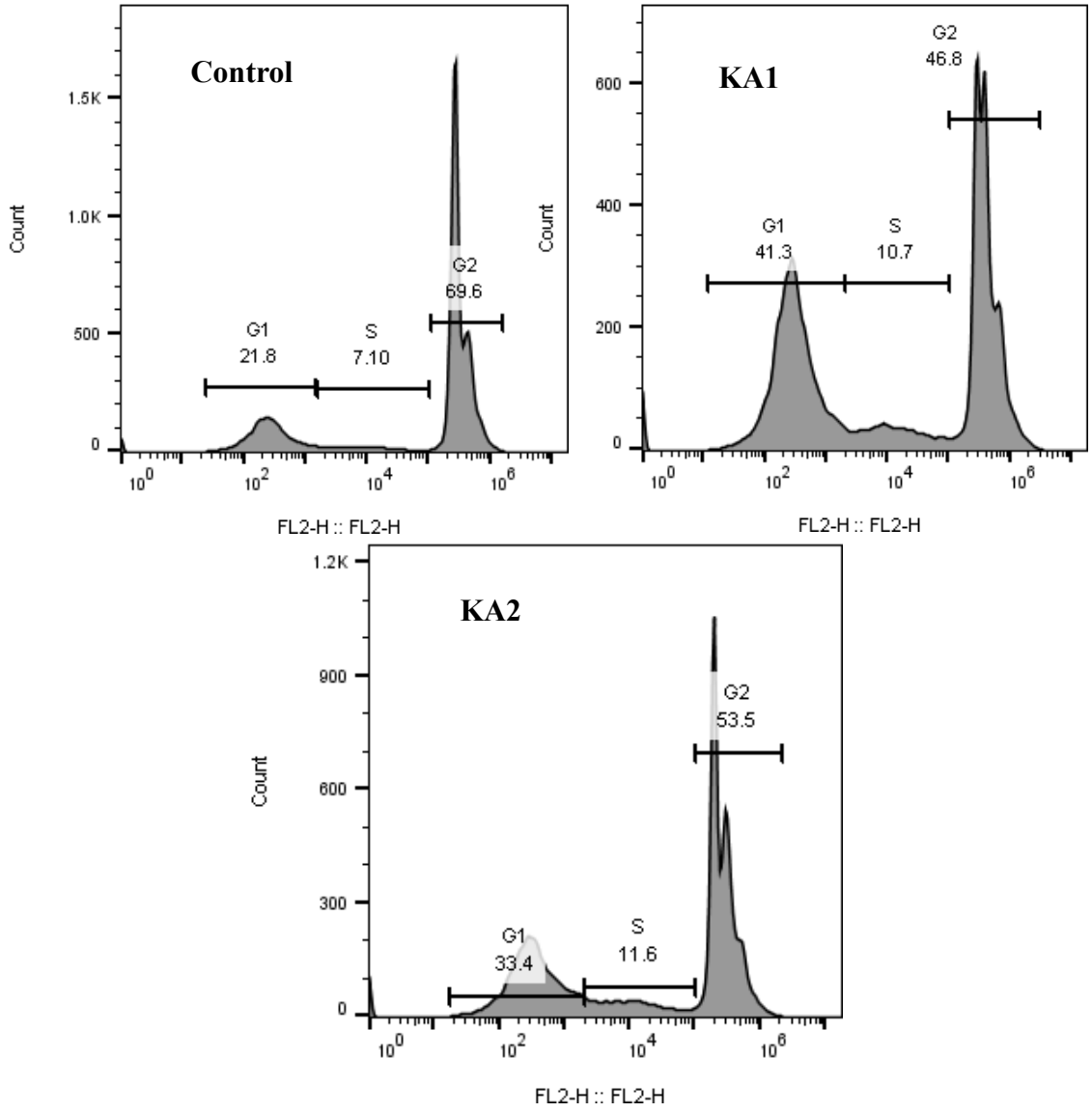

Figure 4.6.A. Cell cycle analysis for KA1 and KA2 after 24

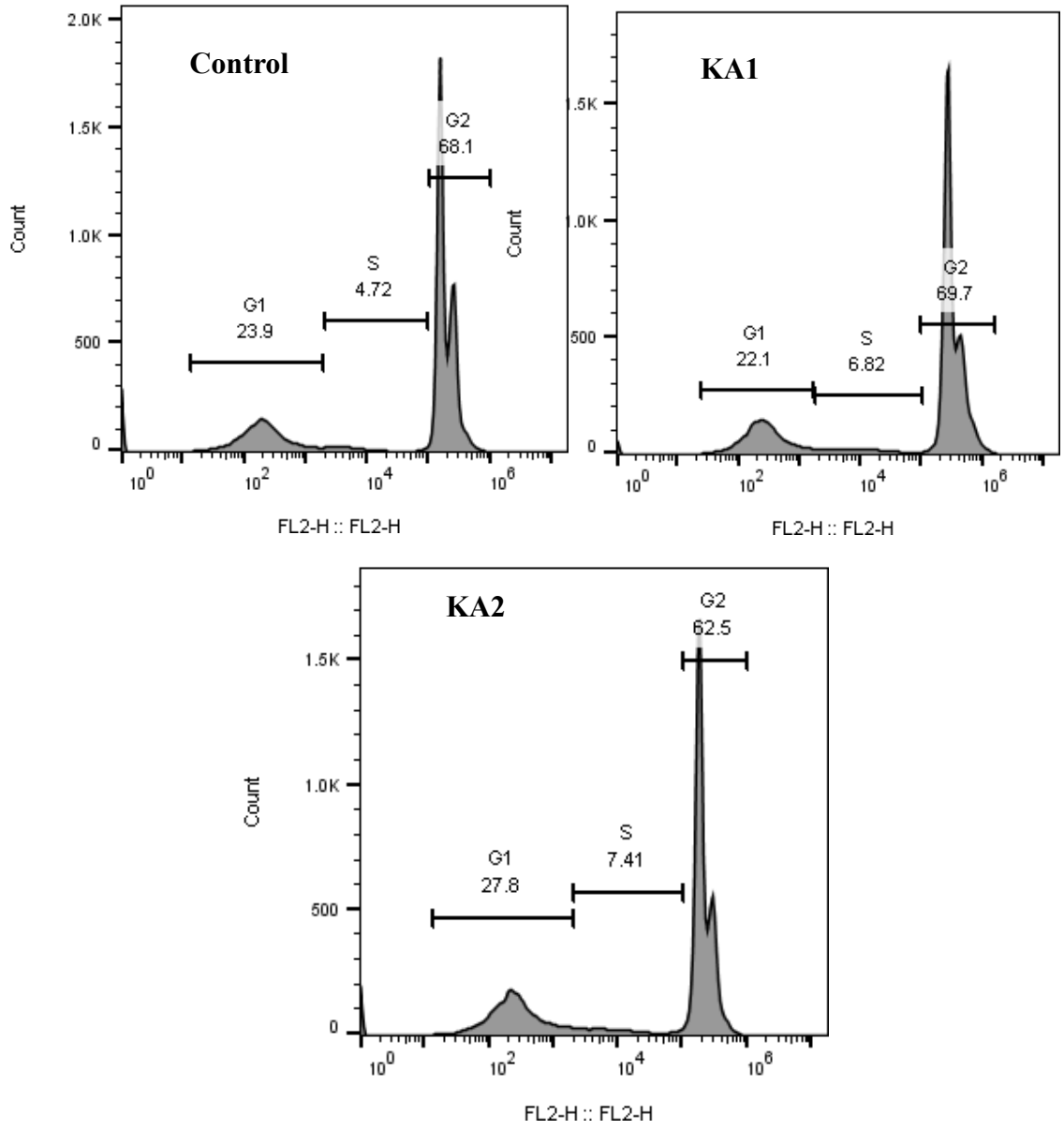

Figure 4.6.B. Cell cycle analysis for KA1 and KA2 after 48.

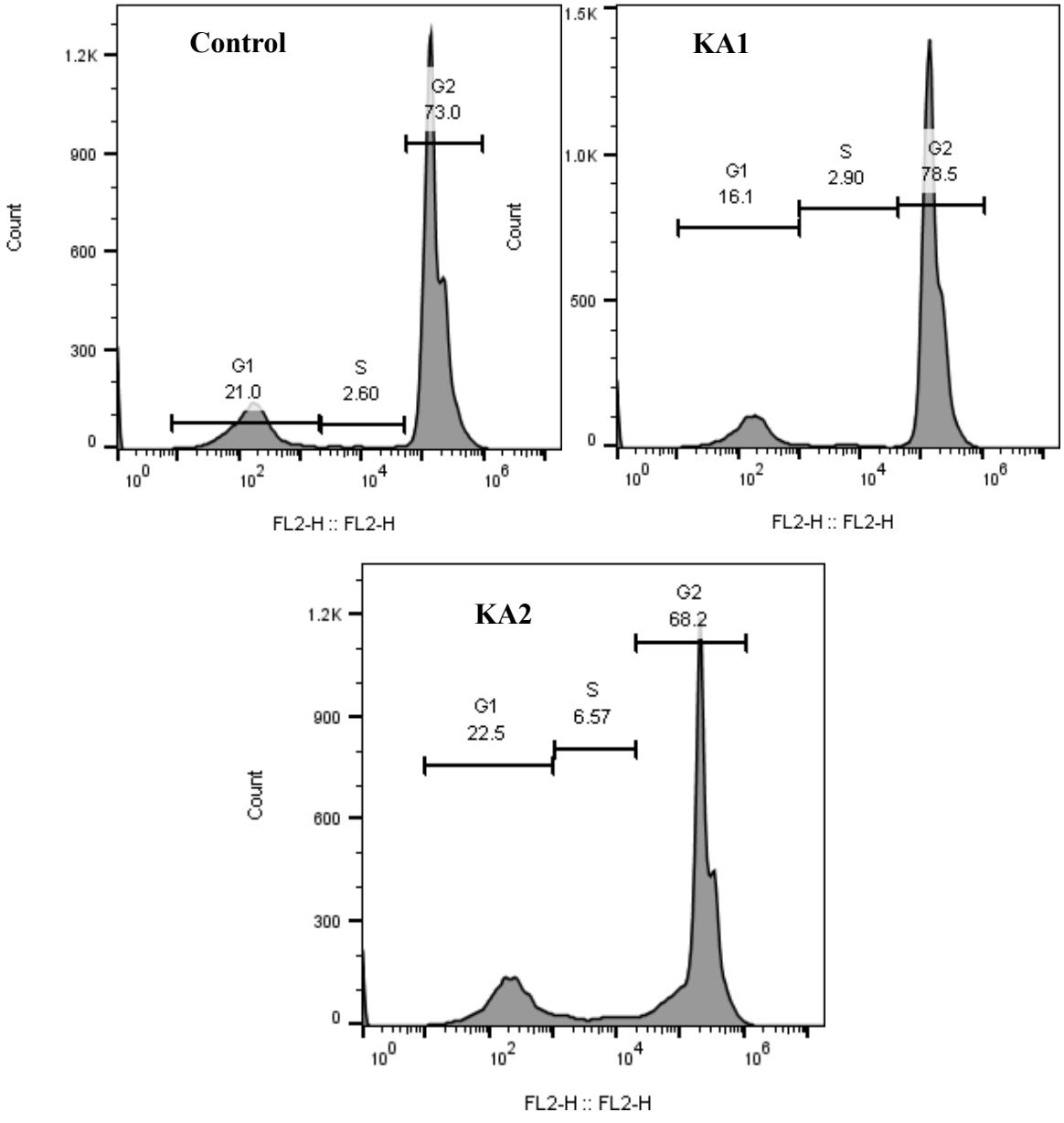

Figure 4.6.C. Cell cycle analysis for KA1 and KA2 after 72.

4.3. Material and methods

4.3.1. Molecular Modeling

The molecular modeling studies were carried using two OpenEye software programs, [28] Omega to generate the conformers of the compounds and FRED to allow rigid exhaustive docking.[29] The targets for the previously mentioned proteins were processed and generated using MakeReceptor®. After the molecular docking was carried out, the consensus scores were visualized using VIDA software.

4.3.2. Chemical Synthesis

General**:**

All chemicals and solvents (ACS grades) were purchased from Fisher Scientific or Sigma Aldrich and used without any additional treatment. Before conducting the experiments, all the glassware and tools were cleaned, washed and dried in a 120 °C oven. Before the reaction the flasks were closed and flushed with nitrogen gas for all of the reaction period, except when mentioned during the experiment. TLC plates (Silica gel, 0.2-mm thick, polyester backed, Sorbtech) were used to analyze the reaction conditions under UV254. All synthetic intermediates and final compounds were purified using column chromatography packed with silica gel 60A, 40-63 μm. ^{1}H and ^{13}C NMR spectra were carried out using Bruker AVANCE-400 MHZ and 600 MHZ NMR spectrometers. The solvents used for the compounds were $CDCl_3$, as will be indicated later. NMR chemical shifts were presented in δ(PPM) using residual solvent peaks as standards ($CDCl_3$, 7.26 (^{1}H), 77.16 (^{13}C)). High resolution mass (HRMS) was performed using Thermofinnigan MAT 95XL mass spectrometer at the Buffalo mass spectroscopy facility. X-ray

crystallography was conducted on KI9 at the University of South Dakota using a Bruker APEX^{II} diffractometer.

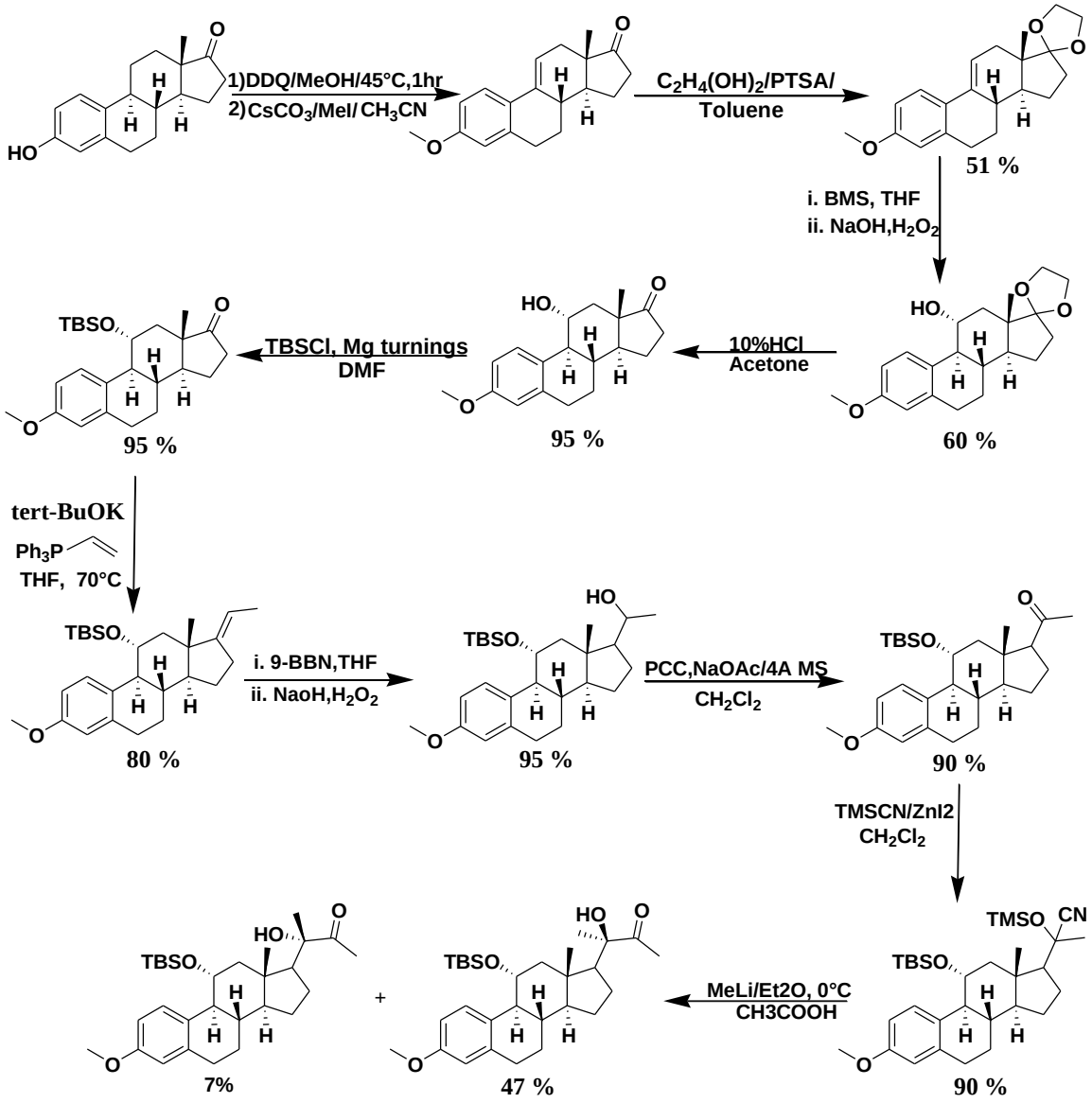

Scheme 1. Synthesis of the main intermediate, KI10.

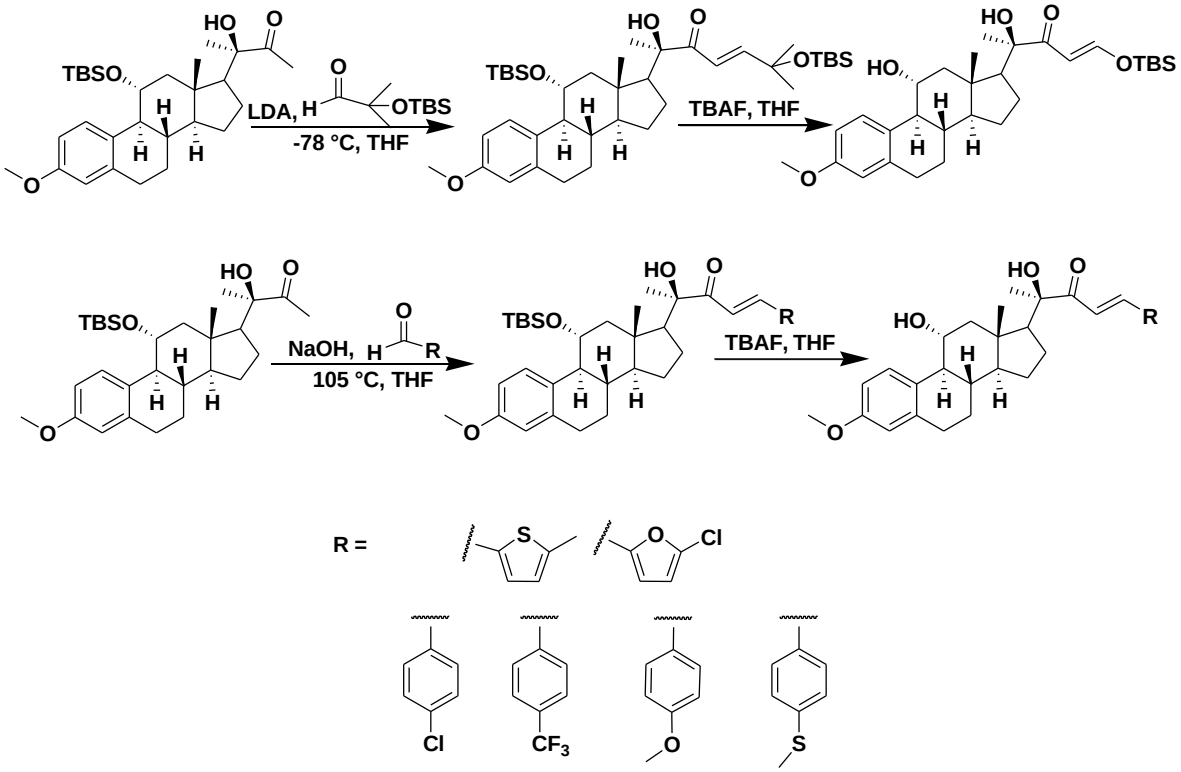

Scheme 2. Aldol condensation and C_{11} hydroxyl deprotection for the hydroxylated CIE analogs.

KI2

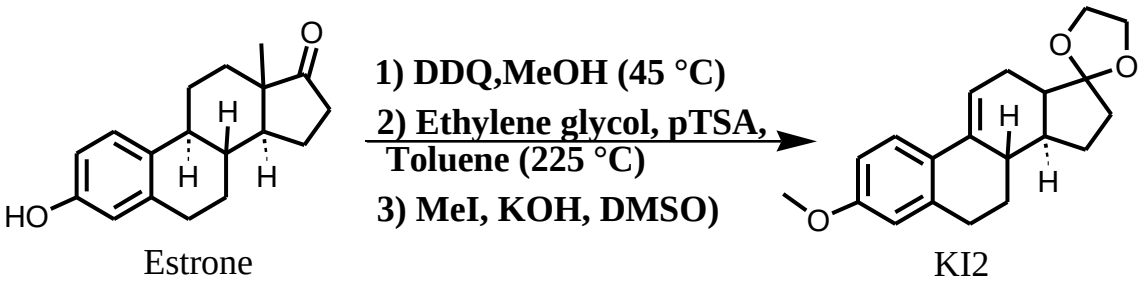

Estrone KI2

To a stirred solution of estrone (5g, 18.49 mmole) in 600 ml of methanol at a temperature of 47 ^{0}C, 2, 3-Dichloro-5, 6-dicyano-1,4-benzoquinone (DDQ) (6.3 g, 27.74 mmole) was added. The reaction was stirred for 5 hrs. and the reaction progress was tested by TLC using 6:4 (hexane: ethyl acetate mixture) followed by the evaporation of methanol using a vacuum. The crude extract was dissolved in 308 ml of toluene to proceed to the next reaction. The solution was heated to 205 ^{0}C. Ethylene glycol (4.53 ml, 81.49 mmole) was poured into one portion, and then *para*-toluene sulfonic acid (0.212 g, 11.19 mmole) was added. The reaction mixture was stirred and refluxed for 8 hours using a Dean-Stark apparatus to eliminate the condensed water; this prevented it from returning to the reaction mixture and reversing the reaction. The reaction was cooled to room temperature, then a saturated $NaHCO_3$ solution was added to quench the reaction. Ethyl acetate (3 ^{x} 100 ml) was used to extract the aqueous layer, then the organic layer was dried over anhydrous $NaSO_4$ and evaporated. The crude material was dissolved in DMSO (90 ml), followed by the addition of crushed granulate potassium hydroxide (4.032 g, 86.46 mmole); next, methyl iodide (2.24 g, 35.94 mmole) was added to the reaction mixture. The reaction was

stirred at room temperature for 2 hours, quenched by the addition of water (400 ml) and stirred for 15 minutes. Ethyl Acetate (3 ^{x}100 ml) was used to extract the aqueous layer, while the organic layer was dried over sodium sulfate anhydrous and concentrated in vacuo to obtain the dry organic portion. Then, the silica gel column was used to purify the crude material using 9:1 (hexane: ethyl acetate) to provide KI 2 (4.3 g, 71.33 %) as a white material.

1H NMR (400 MHz, Chloroform-d) δ 7.52 (d, J = 8.8 Hz, 1H), 6.70 (dd, J = 8.8, 2.8 Hz, 1H), 6.58 (d, J = 2.8 Hz, 1H), 6.12 (dt, J = 5.2, 2.3 Hz, 1H), 3.98 – 3.84 (m, 4H), 3.76 (s, 3H), 2.84 (qdd, J = 14.8, 8.5, 3.8 Hz, 2H), 2.58 (dt, J = 17.6, 3.1 Hz, 1H), 2.15 – 1.97 (m, 3H), 1.94 – 1.66 (m, 5H), 1.38 (dtd, J = 17.0, 12.4, 6.5 Hz, 2H), 0.89 (s, 3H).

^{13}C NMR (101 MHz, CDCl3) δ 158.29, 137.48, 134.50, 127.60, 125.15, 119.06, 117.90, 113.27, 112.66, 65.27, 64.60, 55.23, 46.83, 44.33, 39.19, 33.87, 32.81, 30.17, 28.21 23.25, 14.72.

KI3

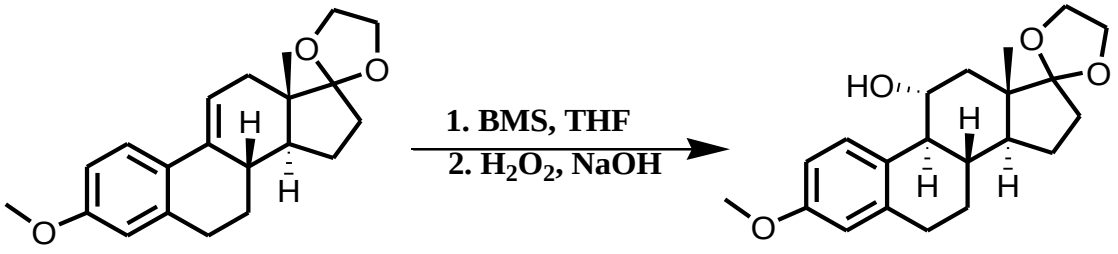

KI3

The KI2 compound (4.3 g, 13.19 mmole) was dissolved in 30 mL anhydrous THF. Then 10 mL (~ 1.5 equivalence) of borane dimethyl sulfide complex solution in THF (2 M) was added portion-wise, stirring under argon, and the reaction was stirred at room temperature for 15 hrs. Next, 3.25 ml NaOH solution (3M) and 3.25 ml H_2O_2 were added portion-wise and the reaction was stirred for 1 hr. under air (Note: the stopper must be removed after the addition of NaOH and H_2O_2 .[30] The aqueous layer was extracted using ethyl acetate (3 x 50 ml) and the organic layer was dried over sodium sulfate anhydrous and concentrated in vacuo. The crude extract was purified using a 7:3 hexane ethyl acetate mixture to obtain KI3 as a white material (3.13 g, 69%).

1H NMR (400 MHz, Chloroform-d) δ 7.88 (dd, J = 8.7, 1.0 Hz, 1H), 6.69 (dd, J = 8.7, 2.9 Hz, 1H), 6.62 (d, J = 2.8 Hz, 1H), *4.10 (d, J = 7.1 Hz, 1H)*, 3.95 – 3.84 (m, 5H), 3.75 (s, 3H), 2.78 (dd, J = 8.0, 6.1 Hz, 2H), 2.13 (t, J = 10.1 Hz, 2H), 2.02 – 1.97 (m, 1H), 1.91 – 1.83 (m, 3H), 1.72 – 1.65 (m, 2H), 1.25 (dd, J = 9.5, 4.8 Hz, 2H), 0.84 (s, 3H).

13C NMR (151 MHz, CDCl3) δ 157.69, 139.05, 132.56, 127.49, 118.88, 113.69, 111.06, *70.95*, 65.30, 64.58, 55.11, 50.36, 48.99, 46.96 , 41.47, 37.58, 34.28, 28.79, 26.83, 22.45, 14.97.

KI4

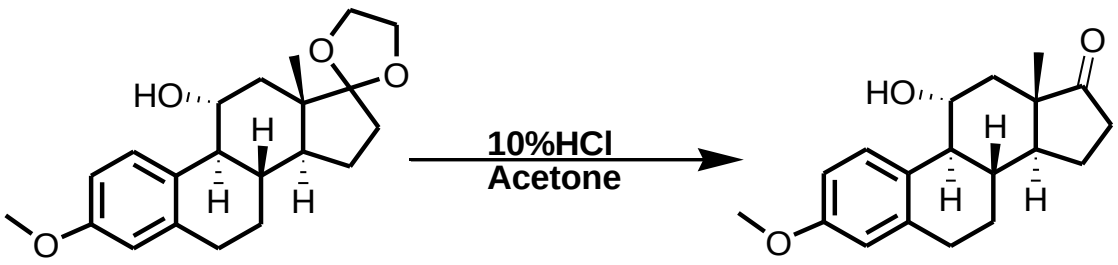

KI4

The 3.13 g (9.10 mmole) of KI3 that was obtained from the previous step was then dissolved in 130 ml (1:1, 10% HCl: Acetone) and stirred at room temperature overnight. The next day, the reaction was quenched by the addition of $NaHCO_3$ to neutralize the excess acid. The reaction mixture was extracted with ethyl acetate (3 X 100 ml) and dried over Na_2SO_3 anhydrous, followed by evaporation in vacuo. The purification process used a 6:4 hexane ethyl acetate mixture to yield 3-methoxy-1, 3, 5(10)-trien-11-ol-17-one (2.5 g, 91%) as a purple solid material.

1H NMR (400 MHz, Chloroform-*d*) δ 7.90 (dd, *J* = 8.7, 1.0 Hz, 1H), 6.74 (dd, *J* = 8.7, 2.9 Hz, 1H), 6.67 (d, *J* = 2.9 Hz, 1H), 4.21 (ddd, *J* = 10.8, 9.7, 5.3 Hz, 1H), 3.79 (s, 3H), 3.46 (s, 1H), 2.85 (t, *J* = 6.8 Hz, 2H), 2.54 (d, *J* = 3.7 Hz, 0H), 2.55 – 2.43 (m, 3H), 2.28 (dd, *J* = 12.5, 5.3 Hz, 1H), 2.21 (q, *J* = 5.7 Hz, 1H), 2.21 – 2.12 (m, 1H), 2.09 – 1.96 (m,

1H), 1.98 (s, 1H), 1.54 (ddd, *J* = 10.4, 8.5, 5.9 Hz, 2H), 1.40 (dd, *J* = 12.5, 10.9 Hz, 1H), 1.29 (s, 2H), 1.28 (s, 1H), 0.95 – 0.80 (m, 1H), 0.87 (s, 3H).

13C NMR (101 MHz, CDCl3) δ 219.88, 157.73, 138.81, 132.11, 127.62, 113.68, 111.13, 77.48, 77.17, 76.85, 70.28, 55.18, 50.27, 49.78, 48.70, 41.71, 36.68, 35.95, 28.61, 26.27, 21.65, 14.28.

KI5

KI5

The purified compound KI4 (2.5 g, 8.28 mmol) was dissolved in 40 ml DMF, followed by the addition of 0.6 g of magnesium turning. With regard to magnesium turnings, the reaction must be facilitated, since the reaction does not work in the absence of a catalyst. Next, 3.75 g of TBSCl was added and the color turned from purple to red. The reaction was run at room temperature for 14 hrs. before it was quenched with water. The reaction mixture was extracted with ethyl acetate (3 X 100 ml) and dried with Na_2SO_3 anhydrous. The TBS-protected compound KI5 was purified using hexane: ethyl acetate (8:2) mixture to obtain 3.3 g (95%).

1H NMR (600 MHz, CDCl3) δ 7.56 (d, J = 8.7 Hz, 1H), 6.49 (dd, J = 8.7, 2.8 Hz, 1H), 6.46 (d, J = 2.7 Hz, 1H), 4.12 (ddd, J = 10.6, 9.5, 5.1 Hz, 1H), 3.59 (d, J = 2.0 Hz, 2H), 2.67 – 2.63 (m, 1H), 2.31 (ddd, J = 13.8, 10.7, 3.0 Hz, 1H), 2.13 (t, J = 9.7 Hz, 1H), 2.07 (dd, J = 12.6, 5.1 Hz, 1H), 2.02 – 1.94 (m, 1H), 1.87 – 1.76 (m, 2H), 1.08 – 1.05 (m, 1H), 0.72 (d, J = 3.2 Hz, 6H), 0.69 (s, 2H), -0.00 (s, 2H), -0.04 (d, J = 2.9 Hz, 2H).

13C NMR (151 MHz, CDCl3) δ 159.94, 141.60, 134.92, 130.94, 115.91, 112.92, 74.61, 57.56, 52.91, 52.34, 51.09, 44.33, 39.46, 38.48, 31.23, 28.77, 28.59, 24.17, 20.70, 16.82, -0.00, -1.55.

KI6

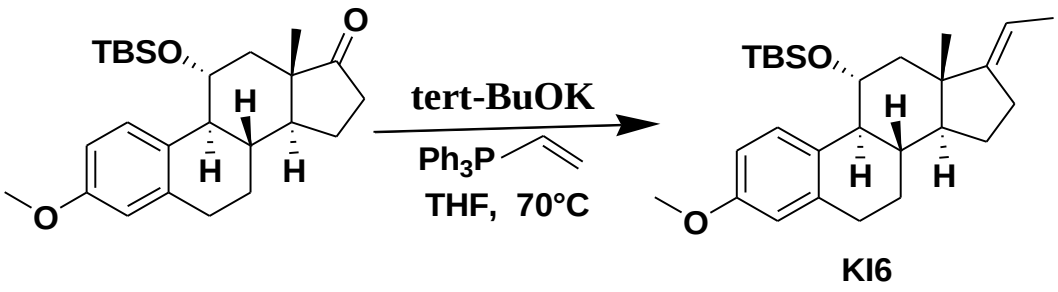

KI6

To a solution of ethyltriphenylphosphonium bromide (8.76 g, 23.58 mm) in 22 ml of THF, potassium *tert*-butoxide (2.47 g, 22 mmole) was added, resulting in an orange mixture that was stirred at room temperature for 1 hr. A solution of (3.3 g, 7.86mmole) KI5 in 15 ml THF was added and the mixture was stirred at 70 °C for 5 hrs. The reaction was allowed to cool to room temperature and NH_4Cl solution was added to quench the reaction, followed by extraction with ethyl acetate (3 X 50 ml) and drying using anhydrous sodium sulfate. The compound KI6 (2.6 g, 80%) was purified using hexane: ethyl acetate (9:1).

13C NMR (101 MHz, CDCl3) δ 160.05 (C3), 152.06 (C17), 141.37 (C5), 135.37 (C10), 130.98 (C1), 116.24 (C20), 115.91 (C4), 113.04 (C2), 75.50 (C11), 57.52 (C3), 57.15 (C13), 52.77 (C9), 50.50, 47.51(C14), 39.36(C8), 33.97(C16), 31.70 (C6), 30.01(C7), 28.79(C12), 26.86(C15), 20.67(C24), 20.18 (C24), 15.66 (C18), -0.00(C22), -1.26(C23).

KI7

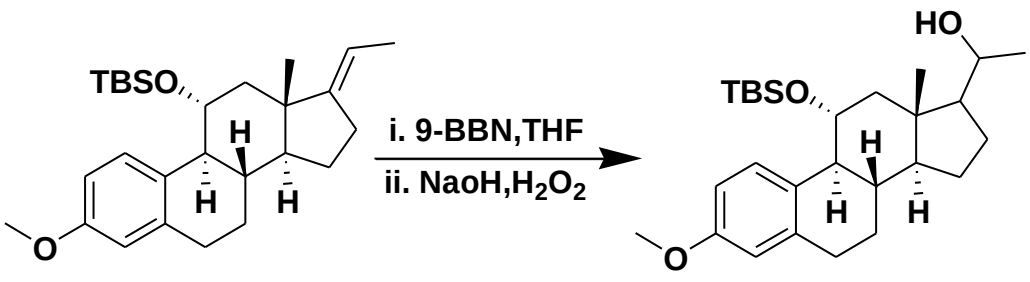

KI7

In a 1 L flask of ***9***-Borabicyclo [3.3.1] nonane, 9-BBN (0.5 M in THF,49 ml, 24.4 mmol) was added portion-wise to KI 5 (2.68 g, 6.288 mmole) at 0 °C and stirred for 30 min. at room temperature. The reaction mixture was run at 60 °C for 18 hr., then run at 0 °C for 10 min., followed by the slow addition of 48 mL of 10% NaOH and 92 mL of 30% H2O. The reaction was then allowed to run at room temperature without closing the system. The mixture was extracted with ethyl acetate (3 X 100 ml) and the organic layers were washed with saturated sodium thiosulfate to reduce any extra H_2O_2. The organic layer was dried with (Na_2SO_4), and concentrated in *vacuo.* The crude extract was moved to the next reaction.

KI8

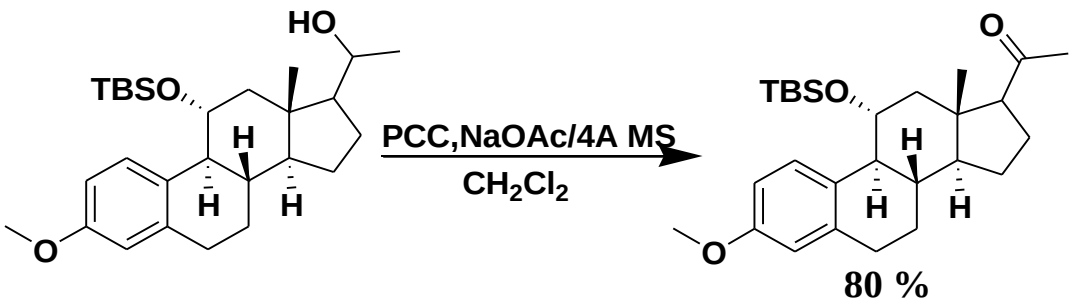

2.65 g (5.97 mmole) of KI7 was dissolved in 28 ml CH_2Cl_2 containing 2.35 g of 4 A° molecular sieves, followed by the addition of (2.34 g, 28.6 mmol) of NaOAc. Next, (2.5 g, 11.92 mmole) of pyridinium chlorochromate (PCC) was added and the reaction was run at room temperature for 5 hrs. The reaction mixture was filtered using normal phase silica to remove PCC and the resulting crude mixture was purified using hexane: ethyl acetate (8:2) to produce KI7 (2.3 g, 80%).

^{13}C NMR (101 MHz, Chloroform-*d*) δ 201.04, 158.22, 152.43, 140.38, 137.69, 132.75, 113.87, 111.41, 72.56, 55.61, 55.20, 46.52, 44.26, 37.04, 34.84, 32.03, 29.67, 27.81, 27.19, 26.50, 20.70, 25.89, 24.22, 22.71, 14.84, -4.31.

KI9

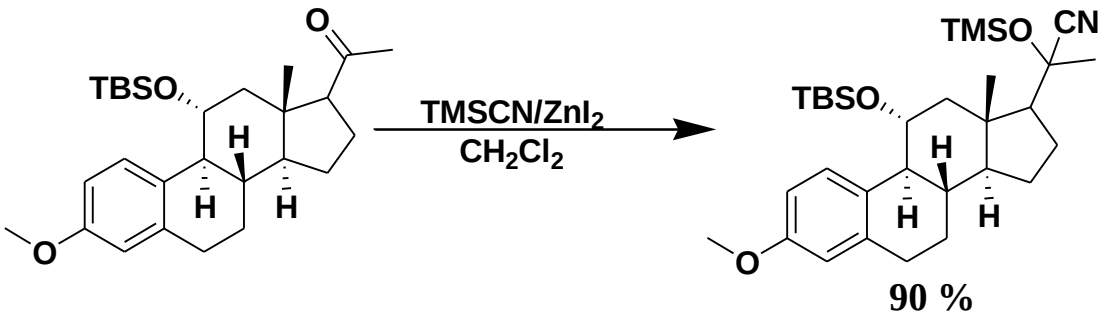

2.11 g (4.77 mmol) of KI8 was dissolved in 10 ml of CH_2Cl_2, while ZnI2 (0.045 g, 0.14 mmole) was added as a catalyst. Next, (0.83 ml, 6.142 mmole) of TMSCN was added to the reaction mixture and stirred at room temperature for 3 hrs. After completion of the reaction, H_2O was added to quench the reaction and extraction was carried out using CH2Cl2 (3 X 50 ml). The crude extract was dried with Na_2SO_2 and concentrated, purified using hexane: ethyl acetate (9:1) to yield 2.9 g (90%) of KI9.

Note. Due to the toxicity of TMSCN, it should be handled under the fume hood.

1H NMR (400 MHz, CDCl3) δ 7.59 (d, J = 8.6 Hz, 1H), 6.52 (dd, J = 8.6, 2.8 Hz, 1H), 6.49 (d, J = 2.7 Hz, 1H), 4.15 (td, J = 10.4, 5.1 Hz, 1H), 3.98 (q, J = 7.1 Hz, 1H), 3.63 (s, 2H), 2.67 (t, J = 6.8 Hz, 2H), 2.41 (dd, J = 12.5, 5.1 Hz, 1H), 2.11 (t, J = 9.3 Hz, 1H), 1.95 – 1.87 (m, 2H), 1.48 (s, 2H), 1.14 – 1.11 (m, 3H), 0.84 (s, 2H), 0.78 (s, 4H), 0.18 (d, J = 3.2 Hz, 6H), 0.04 (s, 2H), -0.00 (s, 2H).

13C NMR (101 MHz, CDCl3) δ 155.90, 137.27, 131.00, 126.60, 120.14, 111.58, 108.78, 70.74, 58.63, 58.29, 53.34, 52.67, 48.66, 48.32, 42.87, 35.20, 29.02, 27.19, 24.45, 19.34, 16.60, 12.57, 11.95, 0.04, -3.88, -5.71.

KI10

To synthesize the main intermediate KI10, (2.9 g, 5.37 mmol) of KI9 was dissolved in 13 ml of Et_2O and stirred for 15 min at 0 °C, followed by the drop-wise addition of MeLi (13 ml). The reaction was run at 0 °C for 2 hrs. Next, 2 ml of glacial acetic acid was added to the reaction and the mixture was stirred for 30 min. before the addition of $NaHCO_3$ to neutralize the acidic environment. The aqueous mixture was extracted with (3 X 50 ml) CH_2Cl_2, dried with Na_2SO_4, concentrated, and purified using gradient mobile phase hexane: ethyl acetate (9:1) then (8:2) to yield KI9 (e.e. 47 %).

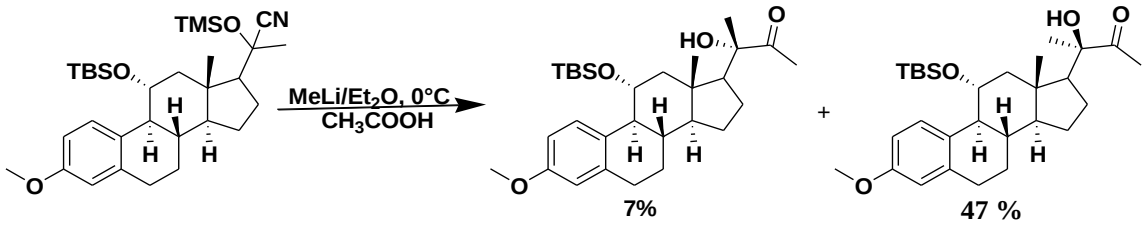

1H NMR (400 MHz, CDCl3) δ 7.63 (d, J = 8.7 Hz, 4H), 6.50 (dd, J = 8.7, 2.7 Hz, 4H), 6.46 (d, J = 2.5 Hz, 3H), 4.15 (td, J = 10.2, 5.0 Hz, 4H), 3.84 (s, 4H), 3.60 (s, 13H), 2.64 (t, J = 6.3 Hz, 8H), 2.43 (dd, J = 12.0, 4.9 Hz, 4H), 2.15 – 2.09 (m, 5H), 2.07 (s, 11H), 1.96 – 0.99 (m, 75H), 0.78 (s, 34H), 0.75 (s, 12H), 0.70 (ddd, J = 6.4, 5.3, 2.3 Hz, 5H), 0.04 (s, 11H), -0.00 (s, 11H).

13C NMR (101 MHz, CDCl3) δ 211.39, 157.55, 139.07, 132.88, 128.40, 113.55, 110.43, 79.93, 72.48, 55.13, 54.87, 51.33, 50.14, 44.88, 36.72, 29.11, 27.55, 26.26, 24.65, 23.75, 23.19, 22.19, 18.46, 14.49, -2.47, -3.90.

TBS – protected aldehyde was prepared as synthesized in our lab previously.

KI11

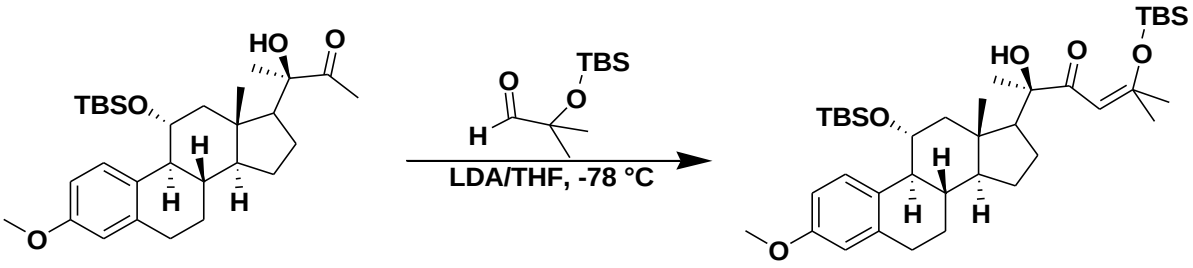

At 78 °C, 0.76 ml (1.85 mm) of *n*-BuLi dissolved in hexane (2.5 M) was added to 1.85 mmole (0.93 ml of 2 M) of diisopropylamine dissolved in THF, and the mixture was stirred for 1 hr. A solution of KI9 0.514 mmole dissolved in THF (1 mL) was then added to produce the enolate and the mixture was stirred for 1 hr. at -78 °C. Next came the addition of 0.085 g (0.44 mmole) TBS protected aldehyde (KI10) that was dissolved in 1.32 ml THF (0.15 M). The reaction was allowed to warm to room temperature and stirred for 24 hrs. After that, the reaction was quenched with the addition of saturated NH_4Cl. The aqueous layer was extracted by ethyl acetate (3 X 50 mL), dried with Na_2SO_4, concentrated, and purified using hexane: ethyl acetate (8:2) to yield (0.470 g, 55%) as a white powder.

^{1}H NMR (400 MHz, $CDCl_3$) δ 7.65 (d, *J* = 8.7 Hz, 1H), 6.94 (d, *J* = 14.9 Hz, 1H), 6.63 – 6.56 (m, 1H), 6.52 (dd, *J* = 8.7, 2.7 Hz, 1H), 6.48 (d, *J* = 2.5 Hz, 1H), 4.18 (td, *J* = 10.2, 5.0 Hz, 1H), 4.02 (s, 1H), 3.63 (s, 3H), 2.66 (t, *J* = 6.6 Hz, 2H), 2.47 (dd, *J* = 12.0, 5.0 Hz, 1H), 2.13 (dd, *J* = 12.4, 6.9 Hz, 1H), 1.69 (dd, *J* = 12.0, 6.8 Hz, 2H), 1.35 (s, 3H), 1.26 – 1.21 (m, 8H), 1.18 (dd, *J* = 12.5, 6.6 Hz, 3H), 1.12 (s, 2H), 0.82 (s, 8H), 0.80 (s, 8H), 0.78 (s, 3H), 0.06 (s, 3H), 0.02 (s, 3H), -0.00 (s, 3H), -0.01 (s, 3H).

13C NMR (101 MHz, CDCl3) δ 204.24, 159.53, 159.52, 140.97, 134.76, 130.38, 120.10, 115.40, 112.47, 80.87, 75.65, 74.47, 57.26, 57.12, 56.57, 53.50, 52.16, 46.86, 38.79, 32.00, 31.87, 31.12, 29.48, 28.25, 27.93, 26.07, 25.76, 24.72, 23.97, 20.36, 20.32, 16.46, 16.17, -0.00, -0.03, -0.70, -1.75.

KA2

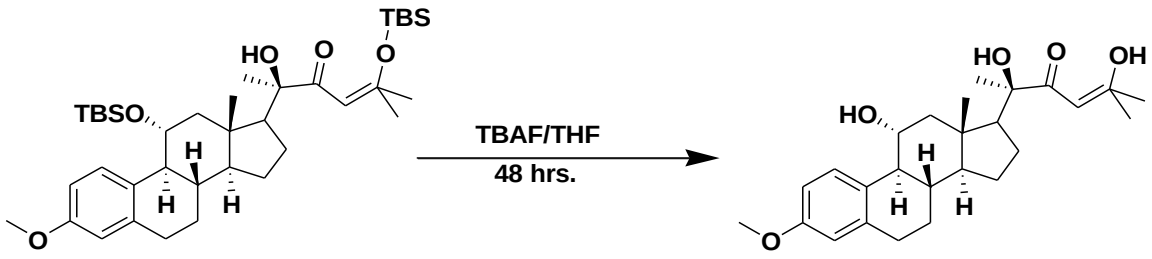

Tetra-butyl ammonium fluoride (TBAF) (8.5 ml, 8.5 mmol) was added to a stirred solution of 11 ml THF containing KI11 (0.470 g, 0.71 mmol) and stirred for 48 hrs. The reaction was then quenched by the addition of NH4Cl solution. The aqueous layer was extracted by ethyl acetate (3 X 50 ml). The organic layer was dried using Na_2SO_4, concentrated *in vacuo*, and purified using hexane: ethyl acetate (6:4) to yield (0.18 g, 59 %) as a white solid powder.

1H NMR (400 MHz, CDCl3) δ 7.78 (d, J = 8.6 Hz, 1H), 7.08 (d, J = 15.2 Hz, 1H), 6.65 (dd, J = 8.8, 2.7 Hz, 1H), 6.61 (d, J = 15.2 Hz, 1H), 6.57 (d, J = 2.4 Hz, 1H), 4.23 – 4.12 (m, 1H), 3.70 (d, J = 2.2 Hz, 3H), 2.82 – 2.69 (m, 2H), 2.55 (dd, J = 11.9, 5.0 Hz, 1H), 2.36 – 2.17 (m, 1H), 2.14 – 2.03 (m, 2H), 1.85 – 1.73 (m, 2H), 1.72 – 1.62 (m, 1H), 1.58 (dd, J = 8.8, 5.2 Hz, 1H), 1.42 (d, J = 7.7 Hz, 3H), 1.39 – 1.29 (m, 9H), 1.18 (s, 3H), 1.15 – 1.03 (m, 2H), 0.90 – 0.82 (m, 3H).

13C NMR (101 MHz, CDCl3) δ 202.14, 157.66, 156.40, 139.03, 132.41, 127.31, 117.94, 113.68, 111.12, 79.02, 71.30, 70.83, 55.20, 54.28, 50.95, 50.29, 45.41, 45.01, 36.52, 29.72, 29.53, 29.46, 28.78, 27.37, 24.15, 23.66, 22.00, 14.50.

General synthesis procedure for (KI12-KI24):

KI10 (0.3 mmol) was dissolved in 1 ml THF, then grounded in NaOH powder (0.87 mm) and 0.36 mmol aldehyde. The reaction mixture was heated in a 20 mL vial for 15 min under 105 °C. After that, the reaction was quenched by water and extracted with 3 X 20 mL ethyl acetate, dried over $NaSO_4$ and purified using 9:1 hexane: ethyl acetate.

KI12

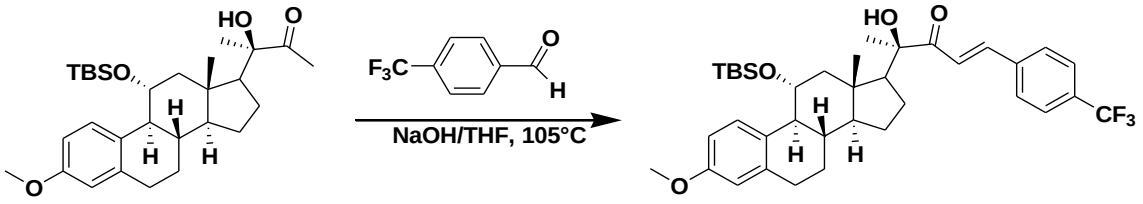

1H NMR (400 MHz, CDCl3) δ 7.61 (d, J = 8.7 Hz, 4H), 7.33 – 7.24 (m, 5H), 6.66 (d, J = 15.2 Hz, 5H), 6.51 (d, J = 3.5 Hz, 5H), 6.49 (d, J = 2.8 Hz, 3H), 6.47 (d, J = 2.8 Hz, 3H), 6.43 (d, J = 2.7 Hz, 5H), 6.13 (d, J = 3.5 Hz, 4H), 4.13 (td, J = 10.2, 5.0 Hz, 5H), 4.00 (s, 3H), 3.58 (s, 12H), 2.59 (dd, J = 14.6, 7.2 Hz, 11H), 2.43 (dd, J = 12.0, 4.9 Hz, 5H), 2.11 (t, J = 9.3 Hz, 5H), 1.71 (dd, J = 17.2, 7.8 Hz, 7H), 1.67 – 1.61 (m, 6H), 1.49 – 1.39 (m, 17H), 1.35 (s, 13H), 1.19 (t, J = 7.9 Hz, 15H), 1.09 – 1.05 (m, 11H), 0.77 (d, J = 2.9 Hz, 36H), 0.75 (s, 14H), 0.04 – -0.01 (m, 27H).

13C NMR (101 MHz, CDCl3) δ 201.44, 158.31, 145.00, 140.91, 134.97, 134.59, 129.92, 128.51, 126.00, 125.14, 122.44, 120.62, 113.45, 110.52, 79.21, 72.51, 55.14, 55.11, 54.78, 51.38, 50.14, 45.02, 36.81, 29.18, 27.44, 26.26, 24.26, 23.68, 22.19, 18.38, 14.66, -2.58, -3.91.

KI13

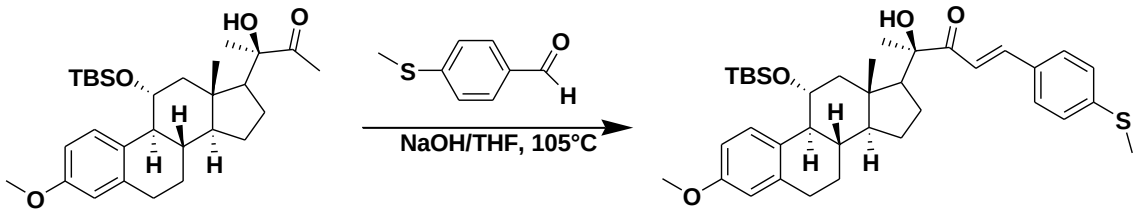

1H NMR (400 MHz, CDCl3) δ 7.69 (d, J = 15.1 Hz, 7H), 7.62 (d, J = 8.7 Hz, 7H), 6.99 (d, J = 3.6 Hz, 6H), 6.57 (dd, J = 3.6, 1.0 Hz, 7H), 6.49 (d, J = 2.7 Hz, 5H), 6.47 (d, J = 3.7 Hz, 6H), 6.44 (s, 10H), 4.13 (td, J = 10.1, 4.9 Hz, 8H), 4.05 (s, 6H), 3.59 (s, 21H), 2.60 (d, J = 7.4 Hz, 15H), 2.47 – 2.40 (m, 9H), 2.35 (s, 20H), 2.11 (t, J = 9.1 Hz, 7H), 1.67 (dd, J = 11.7, 7.7 Hz, 17H), 1.50 – 1.37 (m, 30H), 1.34 (s, 22H), 1.26 – 0.91 (m, 54H), 0.77 (s, 41H), 0.75 (s, 18H), 0.02 (d, J = 12.4 Hz, 40H).

13C NMR (101 MHz, CDCl3) δ 201.28, 157.50, 145.51, 139.04, 138.73, 137.74, 133.79, 132.70, 128.50, 127.06, 115.61, 113.41, 110.48, 78.74, 77.39, 77.07, 76.76, 72.54, 55.16, 55.07, 54.95, 51.35, 50.12, 44.91, 36.82, 29.20, 27.43, 26.27, 24.44, 23.67, 22.12, 18.38, 16.01, 14.60, -2.58, -3.92.

KI14

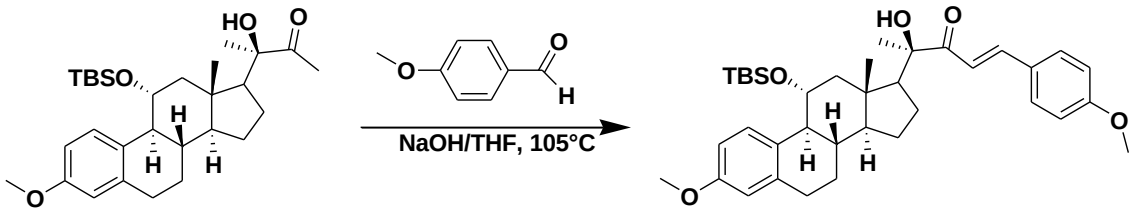

1H NMR (400 MHz, CDCl3) δ 7.87 (d, J = 2.3 Hz, 3H), 7.85 (s, 2H), 7.62 (t, J = 5.7 Hz, 4H), 7.03 (t, J = 2.2 Hz, 1H), 7.01 (d, J = 2.1 Hz, 2H), 6.98 – 6.97 (m, 3H), 6.96 (s, 2H), 6.73 (dd, J = 8.7, 2.8 Hz, 2H), 6.67 (d, J = 2.7 Hz, 2H), 4.39 (dd, J = 10.0, 4.8 Hz, 2H), 4.36 (s, 2H), 3.90 (s, 3H), 3.88 (s, 6H), 3.81 (s, 6H), 2.82 (d, J = 7.0 Hz, 4H), 2.70 (dd, J = 12.0, 4.9 Hz, 2H), 2.34 (t, J = 8.9 Hz, 2H), 1.98 (t, J = 9.6 Hz, 3H), 1.91 – 1.82 (m, 3H), 1.70 – 1.65 (m, 5H), 1.62 (s, 7H), 1.41 (d, J = 4.0 Hz, 8H), 1.30 (d, J = 5.4 Hz, 5H), 1.25 – 1.14 (m, 5H), 1.01 (d, J = 2.7 Hz, 18H), 1.00 (d, J = 2.0 Hz, 6H), 0.97 – 0.86 (m, 9H), 0.28 (s, 6H), 0.25 (s, 6H).

13C NMR (101 MHz, CDCl3) δ 201.50, 162.13, 157.56, 145.83, 138.99, 132.69, 131.99, 130.62, 128.49, 126.98, 115.77, 114.50, 114.33, 113.43, 110.52, 78.83, 77.54, 77.22, 76.90, 72.58, 55.40, 55.08, 54.97, 51.42, 50.04, 44.94, 37.00, 31.65, 29.21, 27.48, 26.30, 24.49, 22.72, 22.18, 18.55, 18.39, 14.65, 14.22, -2.54, -3.89.

KI15

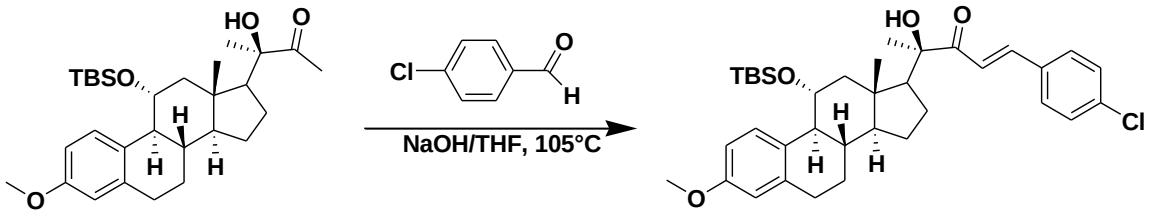

1H NMR (400 MHz, CDCl3) δ 7.63 (s, 1H), 7.60 (d, J = 6.5 Hz, 1H), 7.36 (d, J = 8.5 Hz, 2H), 7.24 – 7.17 (m, 2H), 6.81 (t, J = 10.4 Hz, 1H), 6.49 (dt, J = 8.7, 4.4 Hz, 1H), 6.43 (d, J = 2.5 Hz, 1H), 4.13 (td, J = 10.1, 4.9 Hz, 1H), 3.98 (s, 1H), 3.58 (s, 3H), 2.60 (d, J = 6.8 Hz, 2H), 2.44 (dd, J = 12.0, 4.9 Hz, 1H), 2.15 – 2.05 (m, 1H), 1.75 – 1.61 (m, 3H), 1.38 (s, 3H), 0.77 (s, 8H), 0.02 (d, J = 13.0 Hz, 6H).

13C NMR (101 MHz, CDCl3) δ 201.45, 157.54, 144.52, 138.99, 137.03, 132.72, 132.61, 129.90, 129.34, 128.50, 118.66, 113.45, 110.51, 79.05, 77.42, 77.10, 76.79, 72.52, 55.14, 54.82, 51.40, 50.15, 44.99, 36.81, 29.76, 29.20, 27.45, 26.27, 24.32, 23.69, 22.75, 22.17, 18.38, 14.66, -2.57, -3.90.

KI16

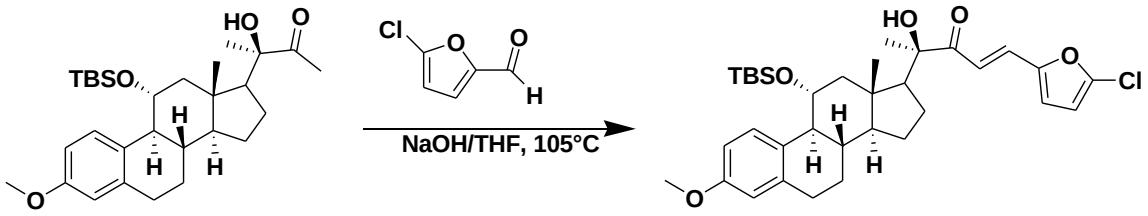

1H NMR (400 MHz, CDCl3) δ 7.61 (d, J = 8.7 Hz, 1H), 7.32 – 7.24 (m, 1H), 6.65 (t, J = 12.5 Hz, 1H), 6.51 (d, J = 3.5 Hz, 1H), 6.48 (dd, J = 8.7, 2.8 Hz, 1H), 6.43 (d, J = 2.7 Hz, 1H), 6.13 (d, J = 3.5 Hz, 1H), 4.13 (td, J = 10.2, 5.0 Hz, 1H), 4.02 (d, J = 19.6 Hz, 1H), 3.59 (d, J = 2.9 Hz, 3H), 2.60 (t, J = 6.3 Hz, 2H), 2.43 (dd, J = 12.0, 4.9 Hz, 1H), 2.11 (t, J = 9.3 Hz, 1H), 1.72 (t, J = 9.6 Hz, 1H), 1.67 – 1.61 (m, 1H), 1.47 – 1.40 (m, 3H), 1.35 (s, 3H), 1.19 (t, J = 7.9 Hz, 3H), 1.07 (dd, J = 11.7, 6.3 Hz, 3H), 0.77 (d, J = 2.8 Hz, 8H), 0.75 (s, 3H), 0.71 (t, J = 2.4 Hz, 1H), 0.02 (d, J = 3.0 Hz, 3H), 0.01 (d, J = 4.5 Hz, 3H).

13C NMR (101 MHz, CDCl3) δ 201.38, 157.47, 150.75, 140.37, 139.11, 132.91, 130.36, 128.56, 119.10, 116.18, 113.42, 110.54, 109.79, 78.91, 72.52, 55.22, 54.74, 51.27, 50.11, 44.96, 36.86, 29.23, 27.51, 26.27, 24.33, 23.75, 22.15, 18.37, 14.67, -2.56, -3.88.

KI17

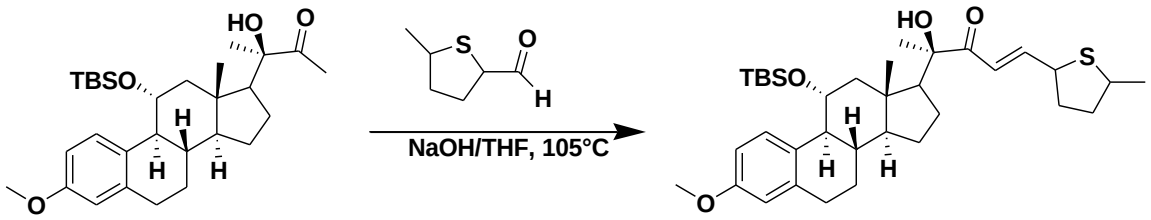

1H NMR (400 MHz, CDCl3) δ 7.63 (d, J = 4.7 Hz, 1H), 7.60 (d, J = 0.9 Hz, 1H), 7.33 (d, J = 8.4 Hz, 2H), 7.04 (d, J = 8.4 Hz, 2H), 6.80 (d, J = 15.5 Hz, 1H), 6.48 (dd, J = 8.7, 2.6 Hz, 1H), 6.43 (d, J = 2.4 Hz, 1H), 4.13 (td, J = 10.1, 4.8 Hz, 1H), 4.05 (s, 1H), 3.57 (s, 3H), 2.58 (d, J = 6.8 Hz, 2H), 2.45 (dd, J = 12.0, 4.8 Hz, 1H), 2.30 (s, 3H), 2.10 (t, J = 8.8 Hz, 1H), 1.72 (t, J = 9.5 Hz, 1H), 1.67 – 1.59 (m, 1H), 1.43 (d, J = 11.1 Hz, 3H), 1.37 (s, 3H), 1.19 (d, J = 14.8 Hz, 3H), 1.11 – 0.90 (m, 3H), 0.77 (d, J = 3.7 Hz, 9H), 0.76 (s, 2H), 0.03 (s, 3H), -0.00 (s, 3H).

13C NMR (101 MHz, CDCl3) δ 201.54, 157.54, 156.34, 145.52, 143.29, 142.06, 139.03, 132.68, 130.62, 129.13, 128.51, 125.87, 117.03, 113.45, 110.52, 78.95, 72.56, 55.17, 55.11, 54.91, 51.42, 50.18, 44.97, 36.79, 29.30, 27.47, 26.24, 24.48, 24.45, 23.69, 22.23, 18.46, 15.06, 14.68, -2.52, -3.85.

KA1

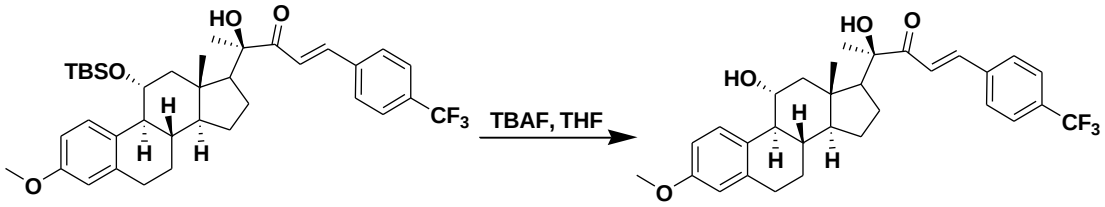

1H NMR (600 MHz, CDCl3) δ 7.74 (d, J = 15.6 Hz, 35H), 7.61 (d, J = 8.3 Hz, 74H), 7.58 (d, J = 8.4 Hz, 75H), 6.88 (s, 32H), 6.73 (d, J = 8.6 Hz, 36H), 6.68 (dd, J = 8.6, 2.6 Hz, 37H), 6.63 (d, J = 2.5 Hz, 37H), 4.38 (s, 33H), 4.02 (s, 34H), 3.79 (d, J = 4.1 Hz, 7H), 3.72 (s, 118H), 2.88 (t, J = 10.2 Hz, 37H), 2.81 – 2.68 (m, 82H), 2.48 – 2.43 (m, 43H), 2.22 (tdd, J = 10.3, 9.6, 6.2 Hz, 60H), 2.04 (dt, J = 12.4, 3.2 Hz, 46H), 1.96 (t, J = 12.8 Hz, 39H), 1.84 (ddd, J = 12.4, 8.6, 5.1 Hz, 96H), 1.73 – 1.57 (m, 237H), 1.56 – 1.50 (m, 73H), 1.44 – 1.25 (m, 403H), 0.91 (s, 111H).

13C NMR (151 MHz, CDCl3) δ 212.87, 159.21, 144.22, 142.23, 138.01, 132.39, 128.86, 128.72, 127.49, 125.97, 125.95, 120.26, 114.43, 113.32, 78.62, 55.27, 53.71, 52.85, 47.85, 47.60, 41.10, 30.02, 29.68, 24.73, 24.07, 23.56, 22.69, 22.27, 20.24, 14.77.

KA11

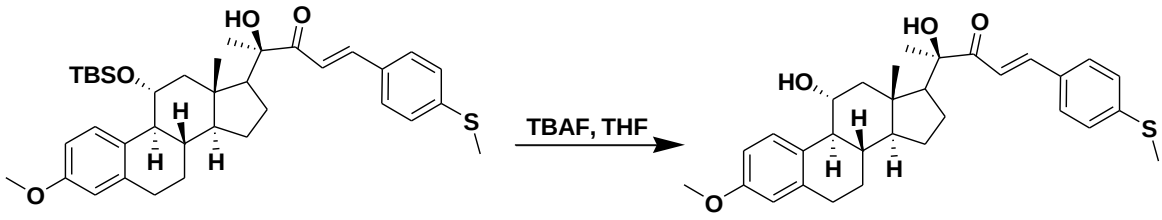

1H NMR (600 MHz, CDCl3) δ 7.90 (d, J = 8.7 Hz, 1H), 7.85 (d, J = 15.5 Hz, 1H), 7.60 (d, J = 8.7 Hz, 2H), 6.97 (d, J = 8.7 Hz, 2H), 6.94 (d, J = 15.5 Hz, 1H), 6.76 (dd, J = 8.7, 2.6 Hz, 1H), 6.68 (d, J = 2.4 Hz, 1H), 4.33 – 4.27 (m, 2H), 3.89 (s, 3H), 3.81 (s, 3H), 2.84 (t, J = 6.6 Hz, 2H), 2.71 (dd, J = 11.9, 5.1 Hz, 1H), 2.19 (t, J = 9.2 Hz, 1H), 1.96 (t, J = 9.7 Hz, 1H), 1.92 – 1.86 (m, 1H), 1.81 (s, 1H), 1.72 – 1.63 (m, 2H), 1.59 (d, J = 16.7 Hz, 4H), 1.47 – 1.27 (m, 5H), 1.22 (td, J = 11.7, 6.4 Hz, 1H), 0.98 (d, J = 10.7 Hz, 3H)

KA5

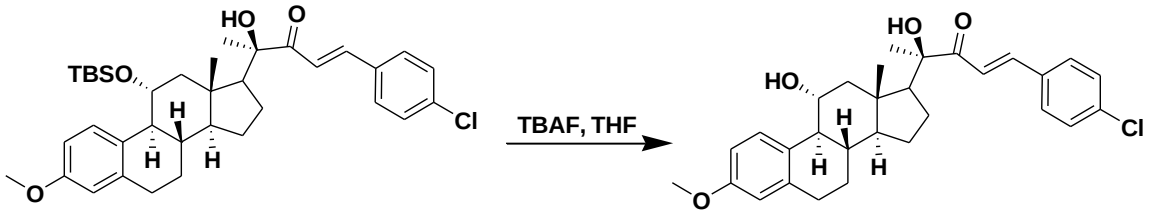

1H NMR (400 MHz, CDCl3) δ 7.77 (d, J = 8.7 Hz, 1H), 7.69 (d, J = 15.6 Hz, 1H), 7.45 (d, J = 8.5 Hz, 2H), 7.30 (d, J = 8.5 Hz, 2H), 6.91 (d, J = 15.6 Hz, 1H), 6.64 (dd, J = 8.6, 2.7 Hz, 1H), 6.55 (d, J = 2.6 Hz, 1H), 4.18 (td, J = 10.3, 5.1 Hz, 1H), 4.06 (s, 1H), 3.68 (s, 3H), 2.71 (d, J = 7.4 Hz, 2H), 2.58 (dd, J = 11.9, 5.1 Hz, 1H), 2.38 – 2.32 (m, 3H), 2.07 (t, J = 9.3 Hz, 2H), 1.85 – 1.78 (m, 2H), 1.76 (dd, J = 5.9, 3.0 Hz, 1H).

13C NMR (101 MHz, CDCl3) δ 201.52, 144.46, 139.08, 137.04, 132.68, 132.35, 129.84, 129.34, 127.26, 118.66, 113.71, 111.12, 79.04, 70.79, 55.30, 55.19, 54.73, 53.67, 51.05, 50.32, 45.07, 36.53, 28.77, 27.36, 24.29, 23.65, 22.74, 22.07, 20.80, 14.50, 14.16.

KA6

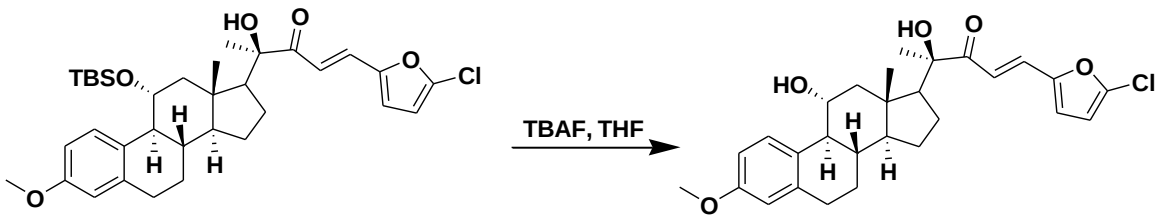

^{1}H NMR (600 MHz, $CDCl_3$) δ 7.36 (d, *J* = 15.2 Hz, 1H), 6.73 (d, *J* = 8.6 Hz, 1H), 6.68 (dd, *J* = 8.6, 2.7 Hz, 1H), 6.64 (s, 1H), 6.62 (s, 1H), 6.62 (d, *J* = 2.2 Hz, 1H), 6.24 (d, *J* = 3.5 Hz, 1H), 3.72 (s, 2H), 2.89 (d, *J* = 12.5 Hz, 1H), 2.79 (s, 1H), 2.73 (d, *J* = 5.7 Hz, 1H), 2.47 (d, *J* = 12.6 Hz, 1H), 2.21 (tdd, *J* = 13.5, 6.1, 3.3 Hz, 1H), 2.03 (dd, *J* = 9.5, 6.2 Hz, 1H), 1.89 – 1.82 (m, 2H), 1.73 – 1.54 (m, 4H), 1.34 (s, 3H), 1.32 – 1.16 (m, 4H), 0.90 (s, 3H).

^{13}C NMR (151 MHz, $CDCl_3$) 200.78, 159.32, 150.49, 140.38, 137.94, 130.64, 128.62, 127.39, 119.36, 115.55, 114.51, 113.35, 109.85, 78.40, 70.79, 55.23, 53.66, 52.89, 47.84, 47.55, 41.15, 24.73, 24.05, 23.60, 22.27, 20.30, 14.65.

KA3

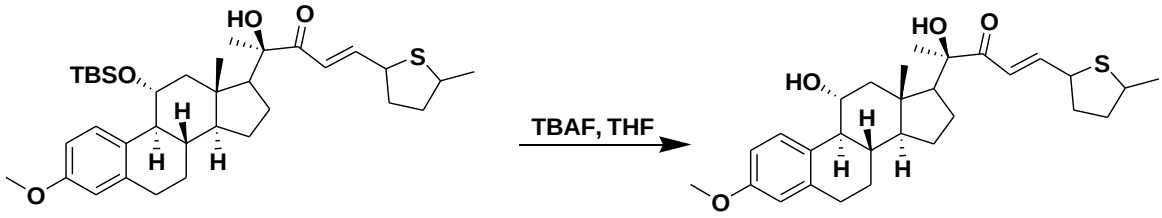

1H NMR (400 MHz, CDCl3) δ 7.78 (d, J = 8.6 Hz, 1H), 7.08 (d, J = 15.2 Hz, 1H), 6.65 (dd, J = 8.8, 2.7 Hz, 1H), 6.61 (d, J = 15.2 Hz, 1H), 6.57 (d, J = 2.4 Hz, 1H), 4.23 – 4.12 (m, 1H), 3.70 (d, J = 2.2 Hz, 3H), 2.82 – 2.69 (m, 2H), 2.55 (dd, J = 11.9, 5.0 Hz, 1H), 2.36 – 2.17 (m, 1H), 2.14 – 2.03 (m, 2H), 1.85 – 1.73 (m, 2H), 1.72 – 1.62 (m, 1H), 1.58 (dd, J = 8.8, 5.2 Hz, 1H), 1.42 (d, J = 7.7 Hz, 3H), 1.39 – 1.29 (m, 9H), 1.18 (s, 3H), 1.15 – 1.03 (m, 2H), 0.90 – 0.82 (m, 3H).

13C NMR (101 MHz, CDCl3) δ 202.14, 157.66, 156.40, 139.03, 132.41, 127.31, 117.94, 113.68, 111.12, 79.02, 71.30, 70.83, 55.20, 54.28, 50.95, 50.29, 45.41, 45.01, 36.52, 29.72, 29.53, 29.46, 28.78, 27.37, 24.15, 23.66, 22.79, 22.71, 22.00, 14.50.

KA4

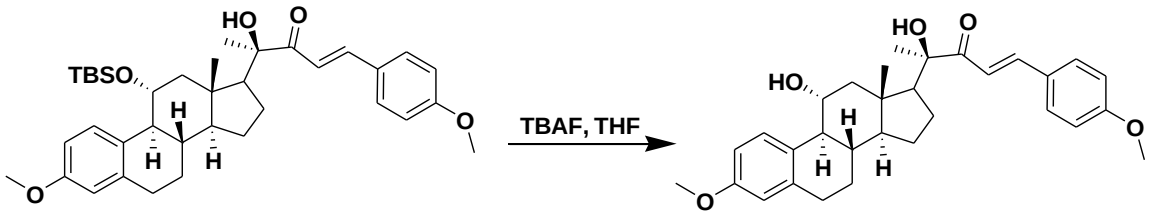

13C NMR (151 MHz, CDCl3) δ 201.61, 162.12, 157.72, 145.80, 139.08, 132.45, 130.58, 127.28, 126.94, 115.77, 114.52, 113.72, 111.12, 78.84, 70.85, 55.50, 55.32, 55.20, 54.90, 51.10, 50.34, 45.04, 36.56, 28.80, 27.38, 24.45, 23.66, 22.07, 14.50.

1H NMR (600 MHz, CDCl3) δ 7.90 (d, J = 8.7 Hz, 1H), 7.85 (d, J = 15.5 Hz, 1H), 7.60 (d, J = 8.7 Hz, 2H), 6.97 (d, J = 8.7 Hz, 2H), 6.94 (d, J = 15.5 Hz, 1H), 6.76 (dd, J = 8.7, 2.6 Hz, 1H), 6.68 (d, J = 2.4 Hz, 1H), 4.31 (d, J = 8.2 Hz, 2H), 3.89 (s, 3H), 3.81 (s, 3H), 2.84 (t, J = 6.6 Hz, 2H), 2.71 (dd, J = 11.9, 5.1 Hz, 1H), 2.19 (t, J = 9.2 Hz, 1H), 1.96 (t, J = 9.7 Hz, 1H), 1.92 – 1.86 (m, 1H), 1.81 (s, 1H), 1.60 (s, 3H), 1.47 – 1.16 (m, 6H), 0.98 (s, 3H).

KA15

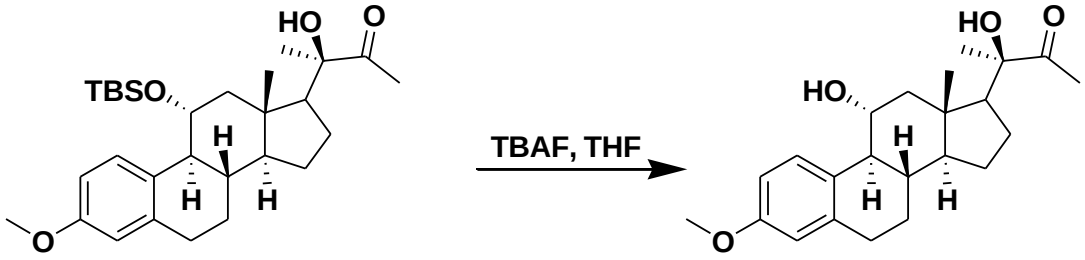

^{1}H NMR (600 MHz, $CDCl_3$) δ 7.73 (d, *J* = 8.4 Hz, 4H), 6.60 (dd, *J* = 8.7, 2.8 Hz, 4H), 6.54 (d, *J* = 2.8 Hz, 4H), 4.03 (q, *J* = 7.2 Hz, 7H), 3.68 (s, 12H), 3.29 – 3.24 (m, 15H), 2.90 – 2.86 (m, 33H), 2.74 – 2.70 (m, 9H), 2.25 (s, 11H), 2.04 (s, 10H), 1.95 (s, 7H), 1.90 – 1.76 (m, 21H), 1.72 – 1.65 (m, 39H), 1.58 (d, *J* = 7.4 Hz, 23H), 1.39 – 1.33 (m, 24H), 1.23 (s, 11H), 1.13 (d, *J* = 3.1 Hz, 5H), 1.10 – 1.05 (m, 9H), 0.87 (s, 10H).

^{13}C NMR (151 MHz, $CDCl_3$) δ 212.87, 157.68, 138.98, 132.51, 127.32, 113.56, 111.02, 79.67, 77.33, 77.11, 76.90, 75.00, 70.35, 58.99, 55.80, 55.14, 52.12, 49.96, 48.88, 43.70, 36.56, 29.68, 28.74, 27.36, 26.33, 25.14, 24.14, 22.85, 22.58, 20.17, 19.76, 14.11, 13.69, 13.56.

4.3.3. Biological evaluations

Cytotoxicity assay

Three cell lines were used to carry out the cytotoxicity assay: PANC-I, PCBX-3 and AsPC-1. In a 96-well plate, a total of $5x10^5$ cells were seeded. After 24 hrs. A serial dilution of the synthesized compounds (from 50 μM down to 3.125 μM as quadruplicate for each concentration) were added to make a total volume of 200 μL/well. Next, incubation was performed at 37 °C and 5% CO2 for 48 hrs. using 0.05% DMSO (Acros Organics) as a negative control and cuc B as a positive control. After 48 hrs, 20 μL of 3-(4, 5-dimethylthiazol-2-yl)-2, 5-diphenyl tetrazolium bromide (MTT) (Sigma Aldrich) and (5 mg/mL PBS) were added to each well and the plate was incubated in the same conditions for 2 hrs. In each well, the solutions were discarded and 200 μL DMSO was added and mixed well. The absorbance was measured directly at 570 nm by Hidex Sense Microplate readers.

Cell Cycle Analysis

PANC-I cells were seeded (3×10^5 cells/well) in a 6-well plate (3mL/ well) and incubated overnight at 37 °C, 5% CO2. Next, the media were removed and replaced by 3 mL media containing 11.23 μM or 7.674 μM from KA19 and KA20, respectively, as a duplicate in each plate, along with cuc B and DMSO as duplicates. After incubating for 24 hrs, the cells were washed twice with ice cold 1X PBS buffer (Hyclone™ Laboratories, Inc) and collected after trypsinization. Then, deactivation with media was completed, by spinning down at 1200 rpm/5 min/4 °C, discarding the supernatant and fixating by cold 70% ethanol: 1X PBS buffer overnight at −20 °C. Next, the cells were spinned down under the same conditions and the supernatant was discarded. Lastly, 500 μL propidium iodide (PI)/ RNase

staining solution (BD Biosciences) and 0.1%tritonx 100 were added and incubated in the dark at room temperature for 30min, then analyzed within 1h by a flow cytometer (BD Accuri C6, Becton-Dickinson, Mountain View, CA). Data was analyzed using MFLT32 software and 10,000 events with slow flowrate were recorded for each sample.

4.4. Conclusion

Design and synthesis of 8 cucurbitacin-inspired estrone analogs functionalized hydroxy group at C_{11} have been achieved based on ligand-based drug discovery approach. 12 synthetic steps was conducted in order to produce each final compound. The stereochemistry of the key intermediate KI10 was determined using crystallography. Molecular modeling data indicate that the calculated binding affinity for the hydroxylated analogs score higher than the dehydrogenated analogs in most of the used molecular targets such EGFR, RAS, RAF, and PI3K. Moreover, *in- vitro* cell viability assay indicate that 3 hydroxylated CIE analogs show promising IC_{50} values. KA1, KA2, and KA4 containing phenyl *para*-trifluoromethyl, cuc, and phenyl *para*-thiomethyl side chains show promising IC_{50} values against 3 pancreatic cancer cell lines PANC-I, AsPC-I, and BXPC-3 with IC_{50},s lower than the dehydrogenated analogs for KA1 and KA2. However, KA4 show higher IC_{50} compared to the previously synthesized analogs. Results of cell cycle arrest analysis show that KA1 and KA2 arrest the cell cycle at G0/G1 phase in a time dependent matter. Our results indicate that hydroxylation of C_{11} increase the antiproliferative activity against three pancreatic cancer cell lines.

4.5. References

1. Hidalgo, M. J. N. E. J. o. M., Pancreatic cancer. **2010,** *362* (17), 1605-1617.

2. Society, A. C., What Is Pancreatic Cancer? **2016**, https://www.cancer.org/cancer/pancreatic-cancer/about/what-is-pancreatic-cancer.html.

3. Malvezzi, M.; Carioli, G.; Bertuccio, P.; Boffetta, P.; Levi, F.; La Vecchia, C.; Negri, E. J. A. o. O., European cancer mortality predictions for the year 2017, with focus on lung cancer. **2017,** *28* (5), 1117-1123.

4. Zhang, X.; Shi, S.; Zhang, B.; Ni, Q.; Yu, X.; Xu, J. J. A. j. o. c. r., Circulating biomarkers for early diagnosis of pancreatic cancer: facts and hopes. **2018,** *8* (3), 332.5.

Advances in Biological Sciences, Guided Tool for Virtual Drug Discovery. **2017**.

5. Beger, H. G.; Rau, B.; Gansauge, F.; Poch, B.; Link, K.-H. J. W. j. o. s., Treatment of pancreatic cancer: challenge of the facts. **2003,** *27* (10), 1075-1084.

6. Yeo, C. J.; Cameron, J. L.; Lillemoe, K. D.; Sohn, T. A.; Campbell, K. A.; Sauter, P. K.; Coleman, J.; Abrams, R. A.; Hruban, R. H. J. A. o. s., Pancreaticoduodenectomy with or without distal gastrectomy and extended retroperitoneal lymphadenectomy for periampullary adenocarcinoma, part 2: randomized controlled trial evaluating survival, morbidity, and mortality. **2002,** *236* (3), 355.

7. Herbst, R. S. J. I. J. o. R. O. B. P., Review of epidermal growth factor receptor biology. **2004,** *59* (2), S21-S26.

8. Seshacharyulu, P.; Ponnusamy, M. P.; Haridas, D.; Jain, M.; Ganti, A. K.; Batra, S. K. J. E. o. o. t. t., Targeting the EGFR signaling pathway in cancer therapy. **2012,** *16* (1), 15-31.

9. Cragg, G. M.; Newman, D. J. J. B. e. B. A.-G. S., Natural products: a continuing source of novel drug leads. **2013,** *1830* (6), 3670-3695.

10. Newman, D. J.; Cragg, G. M.; Snader, K. M. J. J. o. n. p., Natural products as sources of new drugs over the period 1981− 2002. **2003,** *66* (7), 1022-1037.

11. Newman, D. J.; Cragg, G. M. J. J. o. n. p., Natural products as sources of new drugs over the last 25 years. **2007,** *70* (3), 461-477.

12. Gry, J.; Søborg, I.; Andersson, H. C., *Cucurbitacins in plant food*. Nordic Council of Ministers: 2006.

13. Zhou, Y.; Ma, Y.; Zeng, J.; Duan, L.; Xue, X.; Wang, H.; Lin, T.; Liu, Z.; Zeng, K.; Zhong, Y. J. N. p., Convergence and divergence of bitterness biosynthesis and regulation in Cucurbitaceae. **2016,** *2* (12), 16183.

14. Alghasham, A. A., Cucurbitacins–a promising target for cancer therapy. *International journal of health sciences* **2013,** *7* (1).

15. Miro, M. J. P. r., Cucurbitacins and their pharmacological effects. **1995,** *9* (3), 159-168.

16. Fuller, R. W.; Cardellina, J. H.; Cragg, G. M.; Boyd, M. R. J. J. o. n. P., Cucurbitacins: differential cytotoxicity, dereplication and first isolation from Gonystylus keithii. **1994,** *57* (10), 1442-1445.

17. Alsayari, A. S., Anticancer and Antiviral Activities of Cucurbitacins Isolated From Cucumis Prophetarum var. Prophetarum Growing in the Southwestern Region of Saudi Arabia. **2014**.

18. Iwanski, G. B.; Lee, D. H.; En-Gal, S.; Doan, N. B.; Castor, B.; Vogt, M.; Toh, M.; Bokemeyer, C.; Said, J. W.; Thoennissen, N. H. J. B. j. o. p., Cucurbitacin B, a novel in vivo potentiator of gemcitabine with low toxicity in the treatment of pancreatic cancer. **2010,** *160* (4), 998-1007.

19. Molavi, O.; Ma, Z.; Mahmud, A.; Alshamsan, A.; Samuel, J.; Lai, R.; Kwon, G. S.; Lavasanifar, A., Polymeric micelles for the solubilization and delivery of STAT3 inhibitor cucurbitacins in solid tumors. *International journal of pharmaceutics* **2008,** *347* (1), 118-127.

20. Sun, C.; Zhang, M.; Shan, X.; Zhou, X.; Yang, J.; Wang, Y.; Li-Ling, J.; Deng, Y. J. J. o. c. r.; oncology, c., Inhibitory effect of cucurbitacin E on pancreatic cancer cells growth via STAT3 signaling. **2010,** *136* (4), 603-610.

21. Lang, K. L.; Silva, I. T.; Zimmermann, L. A.; Machado, V. R.; Teixeira, M. R.; Lapuh, M. I.; Galetti, M. A.; Palermo, J. A.; Cabrera, G. M.; Bernardes, L. S. C. J. B.; chemistry, m., Synthesis and cytotoxic activity evaluation of dihydrocucurbitacin B and cucurbitacin B derivatives. **2012,** *20* (9), 3016-3030.

22. Ahmed, M. S.; Halaweish, F. T. J. J. o. e. i.; chemistry, m., Cucurbitacins: potential candidates targeting mitogen-activated protein kinase pathway for treatment of melanoma. **2014,** *29* (2), 162-167.

23. Ahmed, M. S.; El-Senduny, F.; Taylor, J.; Halaweish, F. T. J. C. b.; design, d., Biological screening of cucurbitacin inspired estrone analogs targeting mitogen-activated protein kinase (MAPK) pathway. **2017,** *90* (3), 478-484.

24. Mahnashi, M. H., Design, Synthesis and Biological Screening of Novel Cucsinspired Estrone Analogues Towards Treatment of Hepatocellular Carcinoma. **2017**.

25. Ahmed, M. S.; Kopel, L. C.; Halaweish, F. T. J. C., Structural optimization and biological screening of a steroidal scaffold possessing cucurbitacin-like functionalities as B-raf inhibitors. **2014,** *9* (7), 1361-1367.

26. Abou-Salim, M. A.; Shaaban, M. A.; El Hameid, M. K. A.; Elshaier, Y. A.; Halaweish, F. J. B. c., Design, synthesis and biological study of hybrid drug candidates of nitric oxide releasing cucurbitacin-inspired estrone analogs for treatment of hepatocellular carcinoma. **2019,** *85*, 515-533.

27. Fe, NM 87508 ,August 12, 2008; p http://www.apmggroup.net/innovation/molecular_testing/melanoma_pathways/melanoma.html.

28. OpenEye Scientific Software, Inc. : 9 Bisbee Ct, Suite D Santa Fe, NM 87508, 2008

29. OpenEye Scientific Software, I., *FRED Fast Rigid Exhaustive Docking*. 9 Bisbee Ct, Suite D Santa Fe, NM 87508 August 12, 2008; p http://www.apmggroup.net/innovation/molecular_testing/melanoma_pathways/melanoma.html.

30. Stéphan, E.; Zen, R.; Authier, L.; Jaouen, G., Improved synthesis of a protected 11-oxoestrone. Steroids 1995, 60 (12), 809-811.

Chapter Five

Synthesis and Biological Activity of C-11 Ketone Cucurbitacin-Inspired Estrone Analogs Targeting Pancreatic Ductal Adenocarcinoma

Abstract

The treatment of pancreatic cancer is one of the major unsolved health problems today. The high mortality rate of pancreatic cancer patients, among other cancer types, is due to the lack of early diagnosis and of effective treatments. Recently, cucurbitacin B has shown promising antiproliferative activity against human pancreatic cancer cells via decreasing the expression levels of pSTAT3 and pEGFR in a dose- and time-dependent manner. In order to overcome the low yield of cucurbitacin B that prevented its clinical use, a molecular-modeling based drug discovery process was undertaken to install cucurbitacin pharmacophores in the four-membered ring estrone as a carrier scaffold. This resulted in the discovery of **C**ucurbitacin-**I**nspired **E**strone **A**nalogs (CIEA's).

Previously, we confirmed bioinformatically and biologically that the functionalization of C_{11} of the CIE analogs can increase the anticancer effects of this group. Furthermore, the inhibition of pEGFR and pErk expression was demonstrated on pancreatic cancer cell lines. So far, two types of analogs have been synthesized to study the effects of the functionalization of this group. The desaturation of C_{9} and C_{11}led to increased activity compared to the saturated analogs. Upon broader investigation, it was confirmed that the hydroxylation of C_{11}can further increase the activity. In order to increase the potency, both a molecular modeling study and biological data were used to synthesize 8 CIE analogs with

a ketone group at C_{11}. Although only the KA9 analog showed promising activity, it has a greater anticancer effect than previously discovered analogs. Moreover, the results of a Cell Titer assay showed that KA9 had greater anticancer activity on 2D and 3D models of pancreatic cancer cell lines than KA1 and KA2 that were synthesized previously. The anticancer activity was also greater than gemcitabine, since it decreased the micro tumor size after several days of treatment. KA9 demonstrates the inhibition of pEGFR and pErk overexpression, compared to the phosphorylation of mTOR and STAT3. The cell cycle arrest experiment indicated that KA9 inhibited the G1 phase in a time- and dose-dependent manner. KA9 was proven to induce cell death through increased caspase-3 activity on PANC-I cell lines. This result suggests that KA9 is a potential candidate for animal study as a promising pancreatic anticancer agent.

5.1. Introduction

Based on the current incidence, the availability of the treatment and the developing resistance of different cancer types, it is expected that pancreatic ductal adenocarcinoma with liver cancer will be the second and third leading causes of deaths by 2030.[1] Currently, pancreatic cancer is the fourth leading cause of death among cancer types for both men and women.[2] This high mortality rate is attributed to the absence of diagnostic markers in the early stages of pancreatic cancer.[3] The slow progress in finding novel anticancer agents contributes to this expectation of high mortality in the future.[4] Since the disease is generally detected in its late stages, the only option for treatment is chemotherapy, where gemcitabine is the first line of treatment, either alone or in combination therapy. However, its one-year survival rate is 18%, while the 6-month survival rate is 23.8%. The body's resistance to gemcitabine uses many mechanisms, such as a decreased number of

transporters and an overexpression of cytidine deaminase that converts gemcitabine into its inactive metabolite 2',2'-difluorodeoxyuridine (dFdU).[5] This indicates the importance of finding new anticancer drugs with various mechanisms of action.

Epidermal transmembrane factor receptor (EGFR) is a tyrosine kinase that is overexpressed in many cancer types, including pancreatic cancer. EGFR overexpression was found to be related to the advancement of the disease, its low survival rate, and metastasis.[6] One of the important EGFR targeting compounds is **C**ucurbitacin-**I**nspired **E**strone **A**nalogs (CIEA's), which were initially synthesized by installing a 23, 24 α, β- unsaturated ketone side chain in the four membered-rings of triterpene estrone. This compound shows comparable anticancer activity to that of cucurbitacin.[7] CIE analogs have been through several modifications that increase their anticancer activities against different cancer cell lines, including erlotinib resistant HepG2 and multidrug resistance protein (MRP1).[8] Currently, we have shown that the functionalization of rings B and C leads to more potent anticancer agents than the currently available standard treatments.

Previously, we found that the dehydrogenation of C_9-C_{11}, with the installation phenyl *para*-trifluoro and *para*-nitro side chains, can increase their anticancer activity against pancreatic cancer cell lines. Moreover, the α-hydroxylation of C_{11} led to an increase in the anticancer activity with a cuc side chain and phenyl *para*-trifluoro.[9, 10] However, upon testing these compounds in a 3-D model of PANC-I pancreatic cancer, these CIE analogs showed poor penetration and weak anticancer activity, which suggests that further modifications and optimization are needed before moving to an *in vivo* study.

In this study, we report on the molecular modeling of CIEA analogs with ketone C_{11} CIE analogs, a synthesis of the best scoring analogs. We include their bioavailability assay results on PANC-I, AsPC-I, and BXPC-3 pancreatic cell lines, the flowcytometric analysis of KA9, and their inhibition of pEGFR, pER activation using In-Cell Western Analysis. Furthermore, the anticancer activity of KA9 was demonstrated on a 3D model of the PANC-I pancreatic cell line, which indicates a promising potential for KA9 compared to the previously synthesized CIE analogs.

5.2. Results and Discussion

5.2.1. Molecular Modeling Design Strategy

Based on the MTT screening results of CIE analogs, transferring an OH group in C-3 into ether can increase the anticancer activity of MSA7 compared to the same analog with phenolic OH. Also, the molecular modeling studies introduced different side chains, such as *para*-trifluoromethyl phenyl, at C-17 on ring D of estrone, dramatically increasing the antiproliferative activity against hepatocellular carcinoma, breast cancer, colon cancer and others.[10] Upon molecular modeling against an ATP binding site of pEGFR, the KA9 analog was the best scoring analog, which indicates its high affinity upon docking against a pEGFR binding pocket using hydrogen bonding with Ala:18: A (**Figure 5.1**).

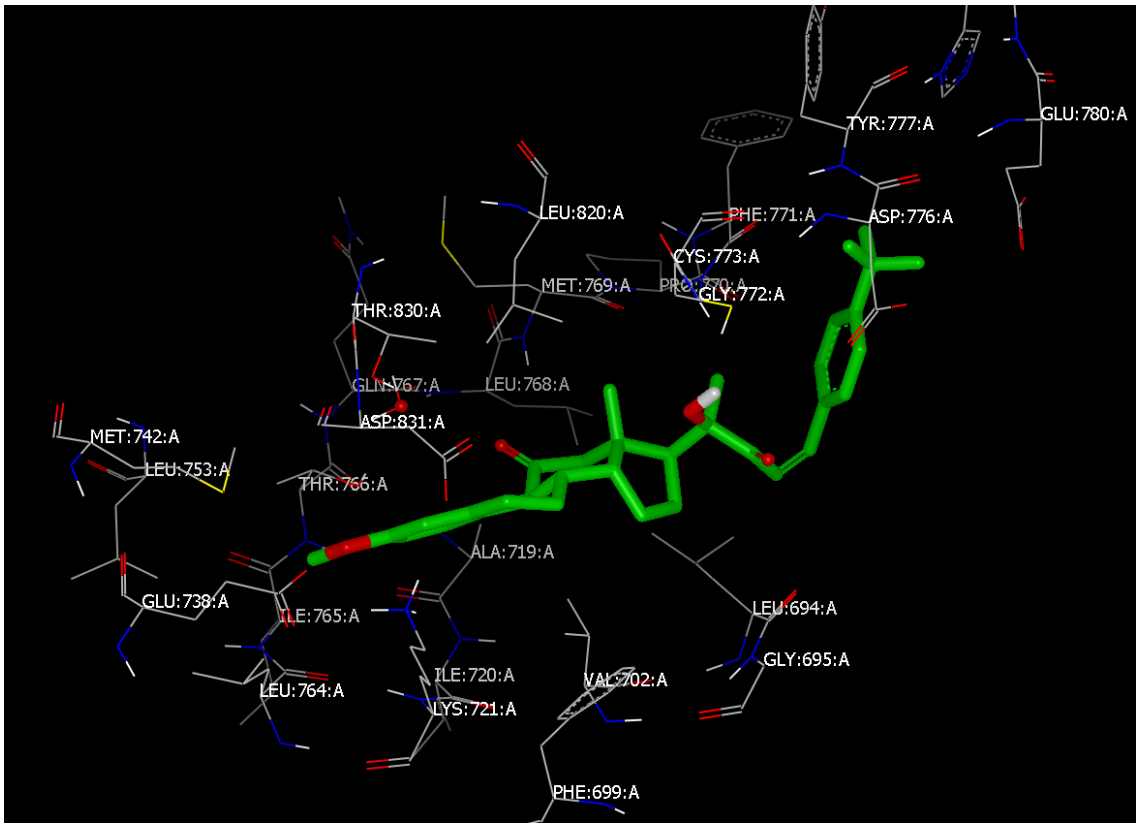

Figure 5.1. Docking profile of the highest scoring CIE analog KA9 on EGFR pocket indicate insertion of the molecule in the pocket by hydrophobic interaction.

Moreover, KA9 demonstrated a promising binding affinity to an RAS binding pocket with a hydrogen bond formation between C_{11} ketone and Ala: 18: A (**Figure 5.2**). The RAS protein is one of the most investigated proteins in pancreatic ductal adenocarcinoma, due to its importance in the resistance mechanism that exists in pancreatic ductal adenocarcinoma patients. It has been reported that nearly 95% of PDAC patients have mutations in KRAS, which is one of the key signaling proteins that leads to an increase in tumor growth, even while inhibiting upstream proteins (KRAS: feeding pancreatic cancer proliferation).

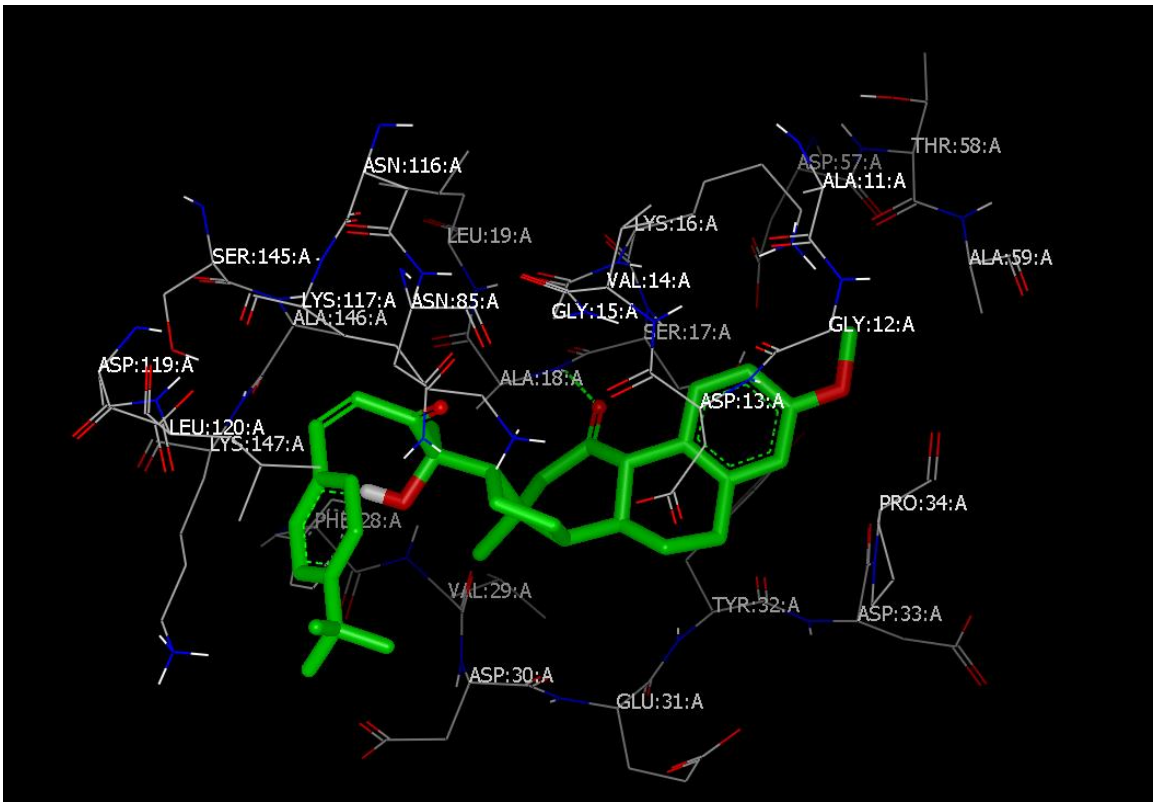

Figure 5.2. KA9 binding in RAS binding pocket show a hydrogen bonding with Ala: 18: A.

5.2.2. Chemical Synthesis

This group of compounds is characterized by the carbonyl group at C_{11}, which contrasts with the previously synthesized compounds that have dehydrogenated C_9 and C_{11} or a hydroxyl group. To obtain the final compounds KA9-KA16, the oxidation of the hydroxyl group is first carried out using the same conditions which oxidize the hydroxylated C_{20}. However, this produced a very small yield of the oxidized product compared to using AlCl3 as a catalyst with a yield of 80%.[11] This confirms that the stereochemistry of the compound hinders the position of C_{11} and requires a catalyst, as in the case of hydroboration hydroxylation and TBS protection.

5.2.3. Biological evaluations:

Two cell lines were used to conduct the cell viability assay against 3 pancreatic cancer cell lines, PANC-I, AsPC-1, and PCBX-3. Most of the synthesized compounds did not show anticancer activity, including KA12, which contains a cuc side chain. This contrasts with the previously synthesized analogs that showed activity from the cuc side chain containing compounds with different modifications. KA9, which contains a phenyl *para*-trifluoro unsaturated side chain, shows greater anticancer potency than any previously synthesized C_{11} functionalized CIE analog. The IC_{50}'s were 4.30, 4.17 and 5.7 μM upon treatment of PANC-I, AsPC-1, and PCBX-3, respectively (**Table 5.1**).

In order to further investigate the effects of KA1 and KA2, an MTT assay was conducted with the addition of HPaSteC cells, which are the main fibroblastic cells of the pancreas. The HPaSteC cells stimulate pancreatic cancer proliferation, inhibit apoptosis, and enhance angiogenesis.[12] Upon co-culturing PANC-I with HPaSteC cells, no main difference was observed between the two results, which indicates the effectiveness of these analogs. Clearly, they are not affected by the inducers of pancreatic cell proliferation (**Figure 5.4**), unlike the standard treatment, gemcitabine.

MTT assay is one of the best known experiments to study the effects of small molecules in terms of cell viability.[13] It measures the concentration of ATP based on the luminescence produced by oxyluciferine after it is formed from luciferine. This assay also has a lower sensitivity than a CellTiter assay. Upon treating the cells with CIE analogs KA1, KA2, and KA9 to PANC-I and PANC-I/ HpaSteC, no noticeable difference was found in IC_{50} results (less than 3 μM), as indicated in Figure 5B and **Table 5.3**.

In order to the study the mechanism by which CEI analogs lead to the inhibition of cancer growth, two mechanism can occur— either inducing cell death or inhibiting cell division. Along with the analysis of cytotoxicity, we measured caspase 3/7 activation in cancer cells using different concentrations of the tested compounds. We revealed that KA1, KA2 and KA9 could cause a 1.5-2-fold increase in caspase activity at sub-toxic concentrations; at toxic concentrations, caspase activity dropped due to a drastic decrease in the cell numbers (**Figure 5.5 B**). At the same time, we observed as much as a 20% increase in caspase activity by GEM and no drop in the considered concentration range (up to 50 μM).

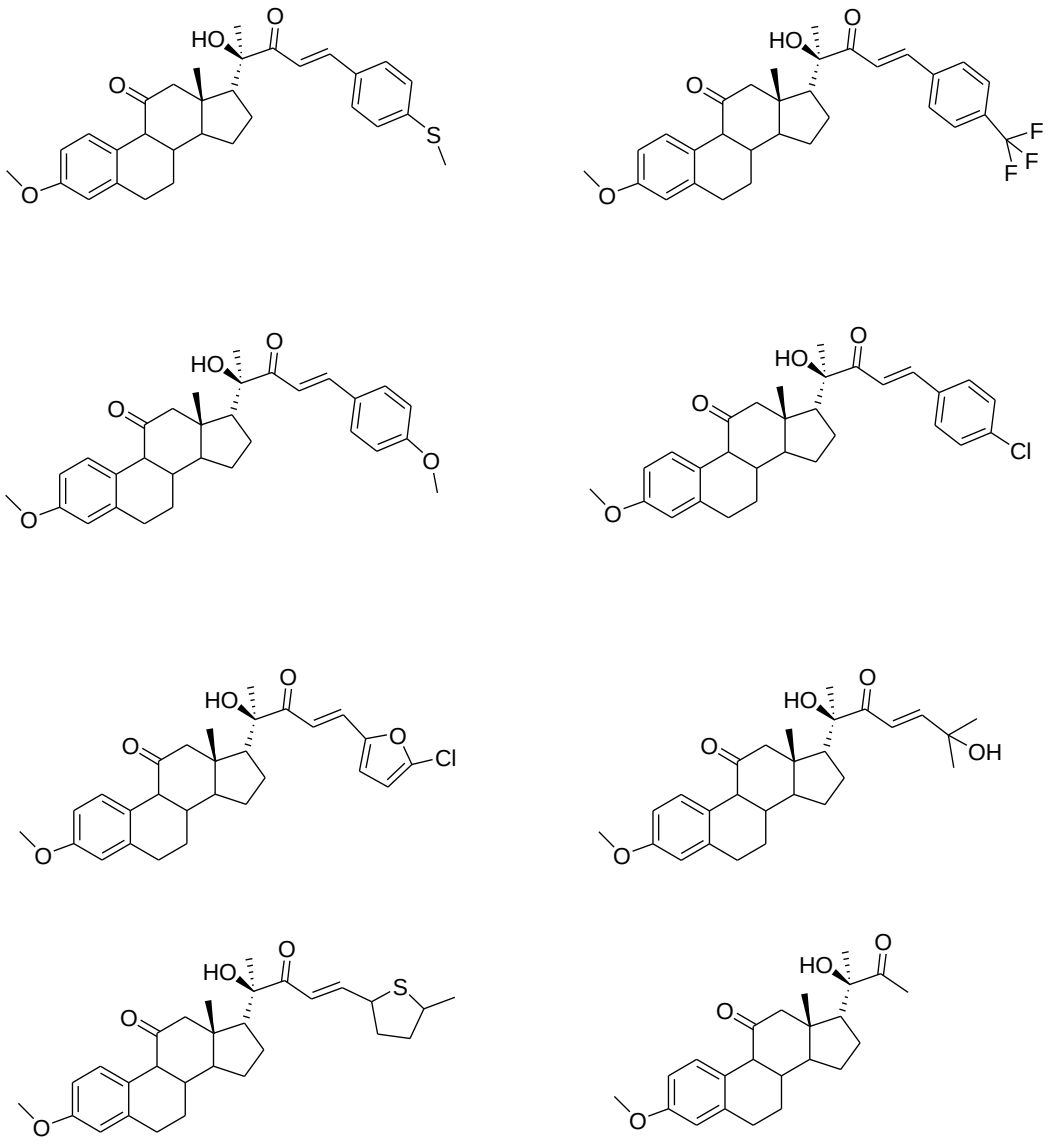

Figure 5.3. The structures of the synthesized oxygenated cucurbitacin-inspired analogs.

Table 5.1. IC_{50}'s in μM of the synthesized CIE analogs upon treatment of PANC-I, AsPC-1, and PCBX-3.

Compound	PANC-I	AsPC-I	BXPC-3
KA9	4.9± 0.3	4.17± 0.9	5.7± 0.65
KA10	NA	NA	NA
KA11	NA	NA	NA
KA12	NA	NA	NA
KA13	NA	NA	NA
KA14	NA	NA	NA

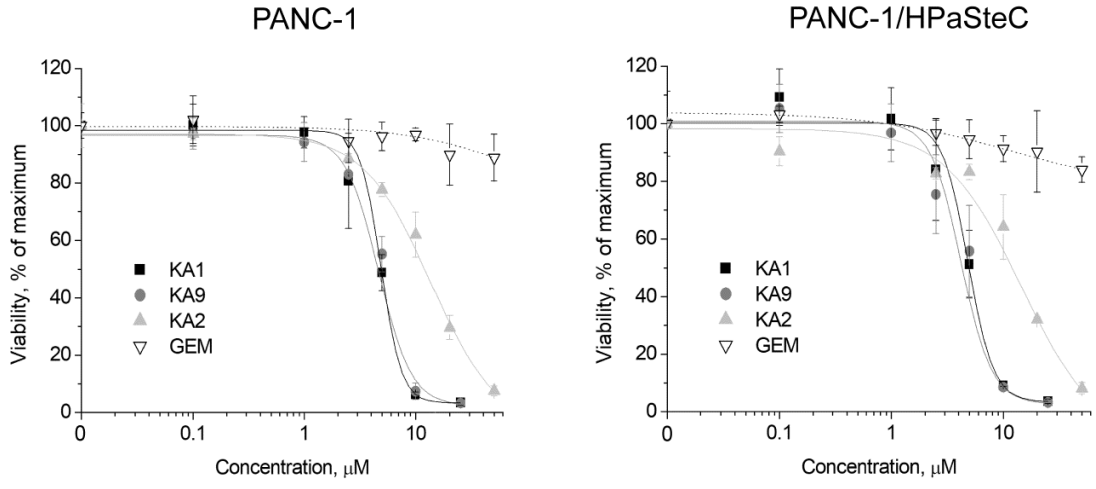

Figure 5.4. MTT assays of PANC-1 and PANC-1/HPaSteC co-culture cell viability after 48 h exposure to cucurbitacin derivatives (KA1, KA2, and KA9) and gemcitabine (GEM). Data are given as means±SD.

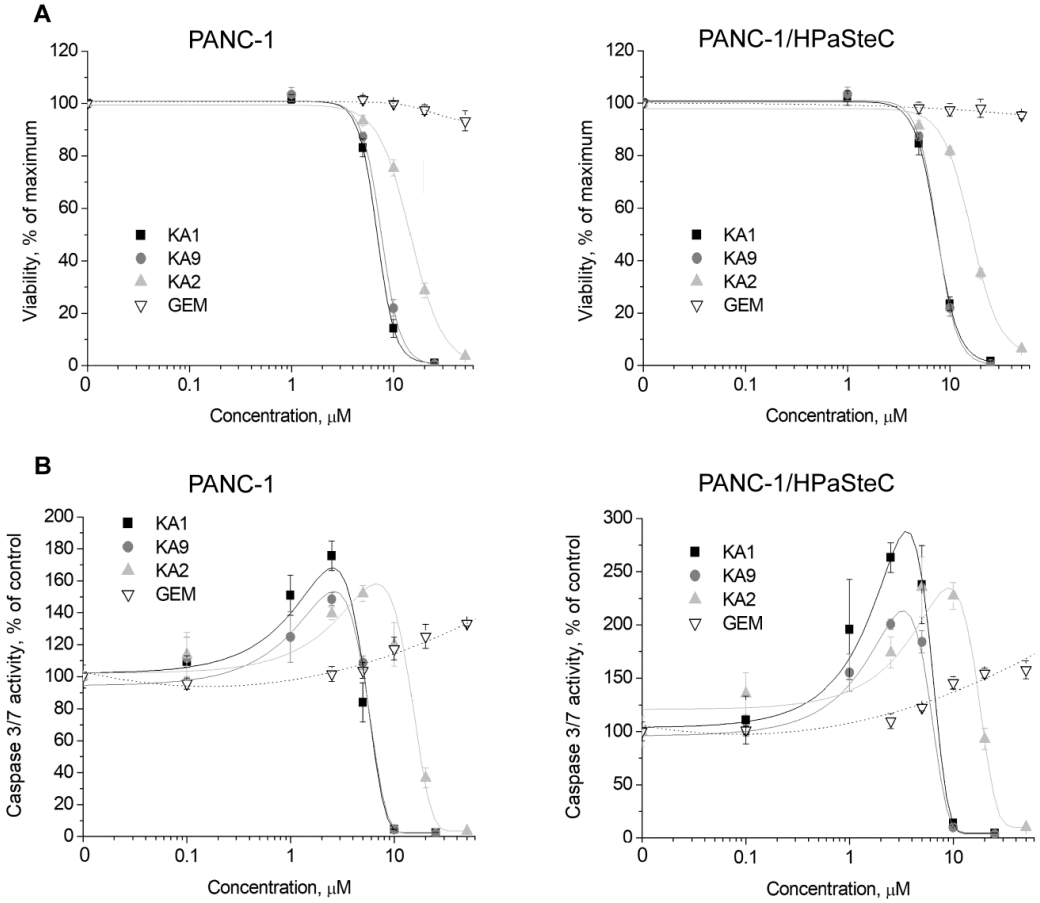

Figure 5.5. Cytotoxic efficacy of cucurbitacin derivatives in monolayers. (A) CellTiter assays of PANC-1 and PANC-1/HPaSteC co-culture cell viability after 48 h exposure to cucurbitacin derivatives (KA1, KA2, and KA9) and gemcitabine (GEM). (B) Caspase 3/7 activity in PANC-1 and PANC-1/HPaSteC 2D co-cultures after 48 h exposure to cucurbitacin derivatives (KA1, KA2, and KA9) and gemcitabine (GEM). Data are given as means±SD.

We then studied the changes that the compounds caused in DNA during different phases of cell growth. According to the mechanism of action of the anticancer agent, a specific growth phase will be affected. If G1 was affected that means the mechanism that is likely

to be is DNA damage or affecting the growth factors; however, if the growth was affected in the S phase, that means the affect was in DNA synthesis.

To further investigate for the effects of active CIE analogs, cell cycle analysis was conducted with these compounds against the PANC-I cell line. The results demonstrated that they accumulate cells at the G1 phase, which indicates that the mechanism of action is similar in these compounds. Moreover, KA9 induced cell cycle arrest in a time- and concentration-dependent manner, as indicated in **Figures 5.6 and 5.7** and **Tables 5.4 and 5.5.**

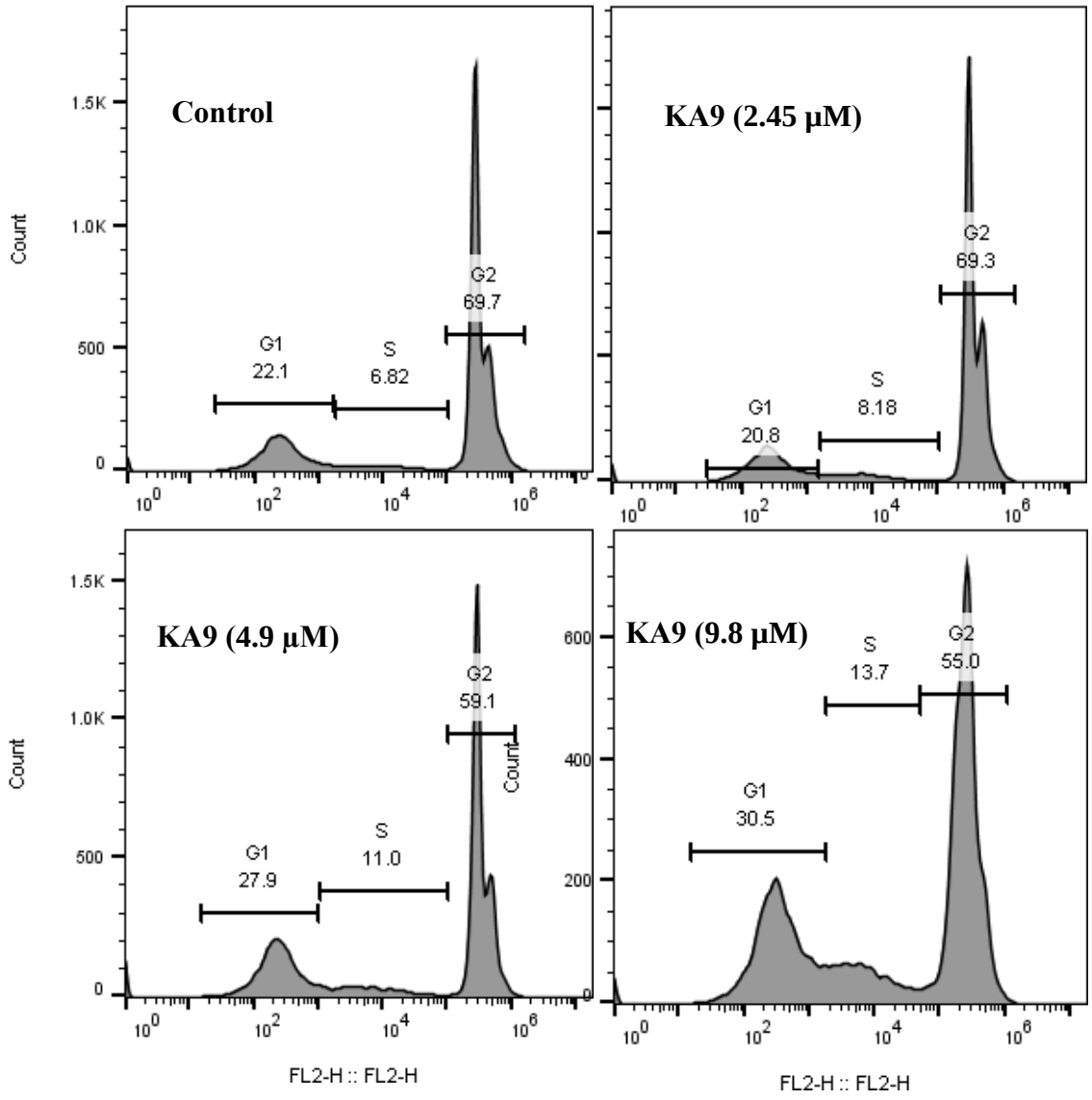

Figure 5.6. Effects of different concentrations of KA9 upon cell cycle indicates G1 phase accumulation after 48 hrs.

Table 5.2. Effects of KA9 treatment on cell cycle upon treatment with different concentrations

Groups	$G_0 - G_1$	S	G_2 - M
Control	22.1	6.82	69.7
KA9 (2.45 µM)	20.8	8.18	69.3
KA9 (4.9 µM)	27.9	11	59.1
KA9 (9.8 µM)	30.5	13.7	55

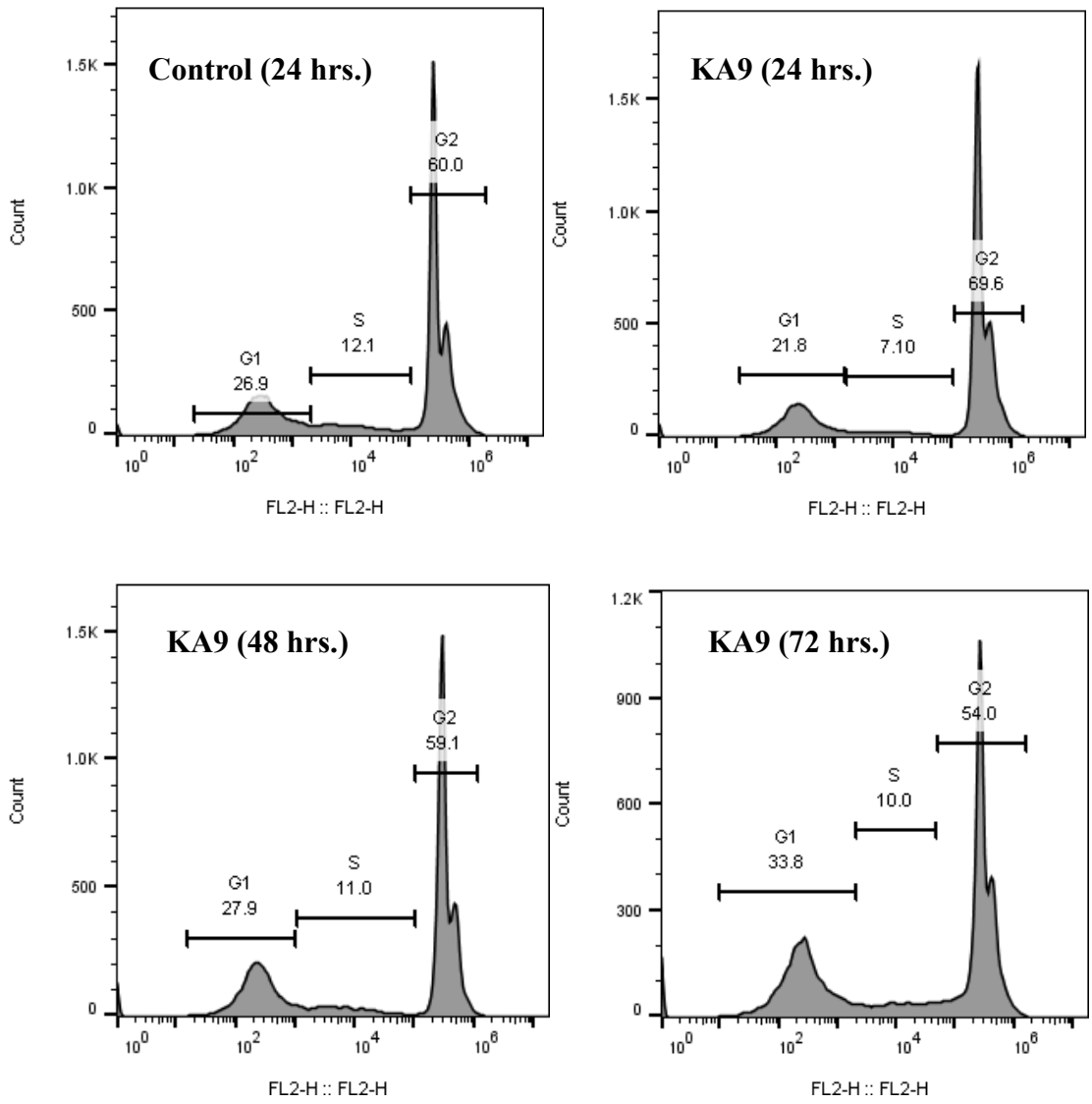

Figure 5.7. Effects of KA9 upon cell cycle indicates inhibition in a time-dependent manner.

Table 5.3. Effect of KA9 upon cell cycle indicates inhibition in a time-dependent manner.

Groups	$G_0 – G_1$	S	G_2 - M
Control (24 hrs.)	21.8	7.10	69.6
KA9 (24 hrs.)	26.9	12.1	60
KA9 (48 hrs.)	27.9	11	59.1
KA9 (72 hrs.)	33.8	10.0	54

The PANC-I cell line was treated with different concentrations of KA9 in order to study the inhibition of various protein activations. Four concentrations, starting with the fourth IC_{50} on PANC-I to twice the $IC_{50,}$ were used to treat the cells. After 24 hrs. KA9, in a concentration-dependent manner, inhibited the phosphorylation of pEGFR and pErk compared to mTOR and pSTAT3, which confirms that the mechanism of action is similar to the previously synthesized CIE analogs (**Figure 5.8**). These results indicate the specificity of KA9 in inhibition of pEGFR and pErk phosphorylation without affecting different routes such as STAT3 and mTOR compared to the broad effect of cucurbitacin. These results indicate that KA9 might have low toxicity compared to cucurbitacin compounds.

In addition to the monolayer cell viability assays, results for the heterospheroids of PANC-1/HPaSteC (2:1) (**Table 5.4**) were obtained, in spite of the reported chemoprotective effect of myofibroblasts on pancreatic cancer cells in co-culture.

Table 5.4. IC_{50} values* for 2D and 3D cell cultures of PANC-1 cells and their co-cultures with HPaSteC.

Compound	2D				3D	
	MTT assay		CellTiter assay		CellTiter assay	
	PANC-1	PANC-1/ /HPaSteC (2:1)	PANC-1	PANC-1/ /HPaSteC (2:1)	PANC-1 120 cells, 2 weeks	PANC-1/ /HPaSteC 120:60 cells, 2 weeks
KA1	4.9	5.1	7.6	7.6	37.5	50.0
KA2	11.8	11.8	13.6	15.8	37.5	39.5
KA9	4.4	4.5	7.5	7.6	21.0	24.3

*All concentration values are given in µM.

Cancer spheroids are considered a more advanced cellular model for screening novel drug candidates, since they mimic the tumor microenvironment to a higher extent and provides better predictive values than cell monolayers.[14] For the cytotoxicity evaluation of cucurbitacin-derived compounds, we used pancreatic cancer homospheroids containing PANC-1 cells, and heterospheroids comprised of PANC-1 and HPaSteC. Both types of spheroids were cultivated for two weeks, reaching a size of approximately 450-500 µm in diameter.

Upon activation in a tumor microenvironment, pancreatic stellate cells play an important role in the progression of PDAC and significantly contribute to the development of the desmoplastic reaction.[15]Here, we studied the expression and architecture of ECM components in both types of spheroids. We found that heterospheroids more extensively

produced collagen I, which form fibrous clusters in spheroid interstitium, whereas in PANC-1 spheroids, it was distributed diffusely (**Figure 5.8**). Furthermore, PANC-1/HPaSteC spheroids produced a fibronectin fibrillary scaffold, while homospheroids did not express this ECM component.

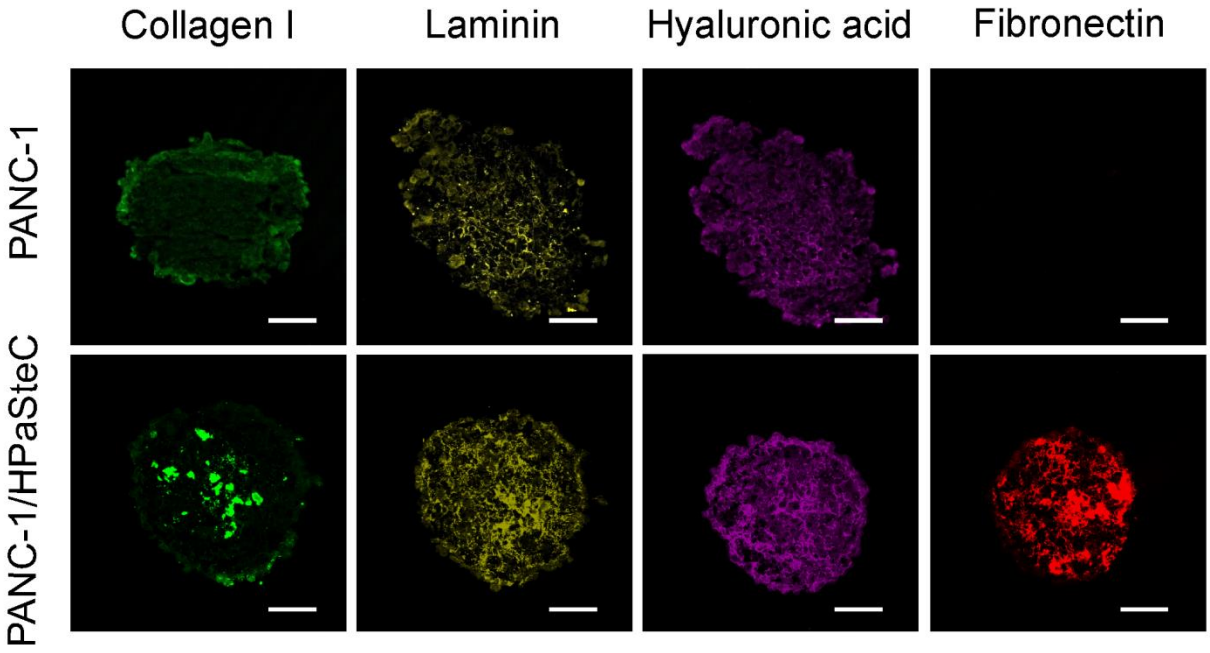

Figure 5.8. Expression of ECM components in pancreatic cancer spheroids. Collagen I (green), fibronectin (red), hyaluronan (purple) and laminin (yellow) in PANC-1 and PANC-1/HPaSteC microtumors were defined in 10 µm-thick spheroid frozen section by immunofluorescent staining. Sections were obtained from spheroids incubated for 2 weeks in growth medium. Scale bar is 100 µm.

To estimate the cytotoxic effects of cucurbitacin derivatives, we used CellTiter assay to compare the values with those obtained for the monolayers of PANC-1 and the PANC-1/HPaSteC co-culture. This test revealed that 3D spheroids are more resistant to all tested compounds than cells in 2D cultures **(Figure 5.9 A, B and Table 5.4**). Moreover, heterospheroids demonstrated slightly higher resistance to all drugs, as compared to homospheroids. Interestingly, in the 3D models, the cytotoxicity trend of the drugs changed

in comparison with the 2D models, resulting in KA9>KA1≈KA2>>GEM. According to our results, KA9 displayed the highest toxicity. This trend was confirmed by another experiment on the inhibition of the spheroid growth rate. We added drugs at final concentrations of 10 µM to 5-day old spheroids and measured their growth. Only KA9 was able to cause a regression of the spheroids, whereas other drugs, including GEM, merely delayed their growth (**Figure 5.9 C, D**).

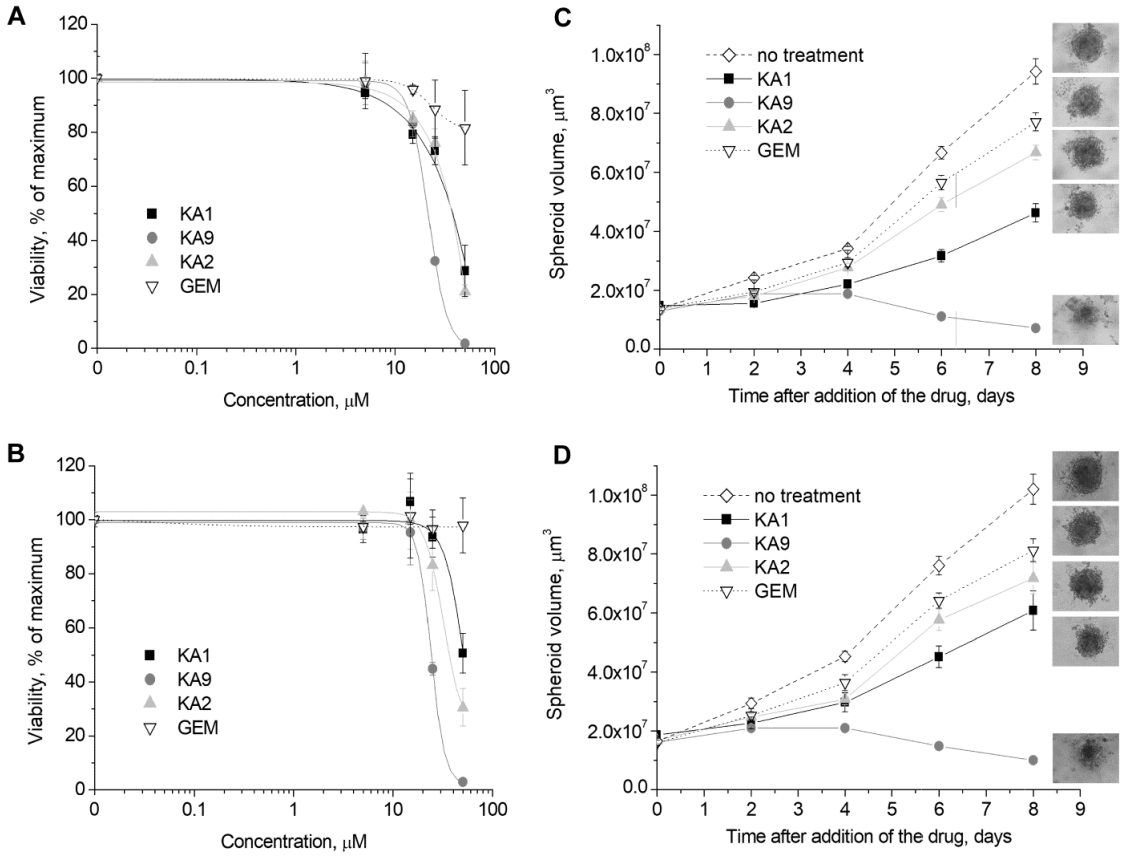

Figure 5.9. Cytotoxic efficacy of cucurbitacin-inspired estrone analogs for pancreatic microtumors. CellTiter analysis of PANC-1 (A) and PANC-1/HPaSteC (B) spheroid viability after 48 h exposure to cucurbitacin derivatives (KA1, KA2, and KA9) and gemcitabine (GEM). For evaluation of spheroid growth inhibition, cucurbitacin derivatives (KA1, KA2, KA9) or gemcitabine (GEM) were added to 5-days old spheroids (day 0). Volumes of PANC-1 (C) or PANC-1/HPaSteC (D) pancreatic tumor spheroids were calculated as L x W x W (length x width x width) every 2 days. All spheroid images in (C) and (D) have a size of 650×450 microns. Data are given as means±SD.

5.3. Material and Methods

5.3.1. Molecular Modeling

The molecular modeling studies were carried using two OpenEye software programs, [13] Omega to generate the conformers of the compounds and FRED to allow rigid exhaustive docking.[14] The targets for the previously mentioned proteins were processed and generated using MakeReceptor®. After the molecular docking was carried out, the consensus scores were visualized using VIDA software.

5.3.2. Chemical Synthesis:

All chemicals and solvents (ACS grades) were purchased from Fisher Scientific or Sigma Aldrich and used without any additional treatment. Before conducting the experiments, all the glassware and tools were cleaned, washed and dried in 120 °C oven, followed by closing and introducing nitrogen gas to the reaction vessel for all the reaction period, except when mentioned during the experiment. TLC plates (Silica gel, 0.2-mm thick, polyester backed, Sorbtech) were used to analyze the reaction conditions under UV254. All synthetic intermediates and final compounds were purified using column chromatography packed with silica gel 60A, 40-63 μm. ^{1}H and ^{13}C NMR spectra were carried out using Bruker AVANCE-400 MHZ and 600 MHZ NMR spectrometers. The solvents used for the compounds are $CDCl_3$ and D-acetone, as will be indicated later. NMR chemical shifts were presented in δ(PPM) using residual solvent peaks as standards ($CDCl_3$, 7.26 (^{1}H), 77.16 (^{13}C). High resolution mass (HRMS) was performed using a Thermofinnigan MAT 95XL mass spectrometer at the Buffalo mass spectroscopy facility. X-ray crystallography was conducted on KI 9 at the University of South Dakota using a Bruker APEX^{II} diffractometer.

To a solution of 0.22 mm of C_{11} hydroxy CIE analogs in DCM (2 mL), AlO3 (0.53 g) was added, followed by PCC (0.659 g). The reaction mixture was heated to 45 for 4 hrs. Next, the reaction mixture was filtered through silica using ethyl acetate, followed by concentrating it under *vacuu* and purifying it through silica using (8:2) hexane: ethyl acetate.

KA12

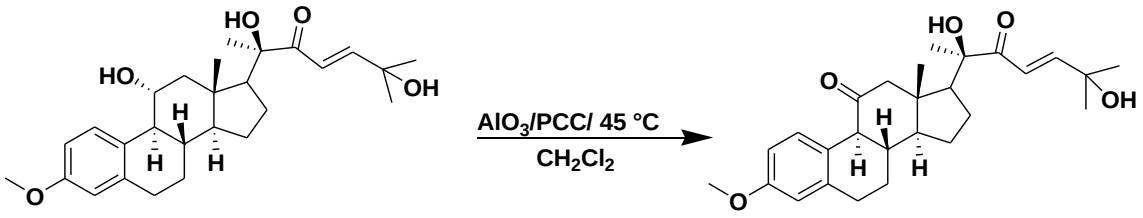

1H NMR (600 MHz, CDCl3) δ 6.89 (s, 4H), 6.69 (d, J = 8.4 Hz, 11H), 6.66 – 6.63 (m, 24H), 4.34 (s, 8H), 3.72 (s, 32H), 2.84 – 2.71 (m, 39H), 2.56 (t, J = 9.1 Hz, 13H), 2.47 (d, J = 12.5 Hz, 13H), 2.23 (tdd, J = 13.6, 6.2, 3.2 Hz, 23H), 2.19 – 2.12 (m, 25H), 2.02 (dt, J = 12.5, 3.2 Hz, 17H), 1.99 (s, 31H), 1.93 (td, J = 12.1, 6.8 Hz, 20H), 1.80 – 1.71 (m, 45H), 1.31 (s, 15H), 0.62 (s, 31H).

KA9

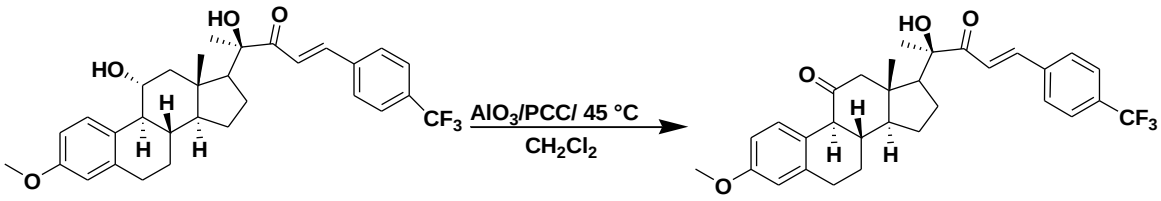

1H NMR (600 MHz, CDCl3) δ 7.74 (d, J = 15.6 Hz, 3H), 7.62 (d, J = 8.3 Hz, 6H), 7.58 (d, J = 8.4 Hz, 6H), 6.91 – 6.87 (m, 4H), 6.72 (s, 2H), 6.69 – 6.67 (m, 3H), 6.63 (d, J = 2.5 Hz, 3H), 3.72 (s, 9H), 2.89 (d, J = 12.5 Hz, 3H), 2.73 (d, J = 5.7 Hz, 7H), 2.45 (d, J = 12.6 Hz, 3H), 2.29 – 2.19 (m, 5H), 2.18 (s, 2H), 2.04 (d, J = 12.5 Hz, 4H), 2.00 – 1.96 (m, 2H), 1.85 (dd, J = 17.1, 7.9 Hz, 8H), 1.72 – 1.68 (m, 5H), 1.67 – 1.57 (m, 11H), 1.37 (s, 9H), 1.33 (dd, J = 10.9, 4.9 Hz, 3H), 1.30 – 1.27 (m, 5H), 0.91 (s, 9H).

13C NMR (151 MHz, CDCl3) δ 213.04, 200.78, 159.32, 150.49, 140.38, 137.94, 130.64, 128.62, 127.39, 119.36, 115.55, 114.51, 113.35, 109.85, 78.40, 55.23, 53.66, 52.89, 47.84, 47.55, 41.15, 24.73, 24.05, 23.60, 22.27, 20.30, 14.65.

KA8

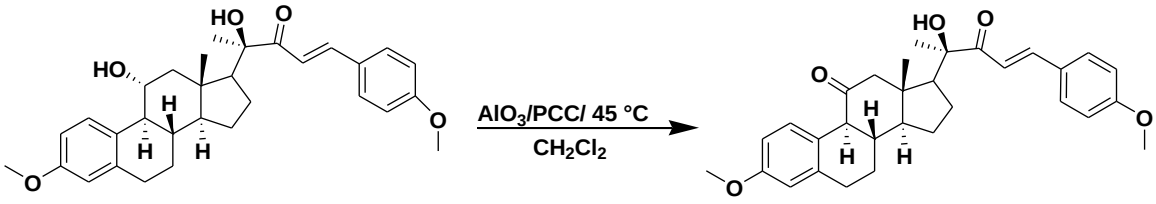

1H NMR (600 MHz, CDCl3) δ 7.71 (d, J = 15.5 Hz, 1H), 7.47 – 7.45 (m, 2H), 7.17 (d, J = 8.7 Hz, 1H), 6.83 – 6.80 (m, 2H), 6.77 (d, J = 15.5 Hz, 1H), 6.64 (dd, J = 8.7, 2.8 Hz, 1H), 6.49 (d, J = 2.7 Hz, 1H), 4.13 (s, 1H), 3.74 (s, 3H), 3.65 (s, 3H), 3.37 (d, J = 11.5 Hz, 1H), 2.82 (d, J = 11.5 Hz, 1H), 2.71 (dd, J = 12.5, 4.9 Hz, 1H), 2.64 (dd, J = 16.9, 3.7 Hz, 1H), 2.59 (d, J = 11.5 Hz, 1H), 2.04 (t, J = 9.6 Hz, 1H), 1.90 – 1.84 (m, 1H), 1.80 (ddd, J = 7.5, 5.6, 2.8 Hz, 1H), 1.71 – 1.57 (m, 3H), 1.38 (s, 3H), 1.32 – 1.16 (m, 3H), 0.83 (s, 3H).

13C NMR (151 MHz, CDCl3) δ 209.38, 201.26, 162.19, 158.00, 146.07, 138.47, 131.13, 130.62, 126.87, 123.71, 115.53, 114.52, 113.76, 111.62, 78.48, 57.92, 55.72, 55.50, 55.45, 55.23, 54.39, 49.05, 39.28, 30.05, 27.93, 24.26, 22.83, 22.52, 14.77.

KA13

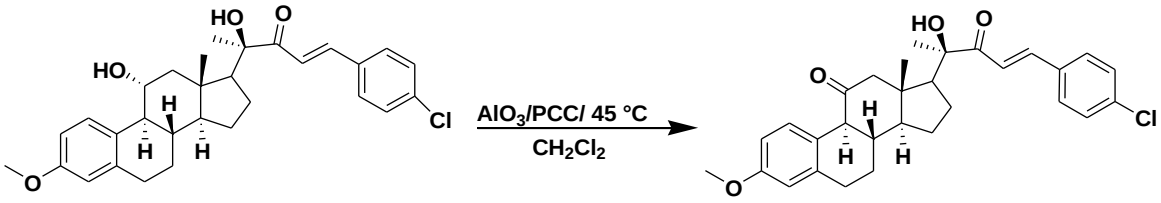

1H NMR (600 MHz, CDCl3) δ 7.73 (d, J = 15.6 Hz, 1H), 7.40 (dd, J = 8.7, 2.4 Hz, 2H), 7.29 (dd, J = 8.7, 2.1 Hz, 2H), 6.79 – 6.76 (m, 1H), 6.64 (s, 1H), 6.61 (d, J = 1.1 Hz, 1H), 6.55 (s, 1H), 3.69 (s, 2H), 2.98 – 2.85 (m, 2H), 2.83 – 2.68 (m, 4H), 2.58 – 2.50 (m, 1H), 2.47 (dd, J = 15.0, 6.1 Hz, 1H), 2.24 – 2.21 (m, 1H), 2.20 – 2.08 (m, 3H), 1.67 – 1.55 (m, 3H), 1.25 (s, 2H), 0.82 – 0.78 (m, 3H), 0.71 (s, 3H).

13C NMR (151 MHz, CDCl3) δ 212.66, 201.65, 182.25, 159.19, 144.31, 137.18, 132.50, 129.94, 129.35, 128.62, 119.15, 114.49, 113.22, 112.63, 78.75, 55.25, 54.61, 51.23, 47.39, 46.89, 41.05, 31.14, 29.73, 26.27, 24.73, 22.94, 20.30, 14.35.

KA10

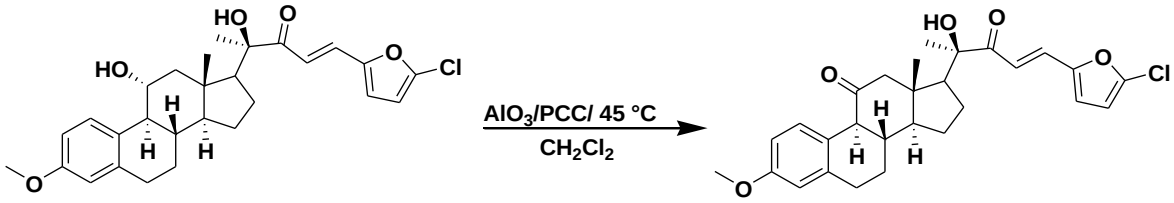

1H NMR (600 MHz, CDCl3) δ 7.36 (d, J = 15.2 Hz, 1H), 6.73 (d, J = 8.6 Hz, 1H), 6.68 (dd, J = 8.6, 2.7 Hz, 1H), 6.64 (s, 1H), 6.62 (s, 1H), 6.62 (d, J = 2.2 Hz, 1H), 6.24 (d, J = 3.5 Hz, 1H), 3.72 (s, 3H), 2.89 (d, J = 12.5 Hz, 1H), 2.78 (dd, J = 13.1, 5.7 Hz, 1H), 2.71 (dd, J = 17.5, 5.7 Hz, 1H), 2.47 (d, J = 12.6 Hz, 1H), 2.24 – 2.17 (m, 1H), 2.04 (dt, J = 12.5, 3.3 Hz, 1H), 1.89 – 1.82 (m, 2H), 1.73 – 1.54 (m, 4H), 1.34 (s, 3H), 1.32 – 1.21 (m, 3H), 0.90 (s, 3H).

13C NMR (151 MHz, CDCl3) δ 213.04, 200.78, 159.32, 150.49, 140.38, 137.94, 130.64, 128.62, 127.39, 119.36, 115.55, 114.51, 113.35, 109.85, 78.40, 55.23, 53.66, 52.89, 47.84, 47.55, 41.15, 24.73, 24.05, 23.60, 22.27, 20.30, 14.65.

KA16

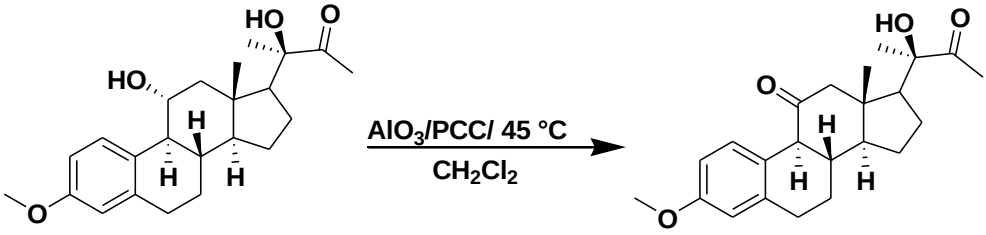

^{1}H NMR (600 MHz, CDCl3 δ 7.73 (d, *J* = 8.4 Hz, 4H), 6.60 (dd, *J* = 8.7, 2.8 Hz, 4H), 6.54 (d, *J* = 2.8 Hz, 4H), 3.72 (s, 3H), 2.89 (d, J = 12.5 Hz, 1H), 2.78 (dd, J = 13.1, 5.7 Hz, 1H), 2.71 (dd, J = 17.5, 5.7 Hz, 1H), 2.47 (d, J = 12.6 Hz, 1H), 2.24 – 2.17 (m, 1H), 2.04 (dt, J = 12.5, 3.3 Hz, 1H), 1.89 – 1.82 (m, 2H), 1.73 – 1.54 (m, 4H), 1.34 (s, 3H), 1.32 – 1.21 (m, 3H), 0.90 (s, 3H).

5.3.3. Biological Evaluations

In a 96-well plate, a total of $1x10^6$ cells were seeded. After serial dilution of each CIE analog (from 25 μM down to 1.625 μM as Quadruplicate for each concentration), they were added with 0.05% DMSO (Acros Organics) as a negative control and cuc B as a positive control. The mixtures were incubated at 37 °C with 5% CO_2 for 48 hrs. Next, 20 μL of 3-(4,5-dimethylthiazol-2-yl)-2,5-diphenyl tetrazolium bromide (MTT) (Sigma Aldrich) (5 mg/mL PBS) was added to each well and the plate was incubated for 2 hrs. In each well, the solutions were discarded and 200 μL of DMSO was added and mixed. The absorbance was measured at 570 nm by Hidex Sense Microplate readers.

Cell Culture: Primary human pancreatic stellate cells HPaSteC (ScienCell Research Laboratories, Carlsbad, CA) were cultured in an RPMI-1640 growth medium with 2% fetal bovine serum, while PANC-1 (ATCC® CRL-1469™) cells were cultured in a DMEM growth medium with 10% (v/v) fetal bovine serum. All cultured cells were grown at 37 °C in a humidified 5% CO_2 atmosphere.[15]

Generation of 3D Pancreatic Spheroids. To generate 3D spheroids, PANC-1 cells were seeded onto round-bottomed 96-well plates with an ultra-low attachment coating (Corning, Kennebunk, ME) at a density of 120 cells per well in a volume of 100 μL. Heterospheroids of PANC-1 and HPaSteC cells were grown at an initial cell ratio of 120:60. After two weeks of incubation at 37 °C in a humidified 5% CO_2 atmosphere, the spheroids were processed for use in other experiments.[16]

Immunostaining and Imaging of Spheroid Frozen Sections. Pancreatic cancer spheroids were washed with PBS and embedded in HistoPrep™ tissue embedding medium, snap-frozen in liquid nitrogen, and kept at -80 °C. Then, the frozen tumor blocks were cut into 10 μm sections, fixed in an acetone-methanol (1:1) mixture for 15 min, and air-dried at room temperature. To determine the ECM components, cryosections were immunostained and imaged with antibodies against collagen I, fibronectin, hyaluronan, and laminin, as described previously.[17]

Cell Viability Assays. The cell viability of pancreatic cells and their co-culture with HPaSteC cells (in a ratio of 2:1) in either monolayers or spheroids was determined after 48 hours of incubation with cucurbitacin derivatives (KA1, KA2 and KA9) and gemcitabine (GEM) at different concentrations. For monolayers, we used MTT and CellTiter assays. In the case of MTT assay, after exposure to the tested compounds, cells were incubated in 0.5 mg mL^{-1} solution of thuazolyl blue tetrazolium bromide (Acros Organics, NJ) in PBS for 1.5-2 hours, followed by extraction of formazan crystals by DMSO:ethanol mixture (1:1, v/v). Optical density was measured at a wavelength of 560 nm using the 96-well plate reader SpectraMax M2 (Molecular Devices, Sunnyvale, CA). The CellTiter assay (Promega, Madison, WI), which measures the content of cell-associated ATP, was carried out in black-wall 96-well plates (Costar, Kennebunk, ME) for both monolayer and 3D cell cultures, according to manufacturer's protocol. Luminescence was measured using GloMax-Multi Detection System (Promega, Madison, WI).

Caspase 3/7 Activity Assay. The Caspase-Glo 3/7 assay (Promega, Madison, WI) was used to measure the activation of caspase 3/7, according to the manufacturer's protocol. After 48 hours of incubation, the caspase 3/7 was measured in monolayers of pancreatic cancer cells in the presence of different concentrations of cucurbitacin derivatives (KA1, KA2 and KA9) and gemcitabine (GEM) (Acros Organics, NJ). Luminescence was measured using the GloMax-Multi Detection System (Promega, Madison, WI).

Spheroid Growth Inhibition: For the evaluation of spheroid growth inhibition, several cucurbitacin derivatives (KA1, KA2, KA9) or gemcitabine (GEM) in concentrations of 10 μM were added to 5-day old spheroids (day 0). Two dimensions (length and width) of PANC-1 (120) or PANC-1/HPaSteC (120:60) pancreatic tumor spheroids were measured every two days using an inverted Axio Observer A1 microscope (Carl Zeiss, Göttingen, Germany) equipped with a ×20/0.4 objective lens microscope. The volumes of the spheroids were calculated as L x W x W (length x width x width).

In-cell western assay (ICW): PANC-I Cell lines were seeded into clear-bottomed, black-walled 96-well plates with a density of 0.5×10^6 cells per mL and allowed to grow to confluence. The next day, the cells were treated with various concentrations of KA9 (1.225, 2.45, 4.9, and 9.8 μM) for 24 h and DMSO was used as a –ve control. Cells were then fixed with 3.7% formaldehyde in 1X PBS for 30 min and then washed, permeabilized with 0.1% TritonX-100 in 1X PBS, and blocked with 1X PBS fish gel solution. Next, they were incubated with an antibody to the following: EGFR (cell signaling technology), Phospho-EGFR (Santa Cruz Biotechnology), MAPK (Erk1/ 2; Santa Cruz Biotechnology),

Phospho-MAPK (p-Erk1/2; Santa Cruz Biotechnology), STAT3 and pSTAT3 (Santa Cruz Biotechnology), mTOR and phosphorylated mTOR (Santa Cruz Biotechnology), and GAPDH (Santa Cruz Biotechnology). The mixtures received gentle shaking for 2 h. They were then incubated overnight at 4 °C without shaking (i.e: stationary). The cells were then washed with 0.1% Tween-20 in 1X PBS four times and then incubated with secondary antibodies conjugated to IR dye for 1 h with gentle shaking (protected from light). Cells were then washed with 0.1% Tween- 20 in 1X PBS four times. After the last wash, any residual liquid was gently pipetted out and the plate was blotted dry using the In-cell western protocol on an Odyssey® imager (LI-COR®), according to manufacturer's directions.[17] Phospho-proteins were normalized for total protein signals. Data are expressed as mean values of at least two runs ± the standard deviation (SD).

5.4. Conclusion

Ligand-based drug discovery approach was used to synthesis 8 cucurbitacin estrone analogs with ketone group at $C_{11.}$ Molecular modeling results indicate that there are some of ketone-C_{11} CIE analogs score high in molecular targets of pancreatic ductal adenocarcinoma such as EGFR, RAS, RAF, PI3K, and STAT3. KA9, CIE analog score higher most of the previous CIE analogs modified with hydroxyl at C_{11} or desaturated at C_9 and C_{11}. However, most of the ketone C_{11} analogs did not show high calculated affinity against the used molecular targets. *In-vitro* MTT and was conducted for the synthesized CIE analogs against 3 pancreatic ductal adenocarcinoma cell lines PANC-I, AsPC-I, and BXPC-3. The results indicate that KA9 show IC_{50} value of 4.9, 4.17, and 5.7 μM's, respectively, which is the lowest IC_{50} among the synthesized 24 analogs which support the conducted molecular docking against the indicated molecular targets. Comparing the best

synthesized analogs, KA1, KA2, and KA9 different biological evaluation assays have been conducted including 2D and 3D cellTiter assays, Caspase-3 activity assay, cell cycle flowcytometery, and in-cell western assay. The results indicate that the cell viability assay on 2D cells with CellTiter assay that the IC50 values for each of these analogs is slightly higher compared to that of MTT assay. All the three analogs KA1, KA2, and KA9 show an increase in caspase-3 activity which an indicated that these analogs induce cell necrosis through cell apoptosis. KA9 appear to arrest cell cycle at G0/G1 phase in a time- and concentration- dependent manner. Interestingly, 3D cellTiter assay experiment show that KA9 was able to decrease the tumor size starting from day 4 of treatment compared to gemcitabine and the hydoxylated analogs which although it has the same analog as KA1 which indicate that two factors is needed to achieve the highest activity through penetration of the tumor spheroids, presence of oxygen and higher hydrophobicity. Our results indicate that KA9 is candidate for *in-vivo* animal study and a promising novel treatment for pancreatic ductal adenocarcinoma.

5.5. References

1. Malvezzi, M.; Carioli, G.; Bertuccio, P.; Boffetta, P.; Levi, F.; La Vecchia, C.; Negri, E. J. A. o. O., European cancer mortality predictions for the year 2017, with focus on lung cancer. **2017,** *28* (5), 1117-1123.

2. Strimpakos, A.; Saif, M. W.; Syrigos, K. N. J. C.; Reviews, M., Pancreatic cancer: from molecular pathogenesis to targeted therapy. **2008,** *27* (3), 495-522.

3. Goess, R.; Friess, H. J. E. r. o. a. t., A look at the progress of treating pancreatic cancer over the past 20 years. **2018,** *18* (3), 295-304.

4. Chen, L.; Li, Q.; Weng, B.; Wang, J.; Zhou, Y.; Cheng, D.; Sirirak, T.; Qiu, P.; Wu, J., Design, synthesis, anti-lung cancer activity, and chemosensitization of tumor-selective MCACs based on ROS-mediated JNK pathway activation and NF-κB pathway inhibition. *European journal of medicinal chemistry* **2018,** *151*, 508-519.

5. Gilbert, J. A.; Salavaggione, O. E.; Ji, Y.; Pelleymounter, L. L.; Eckloff, B. W.; Wieben, E. D.; Ames, M. M.; Weinshilboum, R. M., Gemcitabine pharmacogenomics: cytidine deaminase and deoxycytidylate deaminase gene resequencing and functional genomics. Clinical Cancer Research 2006, 12 (6), 1794-1803.

6. Oliveira-Cunha, M.; Newman, W. G.; Siriwardena, A. K., Epidermal growth factor receptor in pancreatic cancer. Cancers 2011, 3 (2), 1513-1526.

7. Ahmed, M. S.; Kopel, L. C.; Halaweish, F. T. J. C., Structural optimization and biological screening of a steroidal scaffold possessing cucurbitacin-like functionalities as B-raf inhibitors. 2014, 9 (7), 1361-1367.

8. Mahnashi, M. H., Design, Synthesis and Biological Screening of Novel Cucsinspired Estrone Analogues Towards Treatment of Hepatocellular Carcinoma. **2017**.

9. Ahmed, M. S.; Kopel, L. C.; Halaweish, F. T. J. C., Structural optimization and biological screening of a steroidal scaffold possessing cucurbitacin-like functionalities as B-raf inhibitors. **2014,** *9* (7), 1361-1367.

10. Abou-Salim, M. A.; Shaaban, M. A.; El Hameid, M. K. A.; Elshaier, Y. A.; Halaweish, F. J. B. c., Design, synthesis and biological study of hybrid drug candidates of nitric oxide releasing cucurbitacin-inspired estrone analogs for treatment of hepatocellular carcinoma. **2019,** *85*, 515-533.

11. Z Stéphan, E.; Zen, R.; Authier, L.; Jaouen, G., Improved synthesis of a protected 11-oxoestrone. Steroids 1995, 60 (12), 809-811.

12. OpenEye Scientific Software, I., *FRED Fast Rigid Exhaustive Docking*. 9 Bisbee Ct, Suite D Santa Fe, NM 87508

August 12, 2008; p

http://www.apmggroup.net/innovation/molecular_testing/melanoma_pathways/melanoma.html.

13. OpenEye Scientific Software, I., FRED Fast Rigid Exhaustive Docking. 9 Bisbee Ct, Suite D Santa Fe, NM 87508 August 12, 2008; p

14. Riss, T. L.; Moravec, R. A.; Niles, A. L.; Duellman, S.; Benink, H. A.; Worzella, T. J.; Minor, L., Cell viability assays. **2016**.

15. Durymanov, M.; Kroll, C.; Permyakova, A.; O'Neill, E.; Sulaiman, R.; Person, M.; Reineke, J., Subcutaneous Inoculation of 3D Pancreatic Cancer Spheroids Results in Development of Reproducible Stroma-Rich Tumors. *Translational oncology* **2019,** *12* (1), 180-189.

16 Apte, M. V.; Wilson, J. S.; Lugea, A.; Pandol, S. J., A starring role for stellate cells in the pancreatic cancer microenvironment. *Gastroenterology* **2013,** *144* (6), 1210-1219.

17. Hirschhaeuser, F.; Menne, H.; Dittfeld, C.; West, J.; Mueller-Klieser, W.; Kunz-Schughart, L. A., Multicellular tumor spheroids: an underestimated tool is catching up again. *Journal of biotechnology* **2010,** *148* (1), 3-15.

Chapter Six

General Conclusion and Future Directions

In this project, a comprehensive investigation of the functionalization of C_{11} of cucurbitacin inspired-estrone analogs was undertaken. This is part of our lab's investigation into this novel group of compounds in relation to the natural products-based drug discovery process.

Initially, the project was based on previous results regarding the optimization of the analogs that included C_3 and C_{16}. The targeted disease in this study is pancreatic ductal adenocarcinoma, one of the most challenging diseases since it has acquired resistance to the common chemotherapeutic options. This project focused on the C_{11} position, as it previously indicated that it increases the anticancer potency of CIE analogs. Moreover, this position was found to be critical in both CIE analogs and cucurbitacins, as it changes the configuration of the molecule and hence its activity.

The molecular modeling step is an effective beginning step, utilizing putative pancreatic ductal adenocarcinoma's known critical targets, including EGFR, Erk, Ras, JAKI and STAT3 proteins. Upon docking these analogs against the known targets, it was found that different functionalizations offer general trends regarding the affinity to these proteins. For example, amine and oxygenated C_{11} analogs score better in EGFR and STAT3 proteins, while C_9 C_{11} dehydrogenated analogs score better in Erk, compared to the other analogs. This difference in affinity in the functional groups at C_{11}, although with a different 23, 24 α-unsaturated side chain, confirms the importance of this position in the structure-activity relationship of CIE analogs.

The chemical synthesis challenge was one of the main obstacles to overcome in order to reach the proposed synthetic routes, as is the case in any chemical synthesis route. However, the challenges included the optimization of the steps, the yield, the number of synthetic steps, and the performance of different reactions in the hindered C_{11} position. Among these challenges, the optimization of the DDQ reaction was a critical step. Five conditions were tried in this regard and only one of them achieved the desired yield that enabled us to continue. Hydroxylation, as well as three other conditions, were used to achieve the desired product. Moreover, the optimizations of the steps was critical, as working in more than one position delays the synthetic process, since many side reactions can exist. The number of steps was also a challenge, since reaching the final oxygenated products required 13 reactions.

After achieving the synthesis of 24 compounds, biological evaluations were conducted with different pancreatic cancer cell lines. The main cell line used in this biological study was PANC-I. Among the 24 synthesized analogs, 5 analogs indicated promising biological activities on the PANC-I cell line: KA1, KA2, KA9, KA19, and KA20 with IC_{50}'s of 5.52, 12.8, 4.3, 11.23, 7.64 μM, respectively. KA1, KA9, and KA20 all contain a phenyl *para*-trifluoro enone side chain, which indicates this side chain is involved in anticancer activity. KA2 and KA19 contain a cuc D and a phenyl *para*-nitro enone side chain, respectively. Since all CIE analogs containing a phenyl *para*-trifluoro enone side chain have antiproliferative activity, this can be used in their C_{11} functionalization. Regarding C_{11} functionalization of KA9>KA1>KA20 in terms of IC_{50} against the PANC-I cell line, the order of functionalizations is as follows: Ketone>hydroxyl>alkene.

To further investigate the effects of active CIE analogs, cell cycle analysis was conducted against the PANC-I cell line. Results showed that they accumulate the cells in the G1 phase, which indicates that the mechanism of action is similar in these compounds. Moreover, KA9 was shown to induce cell cycle arrest in a time- and concentration-dependent manner.

However, the 3D tests of KA1, KA2, and KA9 against the PANC-I cell line found that KA9 was better able to penetrate cell accumulation than KA1, KA2 and gemcitabine, which confirms the previously hypothesized data that these compounds are transferred to the cells through diffusion.

In order to study the mechanism of action of these compounds in depth, in cell western assay was conducted for KA9 using four proteins: pEGFR, pErk, pSTAT3, mTOR. The results indicate that KA9 was able to inhibit the expression of pEGFR and pErk specifically in a concentration-dependent manner compared to cucurbitacin that has non-specific effect against its targets.

According to our results, then, KA9 appears to be a good candidate for animal study, as it shows a promising IC_{50} and a promising penetration of 3D cells. Additionally, the targets for this compound have been identified. This amount of preliminary data is usually not available for the drugs that are promoted to animal study; however, with KA9, much data can be estimated.

Future Directions and Recommendations

Based on the anticancer activity of the previously mentioned CIE analogs and the molecular docking data, many further investigations are needed to address and investigate

the unanswered questions. These areas include the optimization of C_{16} and C_{17}, based on the desaturation of C_{16} C_{17}, which dramatically changed the anticancer activity of the synthesized analogs. Our current study suggests that hydroxylation, animation, and ketone substitutions may lead to more potent analogs against several cancer cell lines. Moreover, functionalization should include C_{11} and C_{16}, based on the previously obtained data and the results from the recent study.

Another next step based on this investigation is the study of KA9 in an animal model. This would allow further in-depth study of the anticancer activity and the toxicity profile, in order to promote it to clinical trials.

Generally, the CIE analogs from the previously conducted studies should be investigated in animal models in order to broaden the data prior to further in-depth studies.